SOURCES OF ERROR IN RELATING NANOINDENTATION RESULTS TO MATERIAL PROPERTIES

A Dissertation by

Mahdi Saket Kashani

Master of Science, Sharif University of Technology, 2004

Bachelor of Science, Amirkabir University of Technology, 2001

Submitted to the Department of Industrial and Manufacturing Engineering
and the faculty of the Graduate School of
Wichita State University
in partial fulfillment of
the requirements for the degree of
Doctor of Philosophy

May 2010

SOURCES OF ERROR IN RELATING NANOINDENTATION RESULTS TO MATERIAL PROPERTIES

The following faculty have examined the final copy of this dissertation for form and content, and recommend that it be accepted in partial fulfillment of the requirement for the degree of Doctor of Philosophy with a major in Industrial Engineering.

_____
Vis Madhavan, Committee Chair

_____
Suresh Keshavanarayana, Committee Member

_____
Charles Yang, Committee Member

_____
Krishna Krishnan, Committee Member

_____
Ramazan Asmatulu, Committee Member

Accepted for the College of Engineering

_____
Zulma Toro-Ramos, Dean

Accepted for the Graduate School

_____
J. David McDonald, Dean

DEDICATION

To my parents for their unconditional love

ACKNOWLEDGMENTS

I would like to express my deepest appreciation to my advisor, Dr. Vis Madhavan, for his guidance, dedication and most importantly his friendship during the course of my PhD at Wichita State University. He continually and convincingly conveyed a spirit of pursuit of truth, excellence and perfection in regard to research and scholarship. I am really grateful that I had the opportunity to work with an exceptional mentor that taught me beyond what is expected in academia. For everything you've done for me, Vis, I thank you.

I would like to thank my committee members, Suresh Keshavanarayana, Charles Yang, Krishna Krishnan, and Ramazan Asmatulu for their accessibility. I would also like to thank all the members of our research group over the last five years for their friendship, particularly Akbar Aftabi for his help with finite element studies of chapter 4.

Finally, I would like to thank my girlfriend and best friend, Rachel Roberts. Her love, understanding and support during last few years at graduate school have been priceless to me. I thank my parents for their faith in me and for supporting me to follow my heart and intuition. I am truly honored to dedicate this dissertation to them.

ABSTRACT

This dissertation consists of four submission-ready papers that address some of the key error sources that affect the accuracy of interpretation of nanoindentation test results to obtain material properties for elastoplastic materials. The first part of the work is a study of the effect of sample tilt on results of nanoindentation tests. Geometrical relations are used to develop a correction to account for the effect of tilt angle on the contact area. 3D FEA (Finite Element Analysis) shows that the assumptions made in deriving the geometric correction are valid, and the results for contact area, hardness and modulus match the predictions of the analytical model. It is shown that for both materials that sink-in and those that pile-up, the projected contact area for nanoindentation on tilted sample is higher than that estimated by the standard area function, which leads to overestimation of the hardness and elastic modulus. Experimental nanoindentation tests on tilted samples show lower sensitivity to sample tilt compared to FEA results because the compliance of the indenter holder causes the indenter tip to displace in the direction of the surface tilt, reducing the total penetration of the tip into the surface. For tips with very high compliance, this may even lead to significant underestimation of the hardness and modulus.

The second part discusses the various factors that affect the accuracy of FEA of nanoindentation. With the understanding that contact area error arising from discretization of the continuum is a key contributor to noise in the hardness data, a self similar mesh is designed that results in a known amount of maximum error in contact area over a range of depths of penetration of the indenter. Based on the fact that contact area increases in discrete jumps, it is argued that the maximum force that a given area of contact can support, before the next element comes into contact, is the best measure of the true hardness of the material that can be obtained with a given mesh. FEA simulations carried out with meshes of different amounts of error in contact area show that as the discretization becomes coarser, the estimate of the true hardness increases, due to the inability of the mesh to resolve the steep gradients in stress and strain near the end point of contact. It is also shown that results obtained from different meshes with different error percentages can be extrapolated to determine the exact value of hardness that will be obtained with infinitesimally small elements. It is shown that other sources of error, such as the convergence tolerance of the iterative solution process, are small in comparison to the discretization errors.

The third part is a study aimed at identifying the size of the volume underneath a nanoindentation that influences the hardness and modulus measured. FEA simulations of the indentation of a hemispherical particle embedded in a matrix reveal that the hardness of particle can be measured accurately by nanoindentation as long as

the plastically deformed region is confined entirely within the particle. While this may be intuitively obvious in retrospect, this is the first quantitative demonstration that this is so. It is found that an available relationship between the force, yield stress, and the radius of the plastically deformed zone is accurate under the conditions studied. This can be used to determine the maximum penetration depth that can be used if the size of the particle is to be estimated. For modulus of elasticity, it is shown that the modulus measured by nanoindentation method actually represents the elastic response of the entire specimen at the indentation point, which for all penetration depths, is a composite of the elastic response of both the particle and the matrix. A relationship is developed that shows the effect of boundary conditions and the matrix on the modulus measured by indentation at low depths of penetration for a hemispherical particle/matrix system.

The last part describes a new iterative procedure for estimation of the mechanical properties of elastic-perfectly plastic materials by nanoindentation. The key feature of this method is the estimation of the correct contact height, irrespective of whether the material piles-up or sinks-in, using an iterative procedure. It is shown that the proposed method improves the estimation of hardness and modulus compared to the Oliver and Pharr method and also gives a good estimation of the yield stress for materials with plastic index greater than 10.

TABLE OF CONTENTS

TABLE OF CONTENTS (continued)

CHAPTER 1

INTRODUCTION

Nanoindentation testing, also referred to as instrumented indentation testing, is widely used for mechanical characterization of small volumes of elastoplastic materials. The instrument directly measures the indentation force vs. displacement of the indenter, during the loading and unloading steps, from which the hardness and elastic modulus are estimated. However, the level of accuracy of the hardness and modulus values is always is question, since the method is very sensitive to several different parameters.

In this dissertation, which consists of four submission-ready papers, some sources of error that affect the accuracy of nanoindentation tests are addressed. The literature relevant to each subject is reviewed in the introduction section of each chapter and the findings of each study are summarized in the conclusions section.

Our study of the accuracy of nanoindentation tests was motivated by the desire to use this for measuring ductile damage distribution over the primary shear zone in metal cutting process (Figure 1.1). The deformation in this small region is of interest in FEA simulation of cutting, which is very sensitive to changes in material model (Madhavan and Adibi-Sedeh, 2005).

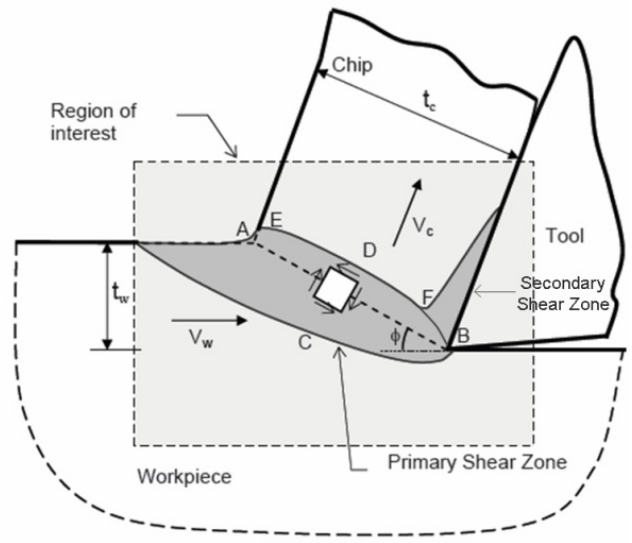

Figure 1.1. Schematic sketch of orthogonal cutting showing the primary shear zone (Madhavan et al. 2010).

We were interested to quantify the amount of damage at each point to include it in constitutive models to improve the accuracy of the simulation of metal cutting process. Damage measurement by nanoindentation and correlating it to mechanical properties has been addressed by some researchers using analytical approaches as well

as FEA and experimental studies (Basaran et al., 2004; Chen et al., 2006; Fleck et al., 1992; Kumar et al., 2001; Tasan et al., 2009; Xiang et al., 2006). Performing a grid of indents over the primary shear zone, it was observed that the noise level in the results obtained from nanoindentation was more than the changes expected in mechanical properties (Saket Kashani and Madhavan, 2007). It was concluded that in order to quantify ductile damage or any other parameter that introduces slight changes in the properties of material, a good understanding of the sources of error in nanoindentation tests was required.

One of the sources of error that we encountered and we needed to address was the effect of sample tilt on nanoindentation results. This was critical for our studies since the presence of slight sample tilt from one specimen to another was unavoidable by the procedures used for mounting and polishing of the specimens. For the case of etched specimens, the local waviness of the surface could also be considered as a significant surface tilt. Lack of a good study on the effects of this factor and incorrect interpretation of sample tilt in available literature (Xu and Li, 2007), led us to a comprehensive study of the effect of tilt on nanoindentation results as presented in chapter 2.

Performing numerous finite element simulations of nanoindentation, it was observed that there is certain amount of noise in FEA results that could sometimes interfere with drawing clear conclusions, especially if the expected changes are small. It was also noticed that several studies reported FEA result of nanoindentation containing clearly perceivable noise (Antunes et al., 2007; Bolshakov and Pharr, 1998; Chen and Vlassak, 2001; Larsson et al., 1996). Reviewing the literature, a need for a comprehensive study of the accuracy of FEA of nanoindentation was felt. This was the motive for the study presented in chapter 3. Using appropriately designed meshes, the contribution of various error sources was quantified and an extrapolation method was developed to reduce the amount of maximum error to arbitrarily small values.

This accurate FEA made possible a critical study to answer the important question: “What is the size of the volume underneath a nanoindentation that influences the hardness and modulus measured?”. The need to answer this question arose from the thought that the damaged region can be treated as a second phase with slightly different mechanical properties. This study also enables interpretation of nanoindentation results in a dual phase material. The study that is presented in chapter 4 identifies the volumes beneath a nanoindentation that influence hardness and modulus and also improves the understanding of the influence of properties of matrix on the modulus measured in a hemispherical particle/matrix configuration. The results of this study help to accurately relate the changes of mechanical properties observed from nanoindentation to different depths to the properties and extent of a second

phase or a damaged region. It also provides empirical rules for allowable depth of penetration for hardness and modulus measurement of small regions.

The other source that was limiting our ability to quantify the change of mechanical properties was the inability of the widely used method (Oliver and Pharr, 1992) to estimate the contact area accurately when the material piles up around the indenter (Bolshakov, 1996; Bolshakov and Pharr, 1998; Cheng and Cheng, 1998, 2000). This was very critical for our studies since it is well known that the less the material work hardens, the more the amount of pile-up is (Cheng and Cheng, 2000; Shu et al., 2007). During the metal cutting test, the large strain imposed causes the material to work harden to the point of saturation and the chip can be considered to be a perfectly plastic material. Therefore a good estimate of mechanical properties could be obtained for parent material, but the results were not accurate for nanoindentation results of the chip. There are several studies in the literature on the effect of pile-up on nanoindentation results and of ways to correct for pile-up (Kese and Li, 2006; Lee et al., 2007; Shu et al., 2007); however, none of them is widely accepted. Our studies on this issue led us to develop an iterative method that accurately estimates the contact area for materials that show pile-up around the indenter. As described in chapter 5, this method results in much better estimation of mechanical properties compared to the O&P method (Oliver and Pharr, 1992).

CHAPTER 2

ANALYSIS AND CORRECTION OF THE EFFECT OF SAMPLE TILT ON RESULTS OF NANOINDENTATION

2.1 Abstract

Finite element simulations have been carried out to study the effect of sample tilt on the results of conical and Berkovich indentation. For the case of conical indentation it is found that, for indentation on a five degree tilted specimen of a material exhibiting sink-in or pile-up behavior, the projected contact area would be underestimated by 8%. The hardness and elastic modulus are consequently overestimated by 8% and 4% respectively. These are significantly less than the overestimation of 130% for the hardness and 50% for the modulus reported in a recent paper (Xu Z-H, Li X. Philos Mag 2007; 87:2299). A generalized definition of the contact area that is also valid for indentation on tilted samples is proposed. We find that for conical indentation on a tilted surface, the boundary of contact lies along a plane; secondly that the plane is nearly parallel to the surface of the tilted sample; and thirdly that the contact depth measured along the indenter's axis is independent of tilt angle! It is found that these conclusions are valid for both sink-in and pile-up materials. This permits a simple geometrical correction for the effect of sample tilt. The validity of this approach is also studied for Berkovich indentation on fused silica by finite element simulations as well as experimental tests. It is found that while FEA show that the correction approach improves the accuracy of estimated hardness and modulus significantly, experimental results indicate an over-correction. The reasons for this are determined.

Keywords: Nanoindentation; Finite element analysis; Hardness; Elastic behavior

2.2 Introduction

Instrumented indentation tests are widely used for mechanical characterization of small volumes of material to obtain the hardness and elastic modulus. The results are very sensitive to numerous instrumentation and sample preparation factors (Fischer-Cripps, 2004) such as surface roughness of the sample, sample compliance and indenter geometry.

The effect of sample tilt on nanoindentation results is another specimen-related factor that can affect the results of nanoindentation tests. Specimen tilt could either be global, arising from non parallelism of the top and bottom surfaces of the sample, or a local tilt of the area under examination arising from surface waviness (Bobji and

Biswas, 1999) and from edge rounding effects near the edges of polished specimens. We have addressed the geometrical effects of surface tilt on nanoindentation results in a recent paper (Saket Kashani and Madhavan, 2008). Analytical equations were derived for calculating the true projected area of indentation of tilted specimens for pyramidal indenters such as Berkovich and cube corner, and also for conical indenters. The true projected area of contact was found to be higher for tilted indentation for the same depth of penetration. The resulting error that would be introduced in the modulus and hardness value was also determined.

Xu and Li (2007) studied the effect of sample tilt on conical nanoindentation test results using finite element analysis, and also presented some experimental results. They simulated several conical indentations with equal depth of penetration on samples tilted different amounts. While they also found that sample tilt will increase the true projected area, their results showed the effect of tilt to be more than ten times higher than ours.

In this paper we use finite element simulation to understand the effect of surface tilt on the results of conical nanoindentation. It is important to resolve this discrepancy since in most experiments the sample has a small, but finite, tilt. Indentation on samples tilted 1 to 5 degrees is studied using 3D finite element analysis (FEA) of half models and compared with a non-tilted sample. It is shown that nanoindentation results are not as sensitive to sample tilt as described in the work by Xu and Li (2007), and are of the magnitude expected based on our geometric analysis (Saket Kashani and Madhavan, 2008). We generalize the definition of contact depth in the manner that instrumented indentation actually measures it, which clarifies the sources of large differences between our result and ones reported in previous work (Xu and Li, 2007). FEA results also help us understand the reason why the analytical correction method based on geometry of the contact area between the indenter and the tilted specimen works so well and can be used to compensate for the slight influence of surface tilt on nanoindentation results.

For the case of Berkovich indentation on tilted samples, there is no FEM study available in the literature, to the knowledge of the authors. It is important to study this since the geometric correction show that a given amount of indentation more than that of the equivalent cone (Saket Kashani and Madhavan, 2008). A similar set of results for the effect of tilt and twist was reported by Ellis et al. (2008) from alignment uncertainty study approach, but no closed form equation was presented.

2.3 Basic theory of nanoindentation

Instrumented indentation tests use the Oliver and Pharr (1992) method to estimate the contact depth (h_c) based on the maximum load (P_{max}) at full penetration depth (h_{max}) and the stiffness of the unloading force curve (S).

This is derived from Sneddon's analysis (Cheng and Cheng, 1997) of the elastic deformation of a half space subject to an axisymmetric displacement boundary condition on the surface akin to that of a cone indenting it. The contact depth is determined using equation (2.1) which has rigorous applicability for elastic indentations but has been shown to be applicable to elastoplastic indentations too (Cheng and Cheng, 1997). The projected contact area ($A_{c\ proj}$) is obtained by substituting the contact depth into the area function of the indenter, which is obtained from a calibration process. The commonly used definition of hardness, the Meyer hardness, is the ratio of the indentation load to the area of the indent projected on a plane perpendicular to the axis of the indenter. The elastic modulus of the specimen can also be obtained from a relationship found in Sneddon's analysis, modified to include a correction found and that accounts for the fact that the loading used in Sneddon's calculation is different from that actually imposed by the indenter (Hay et al., 1999).

$$h_c = h_{max} - \varepsilon \frac{P_{max}}{S} \tag{2.1}$$

$$H = \frac{P_{max}}{A_{c\ proj}} \tag{2.2}$$

$$E_r = \frac{1}{2\beta}\frac{\sqrt{\pi}}{\sqrt{A_{c\ proj}}} S \tag{2.3}$$

$$\frac{1}{E_r} = \frac{1-\nu_s^2}{E_s} + \frac{1-\nu_i^2}{E_i} \tag{2.4}$$

In the above equations, E_r is the reduced modulus, E_s the modulus of specimen, ν_s the Poisson's ratio of specimen, E_i the modulus of indenter, ν_i the Poisson's ratio of indenter, and β and ε are constants that depend primarily on the geometry of the indenter. For conical indentation of fused silica, β can be obtained from analytical equation given by Hay et al. (1999) which is equal to 1.072. While ε turns out to be 0.72 for Sneddon's boundary conditions, experimental results indicate that 0.75 is a better value for Berkovich indenters (Fischer-Cripps, 2004).

2.4 Generalized Definition of Contact Depth

The entire field of depth sensing indentation arose from the ability to estimate the contact depth accurately by compensating for the surface displacement using the approach developed by Oliver and Pharr (1992). The contact depth is calculated based upon the initial slope of the unloading portion of the load-displacement curve and is directly related to the projected contact area at peak load. Oliver and Pharr defined the contact depth as "the vertical distance along which contact is made". Fischer-Cripps (2004) defined it as "the distance from the bottom of the

contact to the contact circle". Both definitions provide a clear description of the contact depth of ideal conical indentations, but are not clear for the case of indentation on tilted samples or pyramidal indentations.

For the case of indentation on tilted samples, the definition can be generalized to be valid independent of the tilt angle. Note that the maximum depth of penetration is measured along the direction along which the indenter is fed into the sample, the indentation direction. This is the way all commercially available nanoindentation machines measure the displacement, using a transducer. Assuming that this direction and the indenter's axis are the same, the contact depth can be defined as: "the distance between the tip of the indenter and the intersection of the indenter's axis with the plane of the boundary of contact" (Figure 2.1). In this work, it is shown that the boundary of contact for conical indentation remains planar, for all sample tilt angles. The above definition degenerates to the traditional definitions for the case of ideal conical indentation with no sample tilt.

For ideal pyramidal indentation, it has been shown by 3D finite element analysis of Berkovich indentation on fused silica that the projected contact area is not a perfect equilateral triangle. The sides of the triangle are curved, attributable to the fact that the contact depth changes locally as the local cone angle varies. For a material that sinks-in, for which the O&P equation is valid, the smaller the local cone angle is (closer to the middle of the face), the smaller the contact radius and the smaller the contact depth. Shim et al. (2007) showed that the contact depth calculated by the O&P method results in a number between the minimum local contact depth (at the middle of the faces) and the maximum local contact depth (at the edges of the pyramid) as shown in Figure 2.2. The geometry of boundary of contact for pyramidal indentation on a tilted surface is further complicated by the tilt angle and also depends on the orientation of the pyramidal faces with respect to the axis of tilt.

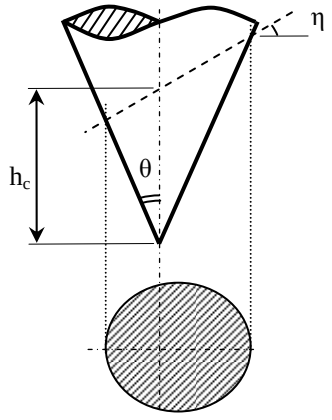

Figure 2.1. Projected area of indent for a contact depth of h_c on a surface tilted η degrees.

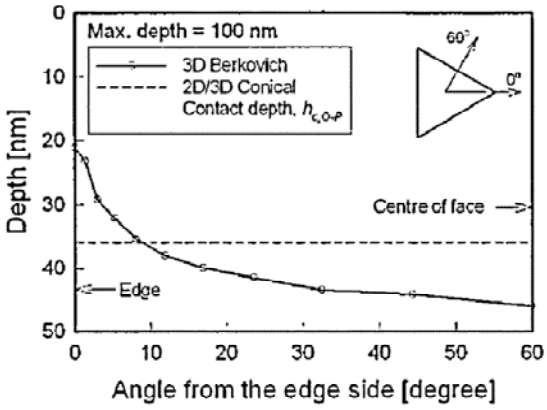

Figure 2.2. Variation of the depth of boundary of contact for a Berkovich indentation compared with that of conical indentation. Note that the conical depth of boundary of contact is between the minimum and the maximum local contact depths of Berkovich indentation (Shim et al.,2007).

2.5 Area function for conical indentation into tilted samples

As stated above, it is assumed that the tilt is only introduced as a result of sample tilt, the conical indenter being mounted accurately, with the geometrical axis of the indenter coinciding with the indentation direction. The depth of indentation is measured beginning at the point where the indenter touches the sample, and is measured in the indentation direction along the indenter's axis.

For an ideal conical indentation without sample tilt, the impression will be circular and the projected area of the impression is given by equation (2.5), where θ is the semi-cone angle, and h_c is the contact depth.

$$A^{\theta}_{c\,proj}=\pi\, h_c^2 \tan^2\theta \tag{2.5}$$

For η degrees of sample tilt, assuming that the boundary of contact lies in a plane, the boundary of contact will be an ellipse. The projected area of contact, along the plane perpendicular to the axis of the indenter, will also be an ellipse as shown in Figure 2.1. The procedure for calculation of this area function is reported in our earlier work (Saket Kashani and Madhavan, 2008). Further assuming that the boundary of contact is parallel to the surface being indented, and defining h_c to be the intersection of this plane with the indenter axis, the area of the projected ellipse can be calculated using equation (2.6).

$$A^{\theta\eta}_{c\,proj}=\frac{\pi\, h_c^2 \tan^2\theta}{(1-\tan^2\theta\tan^2\eta)^{3/2}} \tag{2.6}$$

Using the projected contact area of indentation on ideal surface without tilt given by equation (2.5) as the reference and assuming that h_c remains independent of tilt, the error induced in the projected contact area due to tilt can be written as:

$$\%\text{error}=\frac{A_{c\ proj}^{\theta\eta}-A_{c\ proj}^{\theta}}{A_{c\ proj}^{\theta}}\times 100 \tag{2.7}$$

Figure 2.3 shows the error for a range of cone angles including 70.3º and 42.3º, for which the area functions are the same as that of Berkovich and cube corner indenters, respectively. Notice that the projected contact area with tilt is always more than that without tilt. This can be understood by referring back to Figure 2.1 and noting that the increase in area on the right side of the axis due to tilt is more than the decrease in area on the left. It can be seen from Figure 2.3 that indenters with larger semi-cone angles are more sensitive to sample tilt. A five degree tilt will result in 9.7% underestimation of projected area for the cone angle equivalent to that of a Berkovich indenter, while it results in only 1.0% error for the cone equivalent to a cube corner.

The other useful conclusion that can be drawn is about the specification within ISO 14577 (2002) that the surface tilt should be less than 1º. This recommendation can be seen to be very conservative for indenters with smaller cone angles. Using the equations above, the maximum allowable tilt angle that results in less than 1% error in estimation of area function without any sort of correction strategy is plotted as a function of the semi-cone angle in Figure 2.4. For example, the allowable tilt angle for the cone equivalent to a Berkovich is 1.7º while it is 5.1º for the cone equivalent to a cube corner. This suggests that it may be possible to use indenters with smaller semi-cone angles to expand the applicability of this nondestructive test to cases where local surface tilt is unavoidable, such as with rough surfaces.

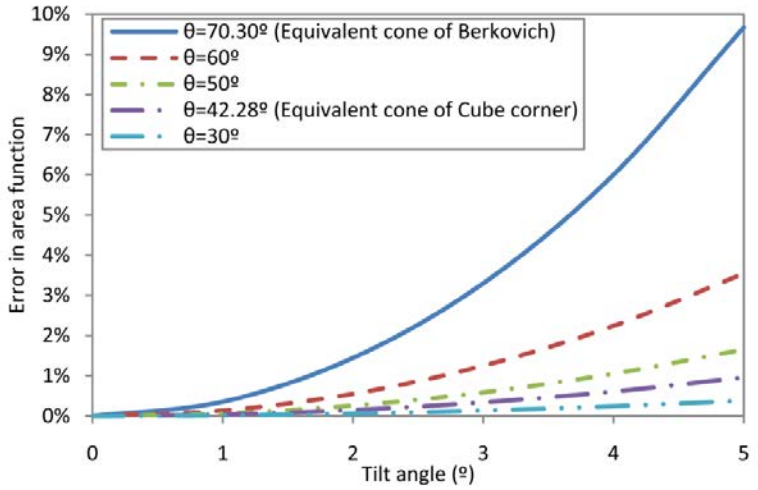

Figure 2.3. Error in projected area versus tilt angle (η) for conical indenters of different semi-cone angles.

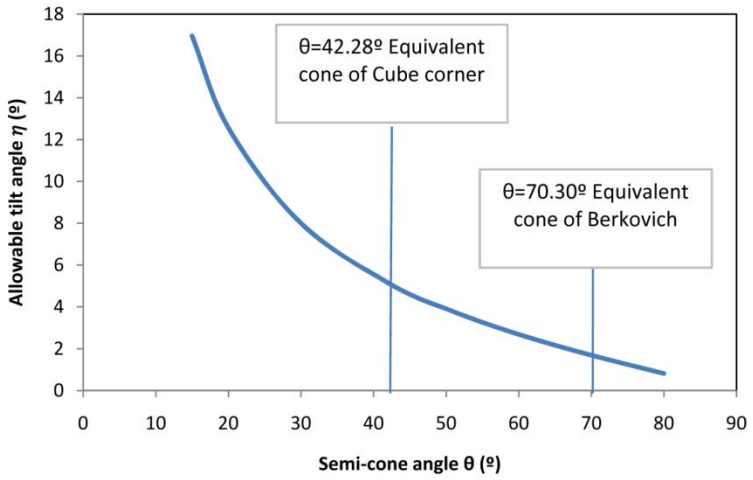

Figure 2.4. Maximum allowable surface tilt angle for the error in projected area to be less than 1%.

2.6 Area function for pyramidal indentation into tilted samples

For the ideal case of indentation without sample tilt, the projected area of a pyramidal indenter would be an equal-sided three sided figure. As discussed before, due to local contact height variations the sides can be either concave outwards (for sink-in) or convex outwards (for pile-up materials). The average contact height can be considered to be the one which would give an area of contact that is an equilateral triangle of contact area equal to that of the area function of the indentation. The projected area is a function of average contact height, h_c, and the face angle of the pyramid, φ, as given in equation (2.8). The face angles of Berkovich and cube corner indenters are 65.27º and 35.26º respectively.

$$A_{c\,proj}^{\varphi} = 3\sqrt{3}\, h_c^2\, tan^2\varphi \tag{2.8}$$

For the case of a tilted sample, the impression corresponding to the average of contact height, h_c, will not be an equilateral triangle anymore. The procedure for calculation of the projected contact area of a triangular pyramidal indentation on a tilted surface was reported in our earlier work (Saket Kashani and Madhavan, 2008). The projected contact area for this case is also a function of the tilt angle (η) and the rotation angle (ζ), as shown in equation (2.9).

$$A_{c\,proj}^{\varphi\eta\zeta} = \frac{3\sqrt{3}\, h_c^2\, tan^2\varphi}{1-3\tan^2\varphi\tan^2\eta-2\tan^3\varphi\tan^3\eta\cos 3\zeta} \tag{2.9}$$

The tilt angle (η) is the angle between the normal vector of the sample surface, $\hat{n}$, and the axis of the pyramid (Z) (see Figure 2.5). The rotation angle (ζ) specifies the direction of the tilt with respect to one of the edges of the pyramid, measured as the angle between the projection of one of the pyramid edges along which the Y angle

is aligned and the projection of the surface normal ($\hat{n}_{xy}$) on the plane perpendicular to the axis of the pyramid (XY plane).

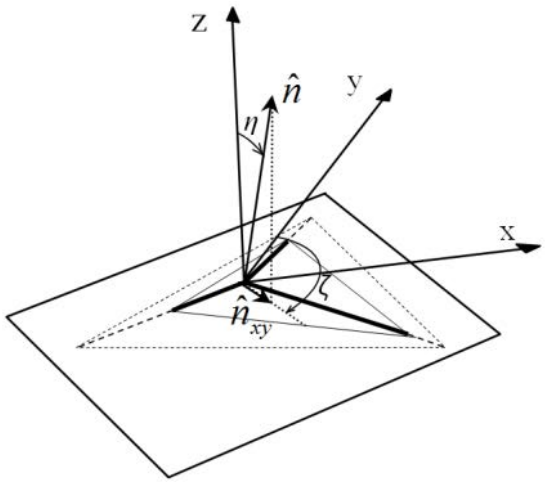

Figure 2.5. Schematic view of a pyramidal indentation into an tilted surface showing the Cartesian coordinate system at the tip of the pyramidal indenter with respect to which the tilt angle η and rotation angle ζ of the surface normal $\hat{\boldsymbol{n}}$ are defined.

Figure 2.6 depicts the normalized projected contact area, the ratio of contact area with and without tilt (equation 2.9 and 2.8, respectively) for a Berkovich indenter (φ=65.27º) as a function of the rotation angle for different tilt angles from 1 to 5 degrees. It can be seen that the maximum error due to tilt occurs when the rotation angle ζ is zero, i.e. the tilt is along an edge of the pyramid.

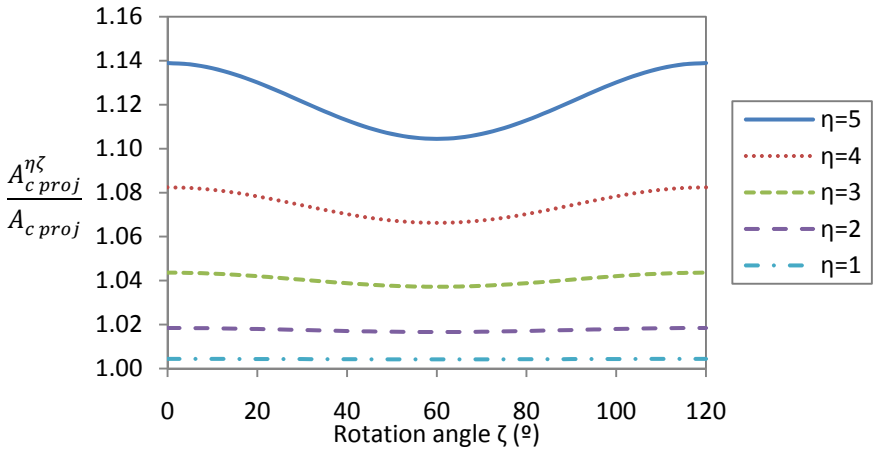

Figure 2.6. Normalized projected contact area of Berkovich indenter versus rotation angle ζ for tilt angles η of 1 to 5 degrees.

In order to compare the effect of tilt for conical and pyramidal indenters, the normalized area versus tilt angle is plotted in Figure 2.7 for Berkovich, cube corner, and their equivalent cones. $\zeta = 0$ is assumed for the

pyramidal ones to study the maximum possible error. It can be concluded that pyramidal indenters are more sensitive to sample tilt than their equivalent cones. This figure also shows that Berkovich indenters are much more sensitive to sample tilt compared to cube corner indenters. This is simply because a Berkovich indenter has a larger equivalent cone angle compared to a cube corner indenter.

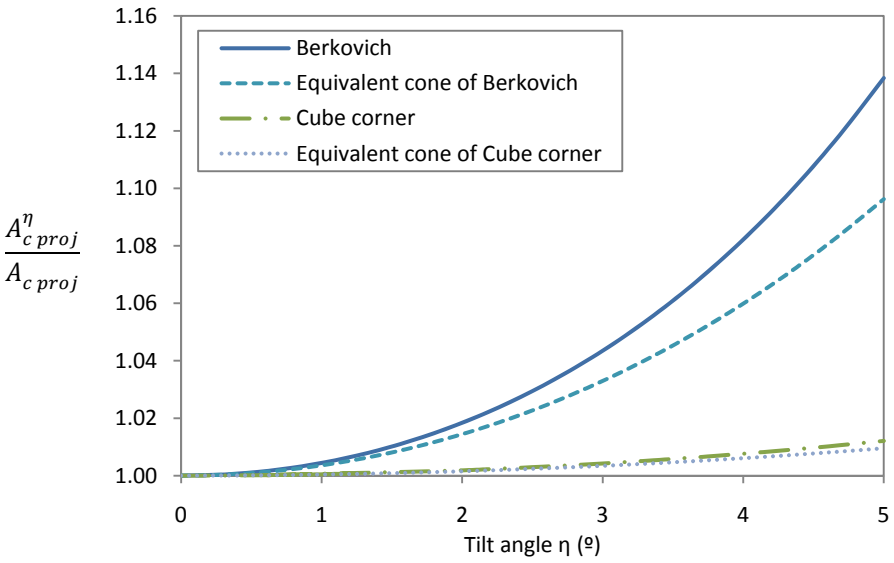

Figure 2.7. Normalized projected contact area for Berkovich, cube corner and their equivalent cones versus tilt angle (η).

2.7 Finite Element Simulations

Three dimensional finite element simulations were carried out using the ABAQUS/STANDARD software package, to check the effect of sample tilt on nanoindentation results. The loading and unloading steps were modeled for a rigid conical indenter with a semi-cone angle of 70.3º and for a rigid Berkovich indenter. Indentation was simulated using displacement boundary conditions on the indenter that resulted in a peak displacement of the indenter tip into the specimen of 90nm (Figure 2.8). The specimen was modeled as a half-cylinder 12.3 μm tall and 24 μm in diameter, tilted from 0º to 5º with respect to the axis of the indenter, and meshed with fully integrated eight-noded hexahedral elements. Symmetry boundary conditions are applied on nodes along the plane of symmetry. The Berkovich simulations are also done using a half model by neglecting the effect of indenter's orientation ($\zeta = 0$). The displacement of nodes along the bottom of the cylinder was constrained as shown in Figure 2.8. Frictionless contact was defined between the indenter and the sample. The element sizes in the contact region were of the order of 15 to 20nm which was found to result in good resolution in the contact area measurement with errors less than 1% (Figure 2.9). For the case of conical indentation two materials were used to study the behavior of both sink-in and

pile-up materials. Elastic-plastic von Mises material with isotropic hardening with $E/\sigma_y=75$ (as a material that sinks in) and $E/\sigma_y=400$ (as a material that piles us) were simulated, with E=100GPa, ν=0.28. Power law work hardening behavior was assumed, of the form $\bar{\sigma}=\sigma_y(E\varepsilon/\sigma_y)^n$ for $\varepsilon \geq \sigma_y/E$ with n=0.1 (Xu and Li, 2007). For Berkovich simulations, fused silica was modeled as an elastic-perfectly plastic material with E=72GPa, ν =0.17 and σ_y =5.5GPa (Shim et al., 2007).

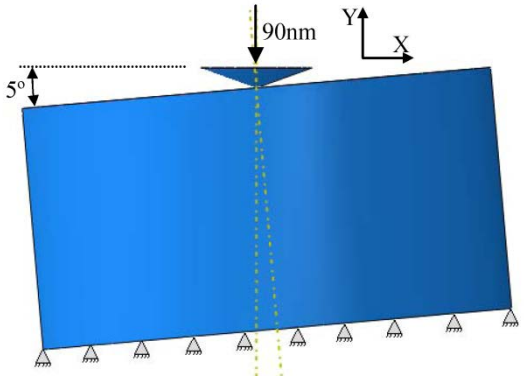

Figure 2.8. Boundary conditions for the finite element model of indentation on a 5º tilted sample. The axis of tilt is along the Z axis, the indenter axis is along the Y axis and the origin of the coordinate system is at the tip of the indenter. The indenter is constrained to displace along its axis and the bottom face of the specimen is fixed.

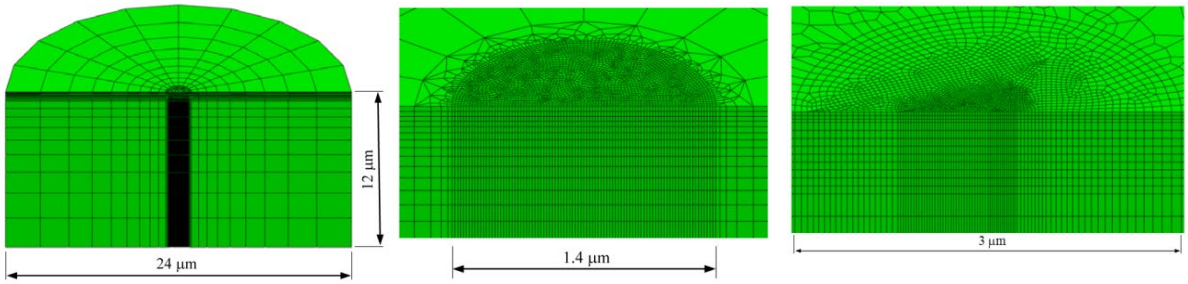

(a) (b) (c)

Figure 2.9. FE model of the specimen. (a) Size of the sample and the mesh used, (b) mesh in the region of interest for conical indentation, with element size of 15 to 20nm, (c) mesh in the region of interest for Berkovich indentation.

2.8 Results

Figure 2.10 shows the load-displacement curves obtained from FEA of conical indentation into surfaces tilted zero and five degrees for sink-in material. It can be clearly seen that the peak load is higher for the tilted indentation, by 8%. It is the case that the initial unloading slope is also greater for the tilted indentation, by 4% in this case.

Figure 2.11(a) shows the distribution of von Mises stress along the top surface and along the symmetry plane of a specimen without tilt and Figure 2.11(b) shows that on a sample tilted 5 degrees with the indenter being vertical in both figures. It can be seen that the stress field for the tilted indentation is skewed, with a larger extent of stressed material on the side with the longer length of contact with the indenter. From the location of the stress contours (corresponding to $\bar{\sigma}=\sigma_y=1333$MPa), it can be seen that size of the plastically deformed material is larger than the size of the contact on the surface. Note that the same view orientation, size and fringe ranges are used for both figures.

The elements in contact with the indenter can be seen in the contact pressure plots shown in Figures 2.12(a) and 2.11(b) for the case of no tilt and tilted samples, respectively. It can be seen that the contact pressure is fairly uniform over the contact region. It can also be noted that the number of elements in contact at maximum displacement (more than 300) is sufficient for accurate determination of the area of contact. The jump in contact area due to each additional element coming into contact is about 0.3% of the maximum contact area at the maximum depth. Since the same element sizes are used for all the simulations, this is the amount of random error to be expected in the contact area and hardness results. Figure 2.13 shows the contact pressure distribution over the projected contact area for Berkovich indentation on non-tilted and tilted samples of fused silica. It can be seen that the true boundary of contact is not an equilateral triangle, but a concave outwards, three sided figure, as observed by others (Shim et al., 2007).

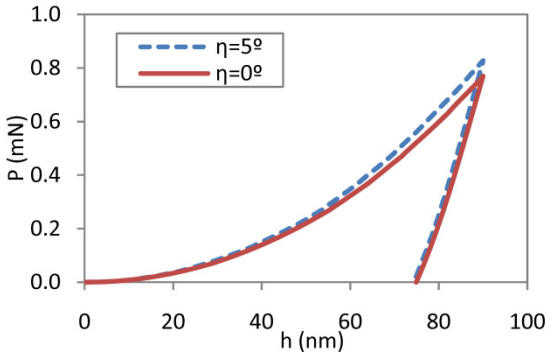

Figure 2.10. Load-displacement curves for indentation into samples tilted zero and five degrees for $E/\sigma_y=75$.

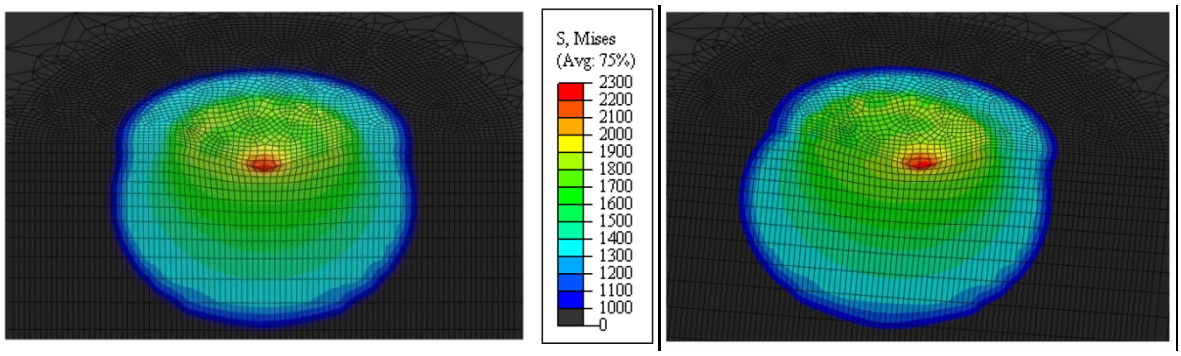

Figure 2.11. Von Mises stress distribution at maximum load in MPa. (a) for sample without tilt, (b) for 5º tilted sample for E/σ_y=75 (σ_y=1333MPa).

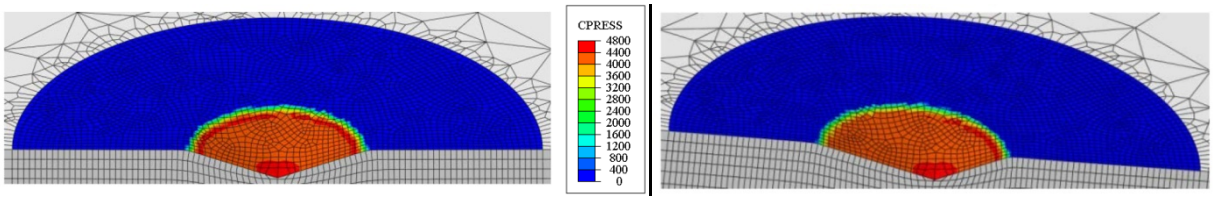

Figure 2.12. Contact pressure (MPa) at maximum load for conical indentation. (a) for sample without tilt, (b) for 5º tilted sample, with σ_y=1333MPa, and E/σ_y=75.

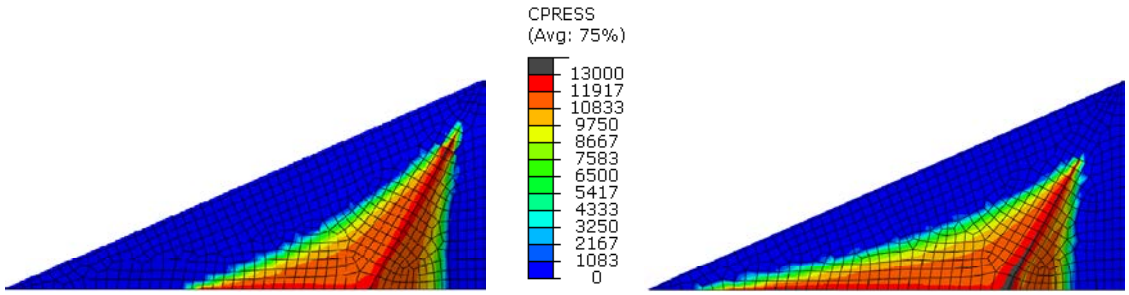

(a) (b)

Figure 2.13. Contact pressure (MPa) at maximum load for Berkovich indentation. (a) for sample without tilt, (b) for 5º tilted sample for fused silica (σ_y=5500MPa).

For obtaining the projected area of contact supporting the indenter, the contact area should be projected onto a plane perpendicular to the indenter axis. The total contact area, which is among the results output by ABAQUS, can be projected in the plane perpendicular to the indenter axis to obtain the projected contact area using equation (2.10) for conical indentation and using equation (2.11) for Berkovich indentation.

$$A_{c\,proj}^{\theta} = A_c^{\theta} \sin\theta \tag{2.10}$$

$$A_{c\,proj}^{\varphi} = A_c^{\varphi} \sin\varphi \tag{2.11}$$

Having the maximum load and projected area at that load, the hardness can be determined using equation (2.2). The hardness of the specimen without tilt is found to be 4.2GPa for E/σ_y=75 and 0.9GPa for E/σ_y=400. The initial slope of the unloading curve is obtained from the load-displacement curve given by the FEA simulation. The reduced modulus of the contact pair is determined by substituting the stiffness and projected area into equation (2.3). The elastic modulus of the specimen can be obtained by substituting the reduced modulus and Poisson's ratio of the specimen into equation (2.4); since the indenter is considered to be rigid, $E_i = \infty$. The elastic modulus of the specimen obtained from FEA simulation of the indentation of samples without tilt is found to be 101GPa for E/σ_y=75 and 102GPa for E/σ_y=400, which are close to the input value of 100GPa.

Figure 2.14 shows the ratio of the projected contact area of indentation on tilted specimens to that on an un-tilted specimen, as a function of tilt angle. The true ratio, obtained from FEA, is found to be matched well by equations (2.1, 2.6), i.e., the projected contact area increases with tilt in accordance with equation (2.6) for both sink-in and Pile-up materials. The geometric parameter ε in equation (2.1) is assumed constant at 0.72 for tilted and non-tilted indentations. Note that, without compensation of the area for tilt, that is with the O&P equations (2.1, 2.5), the small contact area decrease observed in Figure 2.14 with increase in tilt can be attributed to overestimation of the elastic recovery by the O&P equations due to the 8% higher force but 4% higher stiffness. However, the decrease in area estimated by O&P is less than 1%, and the ratio of h_c/h_{max} remains nearly constant independent of tilt for both simulated materials.

Figure 2.15 compares the hardness calculated using the three different measures of the projected area of contact shown in Figure 2.14. It can be seen that the true hardness obtained from FEA remains constant independent of tilt angle – the small (<2%) variation in hardness are due to the contact area error. The area function for indentation without tilt ($A^{\theta}_{c\,proj}$) underestimates the contact area, thereby overestimating the actual hardness of the material. This error increases as the tilt angle increases. The overestimation factor is about 1.08 for the case of five degree sample tilt. It can be noted that using equation (2.6) reduces the error in estimation of hardness for both pile-up and sink-in materials.

Figure 2.16 shows the elastic modulus obtained from the O&P method using the three different measures of the area of contact. Again the standard area function underestimates the area and leads to overestimation of the elastic modulus of the material as the tilt angle increases. The overestimation factor is about 1.04, since the area

appears within a square root in equation (2.3) for the modulus. This shows that the correction method successfully reduces the error in modulus estimation for both pile-up and sink-in type.

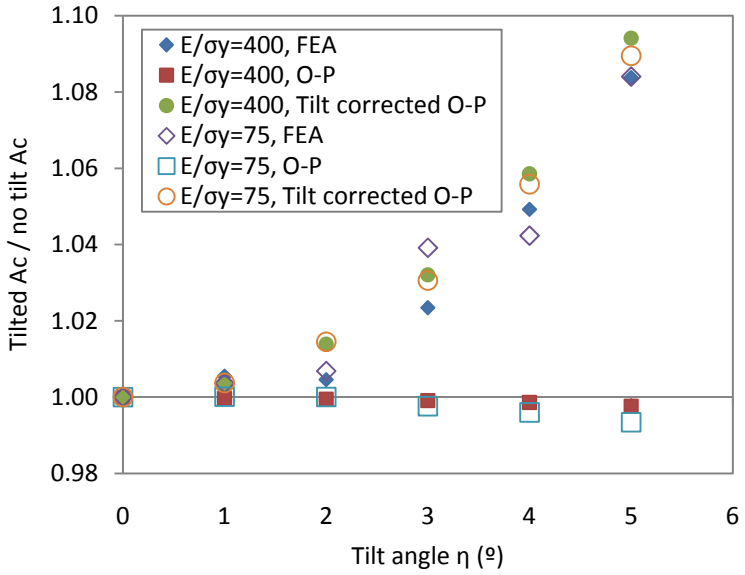

Figure 2.14. Comparison of the projected contact areas of conical indentations obtained from FEA, from O&P method, and from tilt corrected O&P for different tilt angles. Note that while FEA and the tilt corrected area function show an increase in A_c with tilt, the O&P method does not detect the change in A_c.

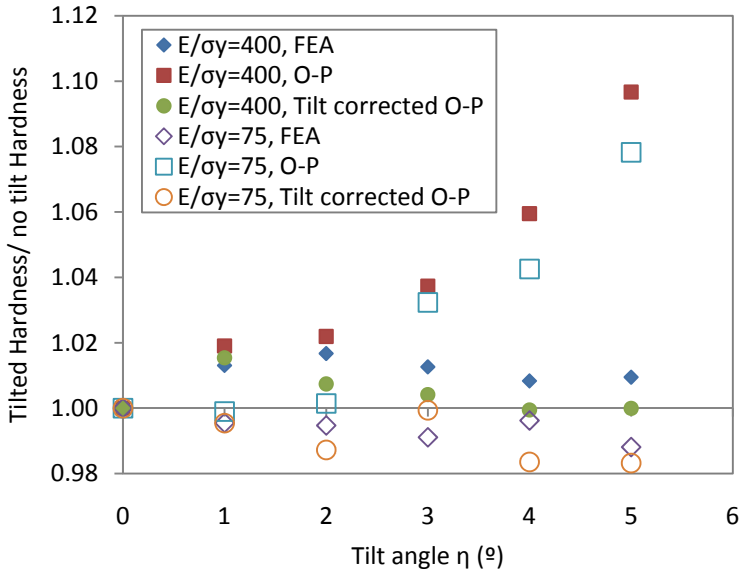

Figure 2.15. Increase in the hardness calculated as a function of tilt angle of the specimen, shown for each of the three different measures of the contact area. Note that while the actual hardness given by FEA is nearly independent of tilt, the hardness estimation by the O&P method is 8 to 10% higher.

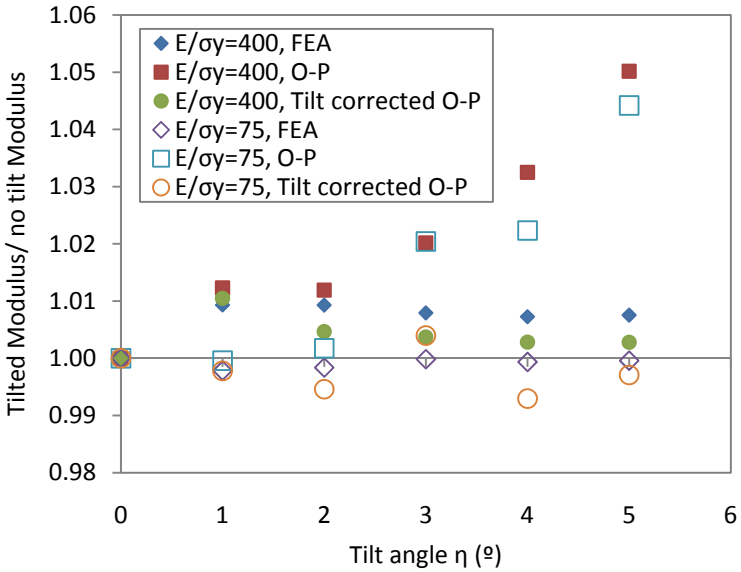

Figure 2.16. Increase in the modulus calculated as a function of tilt angle of the specimen, shown for each of the three different measures of the contact area. Note that while the modulus estimated using true unloading slope and the true contact area obtained from FEA is nearly constant, the modulus estimated by the O&P method is 4 to 5% higher.

2.9 Experiments on tilted specimen of fused silica

Indentations were performed using a Berkovich indenter to study the actual effect of sample tilt on nanoindentation results. Indentations were made on fused silica specimen with and without sample tilt. The sample tilt was introduced using a five degree angle block. In order to make sure the machine compliance is the same for both tests with and without tilt, a zero degree gauge block of the same material and the same height (~ 6-8 mm) was used for the zero degree tests as well. The sample was glued securely to the block and the block was held down by magnetic force. The zero degree tests were performed first and used to obtain the reference area function, which was then used for the tests on the tilted sample. Two sets of 6x6 indents at two different positions with increasing load from 5 to 9mN were performed on the sample with no tilt. This load range resulted in penetration depths between 194 and 267nm. The area function was determined by forcing the reduced modulus to 69.6 GPa for all load curves and was used to process the data. The fitted area function resulted in average hardness and reduced modulus of 10.12 and 69.54GPa respectively. In order to keep the indents on tilted sample within the calibrated contact depth range, the load range was reduced to 6 to 9mN for similar two sets of 6x6 indents at two different positions. This load range resulted in penetration depths between 210 to 260nm.The average of the hardness and reduced modulus of the 72 indents on the tilted sample were 10.60 and 72.87GPa respectively. This shows a clear overestimation

compared to the calibration values both in hardness and modulus; however, the 5% increase in measured hardness and 5% increase in measured reduced modulus do not exactly match the 12% and 6% increase expected based on theoretical and FEA results.

After area function calibration, the same fused silica specimen was mounted on a five degree angle block and two grids of 36 indentations were made. The scanned impressions of indentations with nominal contact depth of 150nm are shown in Figure 2.17 for both untilted and five degree tilted samples. It can be seen that the indentations on tilted sample results in an impression which is not an equilateral triangle, and which has slightly higher projected area for the same contact depth and consequently results in higher indentation loads.

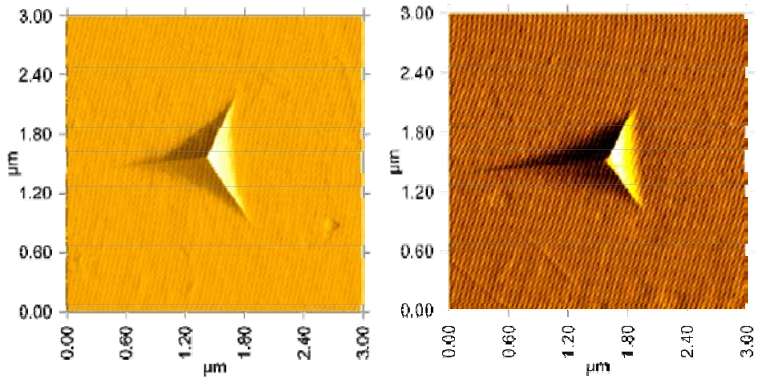

(a) (b)

Figure 2.17. The scanned impression of indentations on fused silica with contact depth of 150nm for (a) the untilted sample and (b) the five degree tilted one.

A closer look at the load curves of indents with same maximum load of 9mN on zero and five degrees tilted samples revealed different creep behavior during the time the load is maintained constant at the peak value. The indentations were done in load control mode that consisted of 5 seconds linear loading, 5 seconds idle at maximum, and 5 seconds linear unloading. The displacement versus time during the idle time of these two load curves are shown in Figure 2.18. It can be seen that the indenter does not creep much into the tilted specimen while the load curve for indentation on zero degree shows about 3nm displacement. Since the load is constant at 9mN during these five seconds, the creep of the zero degree tilted sample means that the material hardness is slightly lower at smaller strain rates. This is an intrinsic character of the material and should not change with slight tilt of the sample; however, Figure 2.18 shows that the indenter creeps less than 1nm into the five degree tilted sample and then retracts. This interesting creep behavior of the tilted sample is interpreted as follows. The stem holding the indenter is deflected slightly to the side due to the side force developed while indenting a tilted specimen. This side force also results in creep to the side, which tends to increase the contact area. The indenter needs to retract to keep the load

constant. The deflection of the stem moves the indenter in the direction of the slope of the specimen surface, causing the true penetration depth to be smaller than the recorded penetration depth.

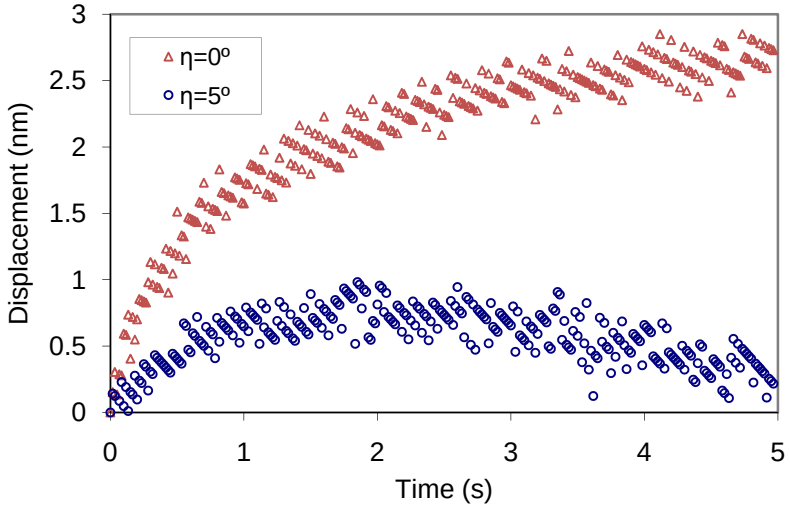

Figure 2.18. The creep behavior of Fused silica during the idle time at constant 9mN load on ideal and five degrees tilted samples

The deflection related overestimation in contact area needs to be compensated in experimental results. A 5nm decrease in maximum depth of penetration is equivalent to about 60nm deflection in the position of the tip over the 5º tilted specimen. Since the stem of the indenter is about 5mm long, it can be seen that the change in angle due to this deflection is negligible. The deflection leads to a smaller maximum penetration into the sample surface than indicated by the instrument, the correction can be done by reducing the maximum depth of penetration used for data processing of tilted indentations (Figure 2.19). A 2% decrease in maximum depth of penetration, which is about 5nm for 9mN indent makes the data agree with the values expected from geometrical estimation of contact area of Berkovich indentation on tilted samples, equation (2.9), and also FEA results of 3D Berkovich indentation on tilted fused silica. The normalized hardness and modulus values are plotted in Figures 2.20 and 2.21 for comparison.

FEA of Berkovich nanoindentation on a 5º tilted specimen of fused silica shows that there is a constant side force, equal to 7.4% of the normal force during the loading step. The side force expected for a load of 9mN is about 0.67mN. The deflection equation for a fixed-end cantilever, of dimensions equal to that in our setup, shows that if the modulus of the indenter's stem is around 10GPa, the 60nm deflection is expected for this side load. The amount of deflection will be dependent on mechanical properties of the stem of the indenter and also the side stiffness of the transducer, which are not the same for different instrumented indenters. It should be also noted that the side stiffness

of the indenter stem and transducer may affect the unloading stiffness slightly. Therefore the modulus measured is affected by the stiffness of the system in horizontal direction, which can be different for different transducers/indenters.

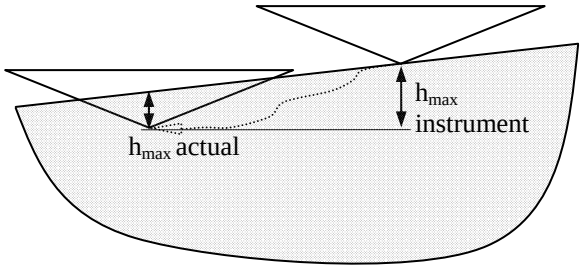

Figure 2.19. Schematic view of the effect of indenter deflection on measured maximum penetration depth. Note that the maximum penetration recorded by the instrument is more than the actual depth.

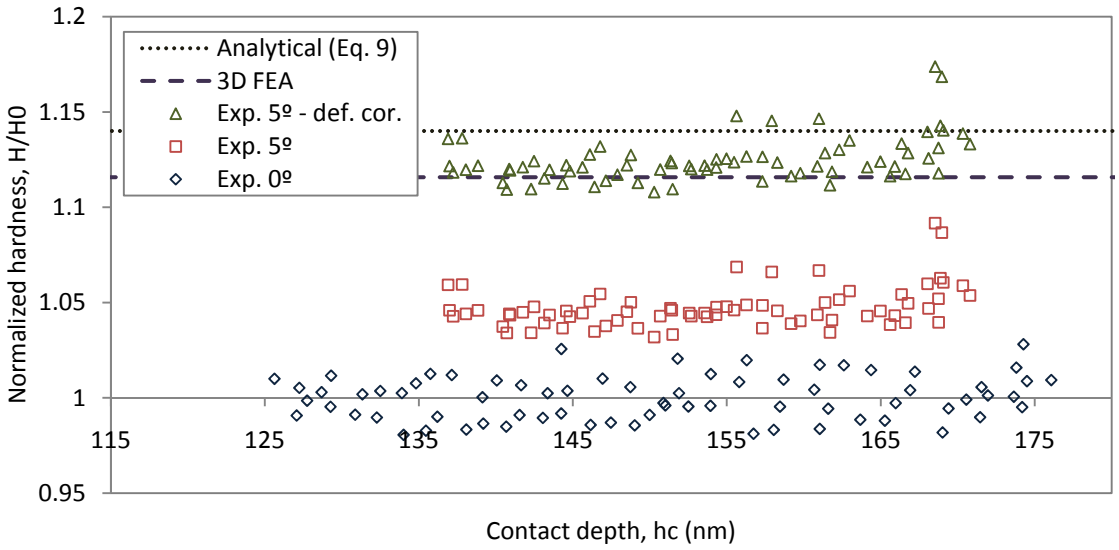

Figure 2.20. Normalized hardness versus contact depth for raw experimental results and those corrected for side deflection, 3D FEA of Berkovich indentation on fused silica, and the expected geometrical overestimation based on equation (2.9).

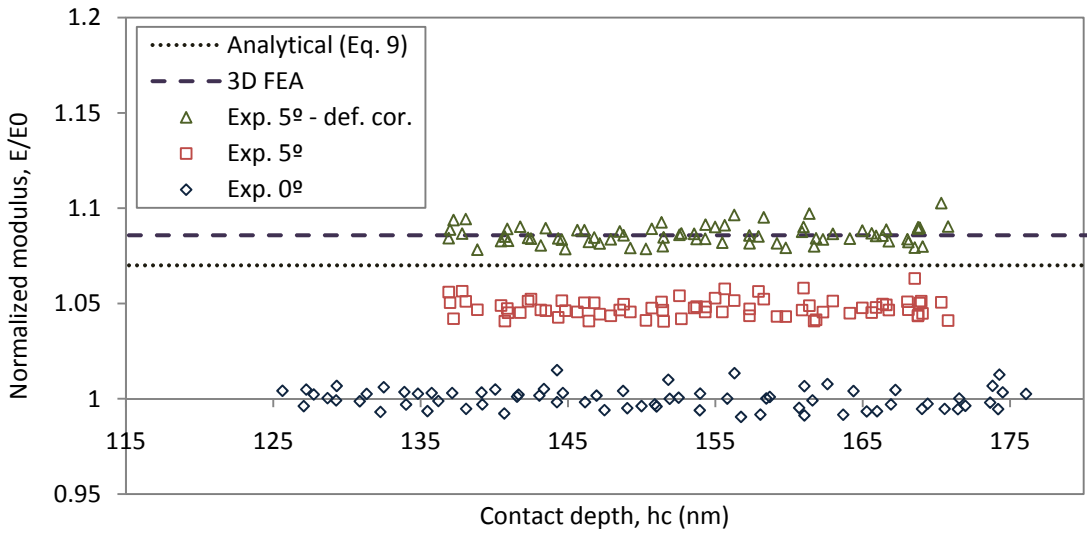

Figure 2.21. Normalized modulus versus contact depth for raw experimental results and those corrected for side deflection, 3D FEA of Berkovich indentation on fused silica, and the expected geometrical overestimation based on equation (2.9).

2.10 Discussion

As noted previously, several assumptions were made in deriving the geometric correction equations for contact area in the presence of specimen tilt. These include (i) the boundary of contact is along a plane (ii) this plane is parallel to the specimen surface and (iii) that the contact depth (measured along the indenter axis) is nearly constant independent of tilt (ε is constant), and can conceivably be obtained by the Oliver and Pharr method, equation (2.1). Given these, it is remarkable that the simplified approach to correct for specimen tilt enables measurements of the hardness and modulus that are very close to true values, within 2% and 0.5% for hardness and modulus respectively. Still, it is of interest to check the degree to which each of these assumptions is valid.

The boundary of the contact area was obtained approximately as the location of the contour line along which the contact pressure is equal to the yield stress. Since the gradient of contact pressure is very high near the boundary (as can be seen from Figure 2.12, 2.13), the actual value chosen to identify the boundary does not affect the contour location or contour shape significantly. Figure 2.22(a) shows the points along the boundary of the projected contact area for indentation into a sample tilted 5º, viewed along the axis of the indenter. Figure 2.22(b) shows the boundary of contact as viewed along the axis of tilt, from which it can be observed that the boundary lies along a plane for conical indentations. By fitting a trend line to the data in Figure 2.22(b), the equation of the plane is obtained to be y=0.082x-6.5 for E/σ_y=75 and y=0.081x+8.0 for E/σ_y=400, both with a goodness of fit R^2=0.999.

From the equations, the tilt angle of the plane which contains the boundary of contact is found to be 4.69º for E/σ_y=75 and 4.63º for E/σ_y=400 and the depth of contact, h_c= 90-6.5= 83.5nm and h_c= 90+8.0 = 98.0nm for E/σ_y=75 and E/σ_y=400 respectively. It is interesting to note that the ellipse in Figure 2.22(a) that seems to fit all the boundary points is actually the ellipse of the contact calculated from analytical equations given in previous work (Saket Kashani and Madhavan, 2007), using the above depth of contact and a tilt angle of 5º.

The boundary of contact for Berkovich indentation on fused silica is also shown in Figure 2.22. It is clear that this boundary is not planar, but to study the applicability of the geometrical correction method, a plane was fitted to the data which has the equation of y=0.098x-30.4. The plane angle is consequently 5.57º which is a close to the tilt angle. Therefore it is expected that the geometrical correction method improves the area estimation which consequently improves the estimation of hardness and modulus. Note that the obtained tilt angle is slightly affected by number of extracted points at each side.

In another approach to study the extent of the contact area, the last nodes in contact with conical indenter along the symmetry plane are plotted in Figure 2.23 for three different tilt angles for E/σ_y=75. From the fact that all three contact 'boundary' lines intersect the vertical axis at the same depth, it can be concluded that the contact depth, h_c, is constant, independent of tilt.

Since each of the three assumptions made in deriving the geometric correction equations are seem to be quite accurate, it is not surprising that, using the contact area given by equation (2.6) within equations (2.2) and (2.3), better estimates for the hardness and modulus are obtained, as shown in Figures 2.15 and 2.16. To implement this procedure as a correction for the effect of sample tilt, a geometrical correction procedure is proposed based on the derived area function to analytically correct the slight influence of sample tilt on contact area. The correction procedure can be simply applied by multiplying the usual area function of ideal indentation by $(1-\tan\theta^2\tan\eta^2)^{-1.5}$ for conical indentation and by $(1-3\tan^2\varphi\tan^2\eta-2\tan^3\varphi\tan^3\eta\cos 3\zeta)^{-1}$ for pyramidal indentation, where θ is semi-cone angle, φ is the pyramid face angle, η is the sample tilt angle, and ζ is the rotation angle. The two latter can be obtained from a post-test scan of the impression of indentation.

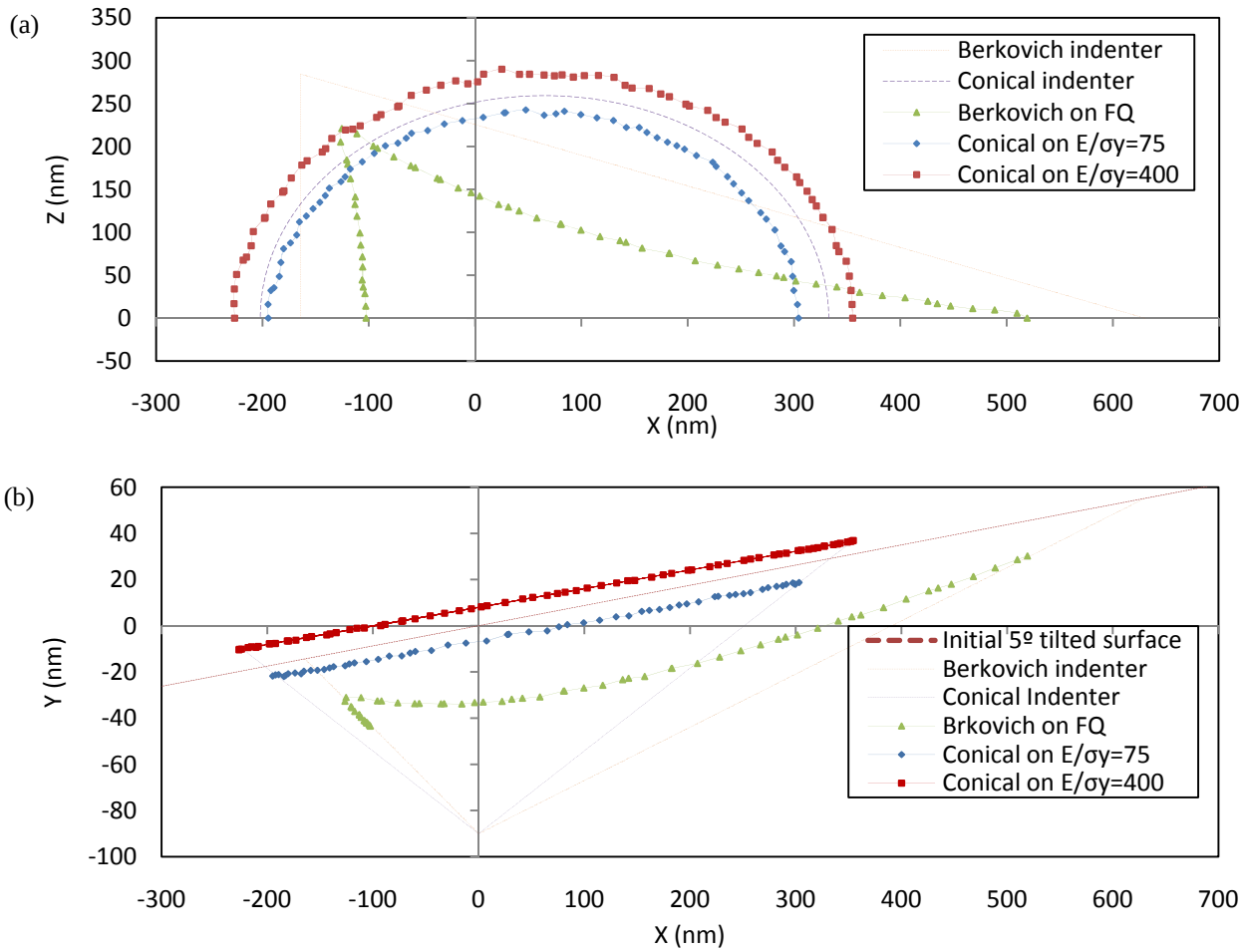

Figure 2.22. Approximate boundary of contact area for indentation into a sample tilted 5º, obtained as the contour of contact pressure equal to yield stress. (a) The view along the axis of the indenter which shows the boundary points of the projected contact area. (b) The view along the axis of tilt, showing that the boundary of contact lies along a plane for conical indentations.

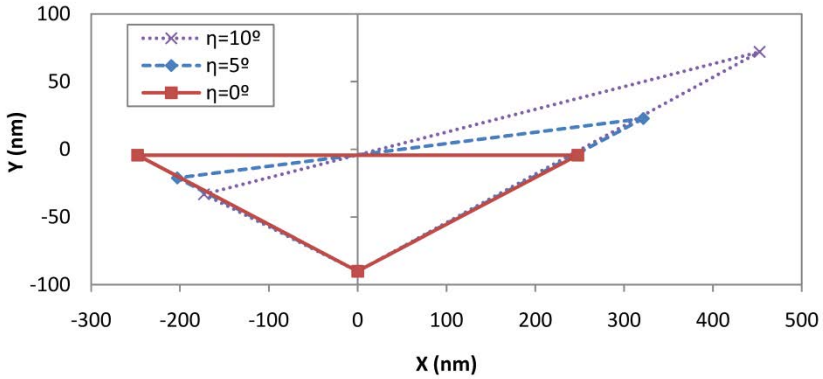

Figure 2.23. Side view of the contact area conical indentation for 0, 5, and 10 degrees of sample tilt from the last node in contact on the symmetry plane for $E/\sigma_y=75$.

The results presented in this work are very different from the ones presented in the work of Xu and Li (2007), except for the case of $\eta=0^o$. They reported the Oliver & Pharr method as being very sensitive to surface tilt. For instance, Xu and Li found that, for a constant penetration depth, the actual contact area of the indenter on a sample tilted five degrees was over two times that on a sample without tilt. This caused the standard O&P method to overestimate the hardness and modulus for a sample tilted by five degrees to be 2.3x and 1.5x the actual values, respectively.

Comparing the results of the simulations of the present work with the results of Xu and Li (2007), it is surmised that a different definition of the contact depth has likely caused the results reported in their paper to be dramatically different. This is inferred from the comparison of their projected area plots with ours, shown in Figures 2.24 and 2.25. The generalized definition of contact depth (h_c) is given earlier in this paper. The elliptical impressions for different amounts of surface tilt would look like those shown in Figures 2.24(a) and 2.25(a) if the contact depth is constant; however if the contact depth is measured as the penetration of the left edge of the indenter (h_1, rather than h_c), the elliptical impressions would look like that shown in Figures 2.24(b) and 2.25(b). This would explain their conclusion that using the standard O&P approach for obtaining the contact area results in underestimation of the projected contact area by up to 200% and consequently leads to significant overestimation of hardness and modulus.

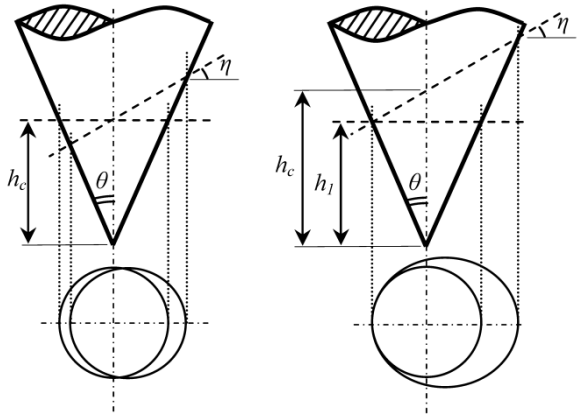

Figure 2.24. Comparison of the projected areas of contact for a conical indenter for tilted and un-tilted samples. (a) Keeping h_c constant which is the actual case in FEA and experimentation. (b) Keeping h_1 constant.

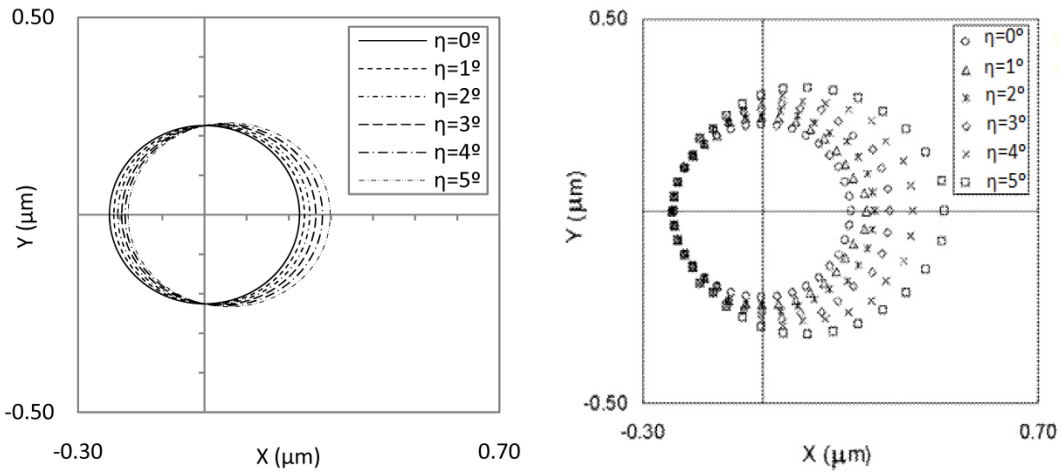

Figure 2.25. Projected contact areas for zero to 5 degrees of sample tilt. (a) Based on this work. (b) Presented in the work of Xu and Li (2007)

In their experimental work Xu and Li (2007) used a 60º conical indenter on three samples with tilt angles of 0, 1 and 3º; however, as shown in Figure 2.3, no significant error is expected for this indenter up to 3º tilt. They reported values of 72.0±0.6, 75.4±0.7 and 72.7±0.8 for modulus and 13.1±0.1, 13.5±0.3 and 14.3±0.6 for hardness, into samples tilted 0, 1, and 3º, respectively. The reason for lack of a clear trend and large variation is their indenter type.

2.11 Conclusions

3D FEA of conical nanoindentation of tilted samples shows that the boundary of contact lies along a plane that is nearly parallel to the surface of the tilted specimen. FEA also shows that the contact depth, measured as the distance between the indenter tip and the intersection of the axis of the indenter with the plane containing the boundary of contact, is independent of tilt angle. These observations justify the assumptions used to model the geometry of the area of contact during conical nanoindentation into tilted specimens. The derived analytical area function equation shows that the contact area increases faster with contact depth than that on non-tilted surfaces. A geometric correction procedure is proposed based on the derived area function to analytically correct the slight influence of sample tilt on contact area. The correction procedure can be simply applied by multiplying the usual area function of ideal indentation by $(1-\tan\theta^2\tan\eta^2)^{-1.5}$ for the case of conical indentation and by $(1-3\tan^2\varphi\tan^2\eta-2\tan^3\varphi\tan^3\eta\cos 3\zeta)^{-1}$ for pyramidal indentation, where θ is semi-cone angle, φ is the pyramid face angle, η is the sample tilt angle, and ζ is the rotation angle. The latter two parameters can be obtained from surface scans of the indentation impression. The accuracy of correction of the area function for tilted indentation is

verified by the results of 3D FEA of nanoindentation of tilted samples. If the sample tilt is not taken into account and the standard area function is used, the contact area would actually be underestimated, leading to overestimation of the hardness and modulus.

For indentation with a cone of semi-cone angle 70.3º, with area function equivalent to the Berkovich indenter, on a specimen tilted five degrees, the contact area is underestimated by 8%, leading to 8% overestimation in hardness and 4% overestimation in modulus; however, a previous study has reported approximately 100% underestimation of contact area, 130% overestimation of hardness, and 50% overestimation of elastic modulus (Xu and Li, 2007). Experimental studies of Berkovich indentation on tilted fused silica confirms that nanoindentation test is not as sensitive to tilt as reported in the previous work. It was found in experiments that compliance of the indenter holder in the horizontal direction causes the actual maximum penetration depth to be lower than that measured by the instrument, which compensates for the underestimation of contact area of tilted indenter, and leads to even less sensitivity of results to tilt angle.

2.12 References

Bobji, M. S. & S. K. Biswas (1999) Deconvolution of hardness from data obtained from nanoindentation of rough surfaces. *Journal of Materials Research,* 14**,** 2259-2268.

Cheng, C. M. & Y. T. Cheng (1997) On the initial unloading slope in indentation of elastic-plastic solids by an indenter with an axisymmetric smooth profile. *Applied Physics Letters,* 71**,** 2623-2625.

Ellis, J. D., S. T. Smith & R. J. Hocken (2008) Alignment uncertainties in ideal indentation styli. *Precision Engineering-Journal of the International Societies for Precision Engineering and Nanotechnology,* 32**,** 207-214.

Fischer-Cripps, A. C. 2004. *Nanoindentation*. New York: Springer.

Hay, J. C., A. Bolshakov & G. M. Pharr (1999) A critical examination of the fundamental relations used in the analysis of nanoindentation data. *Journal of Materials Research,* 14**,** 2296-2305.

ISO14577-2. 2002. International Standard Organization.

Oliver, W. C. & G. M. Pharr (1992) AN IMPROVED TECHNIQUE FOR DETERMINING HARDNESS AND ELASTIC-MODULUS USING LOAD AND DISPLACEMENT SENSING INDENTATION EXPERIMENTS. *Journal of Materials Research,* 7**,** 1564-1583.

Saket Kashani, M. & V. Madhavan. 2007. Study of damage distribution over primary shear zone in metal cutting process by nanoindentation. In *Materials Science and Technology Conference and Exhibition, MS and T'07 - "Exploring Structure, Processing, and Applications Across Multiple Materials Systems"*, 2609-2617. Detroit, MI, United states: Curran Associates Inc., 57 Morehouse Lane, Red Hook, NY 12571, United States.

Saket Kashani, M. & V. Madhavan. 2008. The effect of surface tilt on nanoindentation results. In *ASME International Mechanical Engineering Congress and Exposition, IMECE 2007*, 67-1071. Seattle, WA, United states: American Society of Mechanical Engineers, 3 Park Avenue, New York, NY 10016-5990, United States.

Shim, S., W. C. Oliver, and G. M. Pharr, (2007) A comparison of 3D finite element simulations for Berkovich and conical indentation of fused silica. *International Journal of Surface Science and Engineering*, 1**,** 259-273.

Xu, Z. H. & X. Li (2007) Effect of sample tilt on nanoindentation behavior of materials. *Philosophical Magazine*, 87**,** 2299-2312.

CHAPTER 3

ACCURACY OF FEA OF NANOINDENTATION

3.1 Abstract

The aim of this study is to control and account for various sources of error in finite element analysis of nanoindentation tests and obtain the true hardness of a material as a function of its plastic and elastic properties. Indentation of an elastic perfectly plastic solid by a rigid cone is modeled using axisymmetric first order quadrilateral elements in ABAQUS/Standard. In comparison with small errors arising from the convergence tolerance of the iterative solution process, errors due to discretization are found to be significant. Errors due to discretization arise from discrete jumps in contact area as each additional surface element comes into contact, and from higher indentation forces required for plastic deformation of larger elements near the boundary of contact. It is shown that a graded mesh, that permits self-similar growth of the displacement strain field with increase in indentation depth, can be used to keep the percentage error in hardness due to discretization constant at pre-set values. It is also shown that results obtained from different meshes with different error percentages can be extrapolated to determine the exact value of hardness that will be obtained with infinitesimally small elements. Using this approach, true hardness for a given set of elastoplastic properties commonly used for fused silica is determined to within 0.01%, 100 times more accurately than in earlier work. This extrapolation approach is also applied for calculation of accurate values of the ε correction factor used in the O&P method for estimation of contact depth and of the β correction factor in Sneddon's equation.

Keywords: FEA; indentation; nanoindentation; hardness; elastic modulus; stiffness; error; contact area

3.2 Introduction

Depth sensing nanoindentation has rapidly evolved into an important tool to study material properties over small length scales. The instrument directly measures the indentation force vs. displacement of the indenter during loading and unloading. The Oliver and Pharr method (Oliver and Pharr, 1992) is commonly used to estimate the contact depth, and consequently the contact area from the initial stiffness of the unloading curve. Using the contact area estimated by the O&P method, the Meyer hardness, the force per unit area of contact perpendicular to the

indentation force, can be calculated. The elastic modulus of the specimen that was indented can be estimated from Sneddon's elastic solution for axisymmetric indentation (Oliver and Pharr, 1992).

The true hardness of a material with given elastic and plastic properties is important in a variety of studies where it is important to capture the changes in hardness due to changes in inputs such as in the study of foams, coatings, thin films (Chen and Vlassak, 2001), surface roughness effects (Bobji and Biswas, 1999), tilt effects (Saket Kashani and Madhavan, 2008), etc. Increasingly, support from finite element simulations is used to understand and interpret experimental results. Due to the expense of 3D FEA, axisymmetric models with conical indenters having area functions equivalent to those of pyramidal indenters, are commonly used (Bolshakov et al., 1996). The advantage of finite element analysis is the true area of contact is known and can be used to determine the hardness. FEA can also be used to study the unloading process in detail and relate the stiffness of the unloading curve to the contact area and the elastic modulus.

Comprehensive studies of various aspects of nanoindentation using FEA are available in the literature (Bolshakov, 1996; Hay et al., 1999; Shim, 2007). Several studies have shown that a number of test parameters such as thin film properties (Chen and Vlassak, 2001), influence of residual stress (Bolshakov et al., 1996), Surface properties (Bobji and Biswas, 1999; Warren and Guo, 2006), surface tilt (Saket Kashani and Madhavan, 2008), damage, etc. may cause changes in true or apparent hardness measured by O&P method. If the effect of small changes in these test parameters needs to be determined accurately, it is important to take into consideration various sources of error in FEA and develop a simulation that can study the true effect of the changes without the error in the simulations interfering with the conclusions.

Thus far, the limits of accuracy of FEA of indentation have not been studied in great detail. Many studies show noise in the data obtained by FEA (Shim et al., 2007; Chen and Vlassak, 2001) yet report results to additional decimal places than warranted. In this paper, additional study of the various sources of error is carried out to establish the true hardness of fused silica with commonly used properties to an accuracy of 0.01%. Comparing this to other values reported in the literature for the same properties (Shim et al., 2007), it is found that the error in hardness reported by others can often be more than 1%.

3.3 Basic theory of nanoindentation

The basic equations in nanoindentation data processing are Oliver and Pharr's equation for estimation of contact depth, the area function, the Meyer hardness equation, Sneddon's equation for the reduced modulus, and the

equation for determining the sample's modulus from the reduced modulus, equations (3.1) to (3.5) respectively (Oliver and Pharr, 1992).

$$h_c = h_{max} - \varepsilon \frac{P_{max}}{S} \tag{3.1}$$

$$A_{c\,proj} = A\,(h_c) \tag{3.2}$$

$$H = \frac{P_{max}}{A_{c\,proj}} \tag{3.3}$$

$$E_r = \frac{1}{2\beta}\frac{\sqrt{\pi}}{\sqrt{A_{c\,proj}}} S \tag{3.4}$$

$$\frac{1}{E_r} = \frac{1-\nu_s^2}{E_s} + \frac{1-\nu_i^2}{E_i} \tag{3.5}$$

In these equations h_c is the contact depth, P_{max} is the maximum load, h_{max} is the maximum depth of penetration, S is the stiffness of unloading curve, A is the area function of the indenter, H is the Meyer hardness, $A_{c\,proj}$ is the projected contact area, E_r is the reduced modulus, E_s is the modulus of specimen, ν_s is the Poisson's ratio of specimen, E_i is the modulus of indenter, ν_i is the Poisson's ratio of indenter, and β and ε are constants that depend primarily on the geometry of the indenter.

3.4 Errors in FEA of nanoindentation

Prchlik (2004) carried out a sensitivity analysis of hardness and elastic modulus evaluated from indentation load-displacement records (by the Oliver and Pharr method) to relative errors in force and penetration depth. This was done by differentiating the relations used in the O&P method. Assuming constant relative error over the entire depth and load ranges, the sensitivity relations for sharp indenters simplify to equations (3.6) and (3.7).

$$\frac{\Delta H}{H} = -2\left(\frac{\Delta h}{h}\right) + \left(\frac{\Delta F}{F}\right) \tag{3.6}$$

$$\frac{\Delta E_r}{E_r} = -2\left(\frac{\Delta h}{h}\right) + \left(\frac{\Delta F}{F}\right) \tag{3.7}$$

While errors in measurement of contact height and force would lead to uncertainty in hardness and modulus measurements as shown above, for both experiment and FEA, the reasons for error in contact height and force are different in FEA than in experiments. Assuming that the test is modeled accurately and the properties and boundary conditions are assigned appropriately, there are still some sources of error that affect the contact height and indentation force.

a) *Contact area error due to discretization.* While the height of penetration of the indenter (h_{max} in Figure 3.1 and 3.2) increases smoothly and continuously, the contact height, h_c, exhibits discontinuities, with the height of the steps being dependent on the deformed size of the surface element and the indenter angle θ. Using the last node in contact to determine the contact height, the mesh size at the boundary of contact (L_e) is related to the granularity of contact height determination by $\Delta h_c = L_e \cos\theta$.

The relative error in projected contact area of any self-similar indenter for which $A \propto h^2$ (such as ideal cone, Berkovich and Vickers) can be determined as $\Delta A/A = 2\,\Delta h/h$ (Prchlik, 2004). The relative error in projected contact area can be determined as a function of element size, contact radius, and semi-cone angle of the cone (equation (3.8)).

$$\frac{\Delta A}{A} = 2\frac{\Delta h}{h} = 2\frac{L_e \cos\theta}{h_c} = 2\frac{\Delta R}{R} = 2\frac{R_e}{R_c} = 2\frac{L_e \sin\theta}{R_c} \tag{3.8}$$

This error can be alleviated by controlling the solution step size and recording the force data with high resolution around the point of discontinuous change in contact area, so that the maximum force prior to a jump in contact area can be detected. If the maximum force prior to the jump in contact area can be accurately determined, the hardness (the maximum force a certain projected area of contact can support) can be determined accurately.

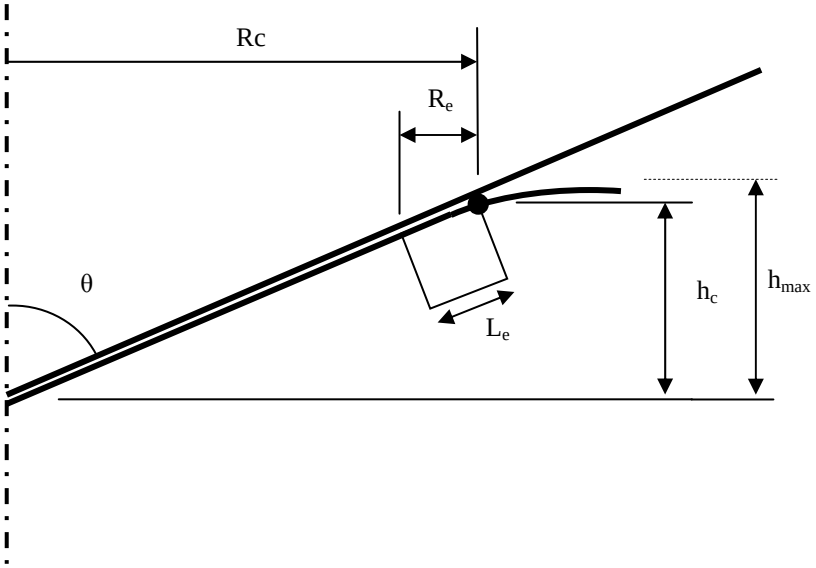

Figure 3.1. Schematic view of last element in contact in conical indentation

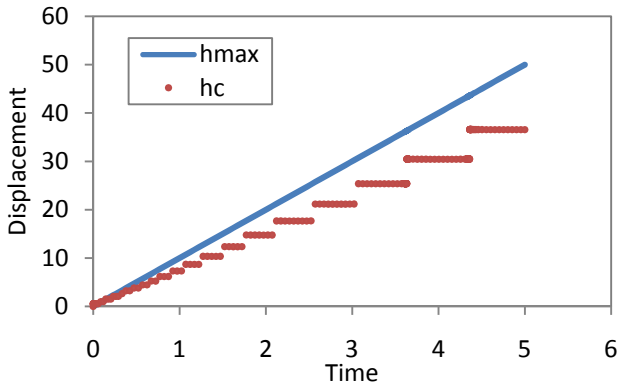

Figure 3.2. The height of penetration of the indenter, h_{max}, increases smoothly and continuously while the contact height, h_c, exhibits discontinuities, with the height of the steps being dependent on the deformed size of the surface element and the indenter angle θ.

b) *Error in force due to discretization.* This is another source of error in FEA of nanoindentation test, which arises from approximating the load carrying capacity of a continuum by that of a discretization of the continuum. This error can usually be reduced by refining the mesh in the regions where stress or strain gradients are relatively high, typically around the boundary of contact. The effect of a coarse mesh can be observed by noting the jumps in stress across elements. This error in force will cause the maximum force supported by the contact area (prior to the jump in contact height) to be typically higher than that of the continuum. Additionally, while the contact area error is only a result of the mesh size at the contact surface, the error in force due to the discretization is affected by the mesh both at and below the boundary of contact.

c) *Convergence tolerance.* The nonlinear response of the elastoplastic continuum necessitates iterative solution of the equilibrium equation in the implicit integral solution procedure used in ABAQUS/Standard. Convergence of the iteration can be judged using a variety of criteria. The criteria as well as the tolerances can be adjusted in ABAQUS simulations. There are numerous parameters that can be adjusted, but most of them rarely need to be reset from their default values according to ABAQUS theory manual. The convergence criterion for the ratio of the largest residual force to the average internal force for convergence (default 0.005) and convergence criterion for the ratio of the largest solution correction to the largest corresponding incremental solution value (default 0.01) were both reduced by a factor of 1E-16. In the case of this quasi-static simulation this just resulted in a slightly smaller force noise at the contact nodes, but much longer simulation time because of smaller step sizes for these simulations.

d) *Number of significant digits.* During the course of data processing it was noticed that the number of significant digits exported from ABAQUS can have significant influence on the noise level of calculated parameters like hardness and modulus. The modulus is especially sensitive to this because it is a function of slope of unloading curve, for very small steps, small round-off error in displacement, force and contact area values can add up and result in significant noise in final modulus values. Therefore it is recommended to use the maximum number of digits possible to minimize the effect of rounding the values exported from ABAQUS.

3.5 Finite Element Model

Using the dependence of the jumps in contact area on the mesh size described in the previous section, a mesh can be designed to control the maximum error from area measurement. To keep the maximum area measurement error constant, the element size at any given contact radius can be determined from equation (3.7). Therefore the contact surface of the specimen should be meshed with a linear gradient. The simplified form of the relation $L_e = C\ R_c$ means that the element size should increase with increase of the radius. Using the same relation to mesh the interior region also, self-similar mesh having a constant discretization error can be realized.

Four different values for contact area measurement error were considered in this study: 31.6%, 10%, 3.16%, and 1% which means the ratio $\Delta R/\ R$ should be 0.158, 0.05, 0.0158, and 0.005, respectively. For a cone with semi-cone angle of 70.3º, the specimen is meshed to follow this rule between radius of 10nm and 500nm. The indenter is loaded in displacement control mode into the material for 50nm. The specimen which is shown in Figure 3.3 was considered as a 200μm radius semi-sphere to minimize the effect of boundary conditions.

Figure 3.4(a) shows the close up of the controlled gradient mesh between 10 and 500nm for the mesh designed for 10% error and Figure 3.4(b) shows the initial 10nm. The element sizes at radius of 10 and 500nm and the number of elements on the surface between these points and also the number of elements for the whole model are listed for all four meshes in Table 3.1. It was verified that the mesh for the initial 10nm does not affect the results, by running similar simulations with only changing the mesh in that region. Four-node axisymmetric linear full integration elements (CAX4) were used for meshing the models.

The indenter was modeled as an analytical rigid surface, representing a perfect conical indenter with a semi-cone angle of 70.3º which is a cone with area function equivalent to that of the Berkovich indenter. The material properties of fused silica used in this study were the same as reported by Shim et al. (2007): elastic-perfectly-plastic material with a yield strength of 5.5 GPa, elastic modulus of 72GPa, and Poisson's ratio of 0.17.

Frictionless contact was used between indenter and the specimen surface. Even though frictionless contact will increase the chance of radial displacement of the nodes and thus the deviation from the estimated error, it has been used in order to allow comparison of results with other works in the literature (Shim et al., 2007). On the other hand, this deviation makes the design a conservative one since the elements can move outward which reduces the radial width of the elements. Therefore, for the case of the mesh designed for 1% error in contact area, the maximum expected error in contact area is 1%, independent of friction value. It is important to remember that the error that is controlled here is the range of variation in results due to discrete jumps in contact area, not the deviation from true indentation results, as will be discussed in more detail later.

TABLE 3.1

SIZE AND NUMBER OF ELEMENTS FOR FOUR DIFFERENT MESHES DESIGNED TO RESULT IN 31.6%, 10%, 3.16%, AND 1% ERROR IN HARDNESS

Mesh error		Element size (nm)		Number of elements on the surface between R=10nm and R=500nm	Number of elements in the whole model
$\frac{\Delta A}{A}$	$\frac{\Delta R}{R}$	@ R=10 nm	@ R=500 nm		
1%	0.005	0.05	2.66	736	17754
3.16%	0.0158	0.17	8.39	232	6358
10%	0.05	0.53	26.55	73	1770
31.6%	0.158	1.68	83.91	22	825

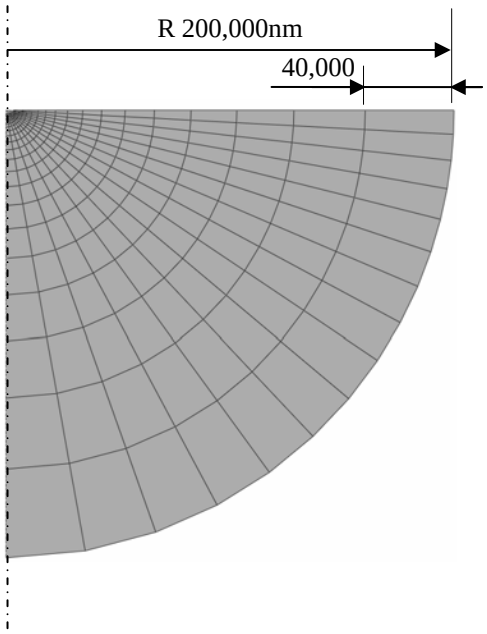

Figure 3.1. Hemispherical axisymmetric model for 10% jumps in contact area.

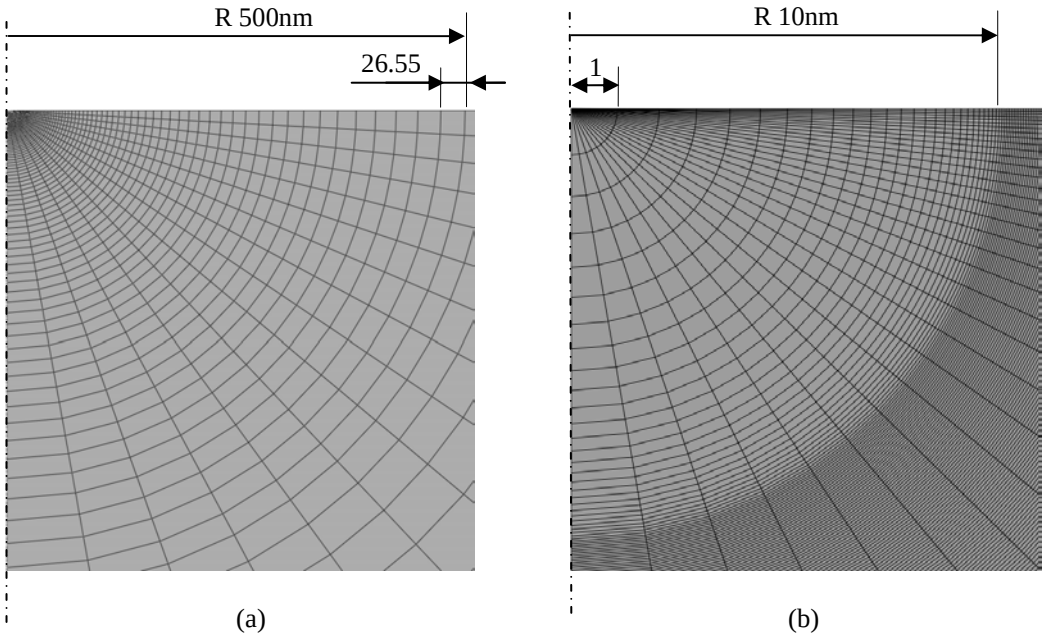

Figure 3.2. Detail of the mesh. (a) Close up at the contact region which is meshed to have less than 1% jumps in contact area, (b) Initial 10nm with relatively coarse mesh.

Figure 3.5 shows the distribution of von Mises stress at the maximum penetration for each of the four meshes. The differences in smoothness of stress contours can be observed, which will be shown to cause the discretization error in final results. Closer views of contours of von Mises stress near the end of contact are also shown in Figure 3.5. Note that for fused silica, the plastic zone is nearly hemispherical with a radius nearly equal to

the radius of contact. The equivalent plastic strain distributions beneath the indenter are also shown in Figure 3.6 for all four cases.

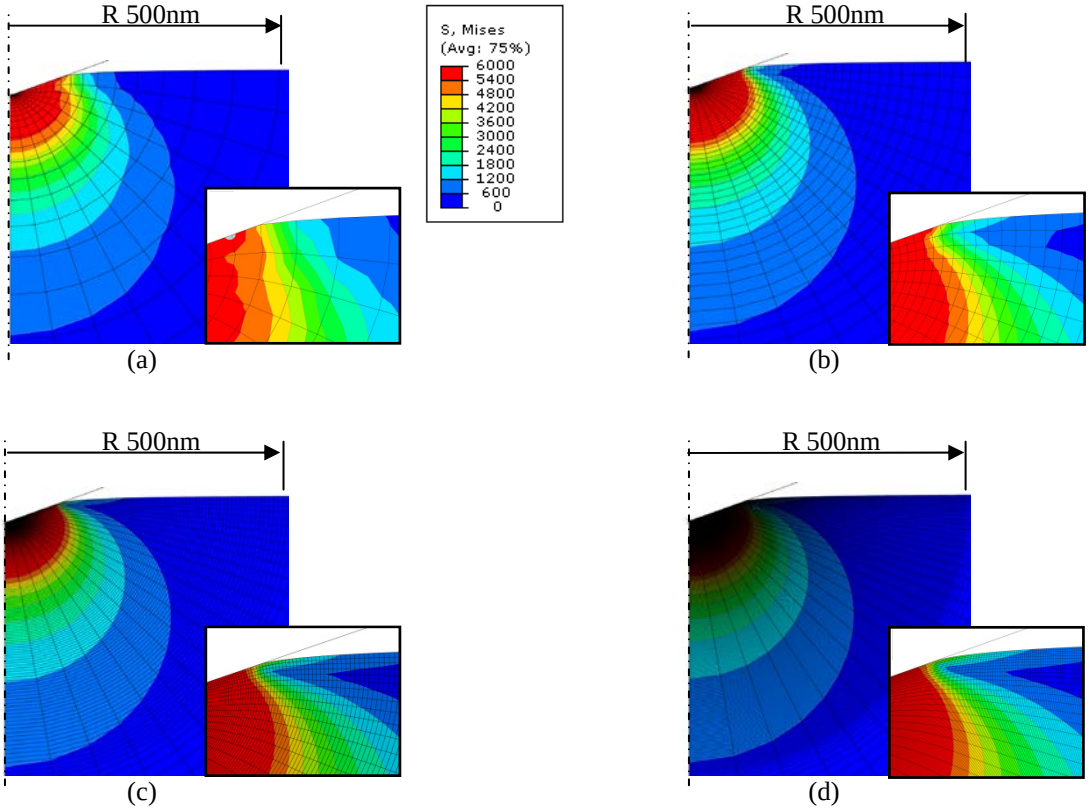

Figure 3.3. Distribution of von Mises stress at maximum depth of penetration, h_{max}=50nm, with a close-up of the nodes in contact for the case of (a) 31.6% Mesh, (b) 10% Mesh, (c) 3.16% Mesh, and (d) 1% Mesh.

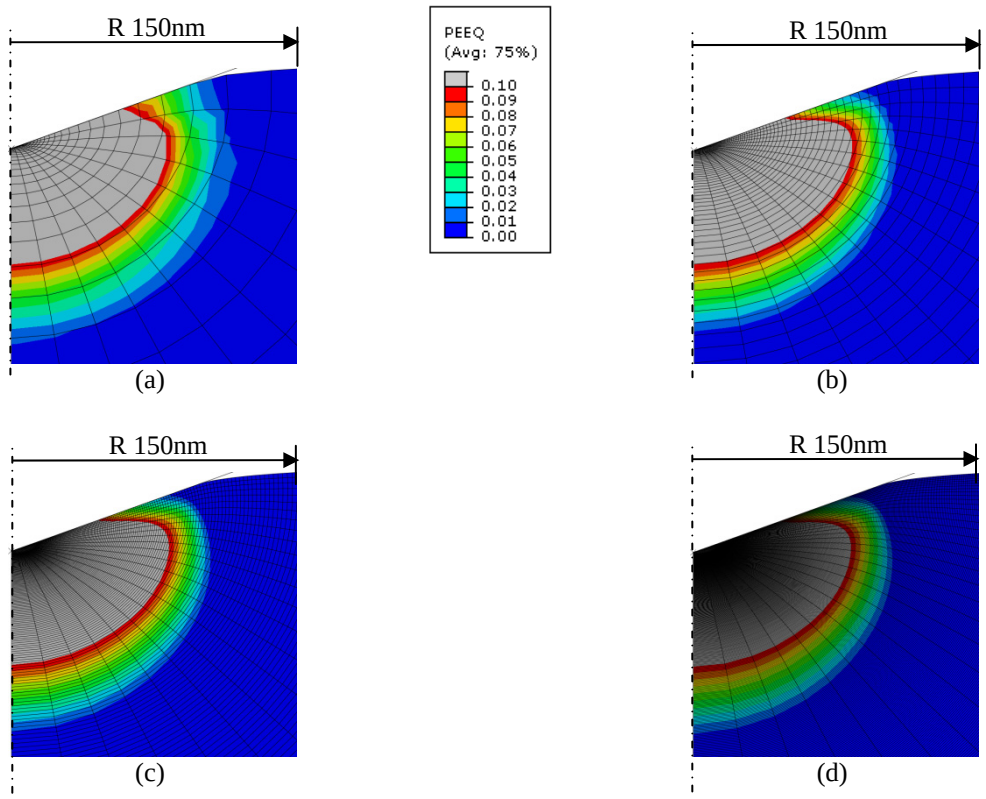

Figure 3.4. Distribution of equivalent plastic strain at maximum depth of penetration for the case of (a) 31.6% Mesh, (b) 10% Mesh, (c) 3.16% Mesh, and (d) 1% Mesh.

The variation of stress in y direction, σ_{yy}, as a function of radius is shown in Figure 3.7 for the points on the surface of the specimen at the maximum penetration of 50nm. It can be seen that the coarser the mesh is, the larger is the deviation from expected value. The stress distribution plots around the last point in contact show that the gradient of stress in this region is not captured properly. Figure 3.8 shows the gradient of σ_{yy} of the points on the surface of the specimen as a function of radius at the maximum penetration of 50nm. This figure clearly shows that finer mesh captures the high gradient of stress in this region while the coarse mesh is not capable of doing so. It is also of value to look at the distribution of equivalent plastic strain on the surface of the specimen as shown in Figure 3.9. It can be seen that the plastic strain required for deforming a fine mesh is smaller than that required for deforming a coarse mesh.

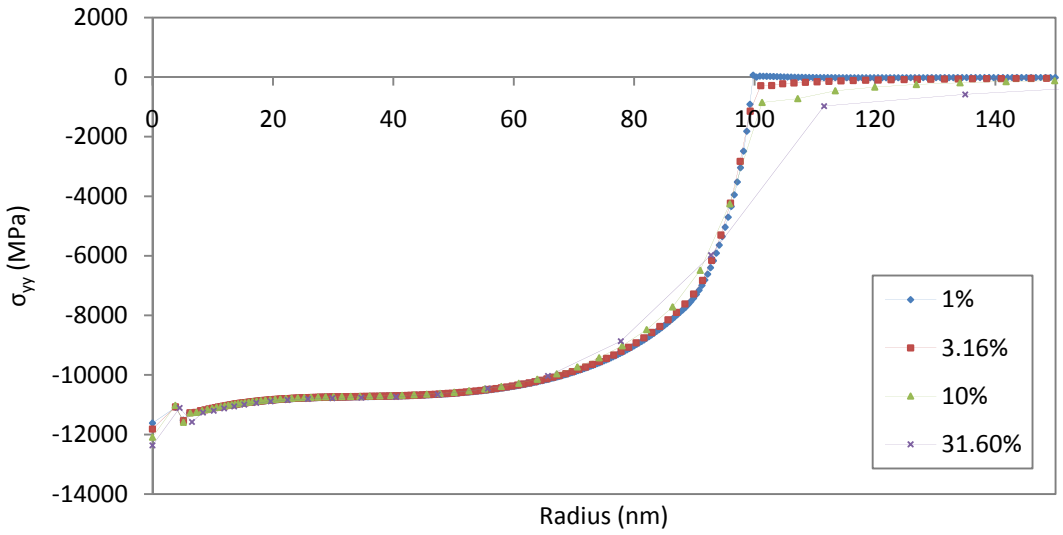

Figure 3.7. The variation of stress in y direction, σ_{yy}, at the maximum penetration of 50nm for the points on the surface of the specimen as a function of radius.

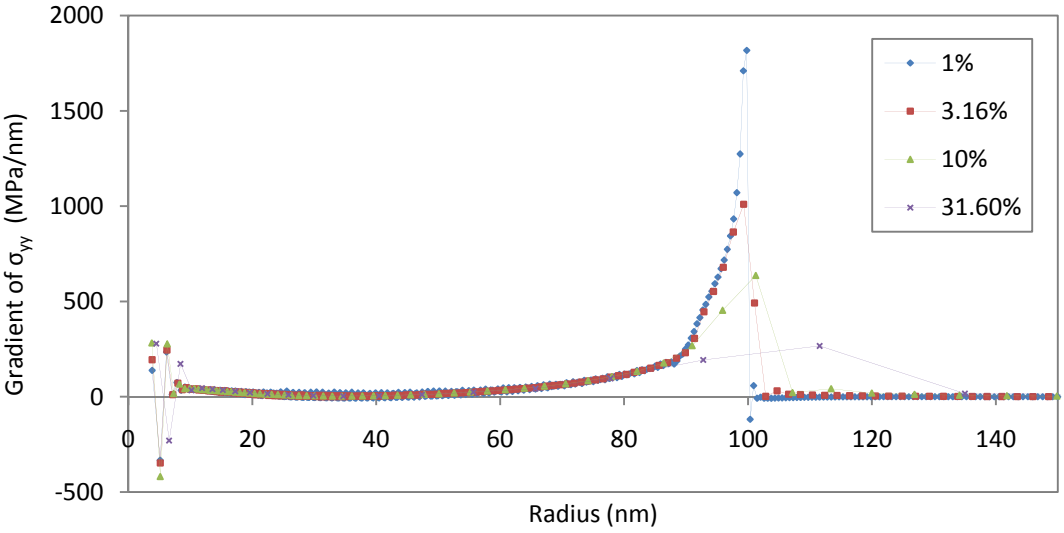

Figure 3.8. The variation of the gradient of σ_{yy} at the maximum penetration of 50nm for the points on the surface of the specimen as a function of radius. Note that the plastic strain required for deforming a fine mesh is smaller than that required for deforming a coarse mesh.

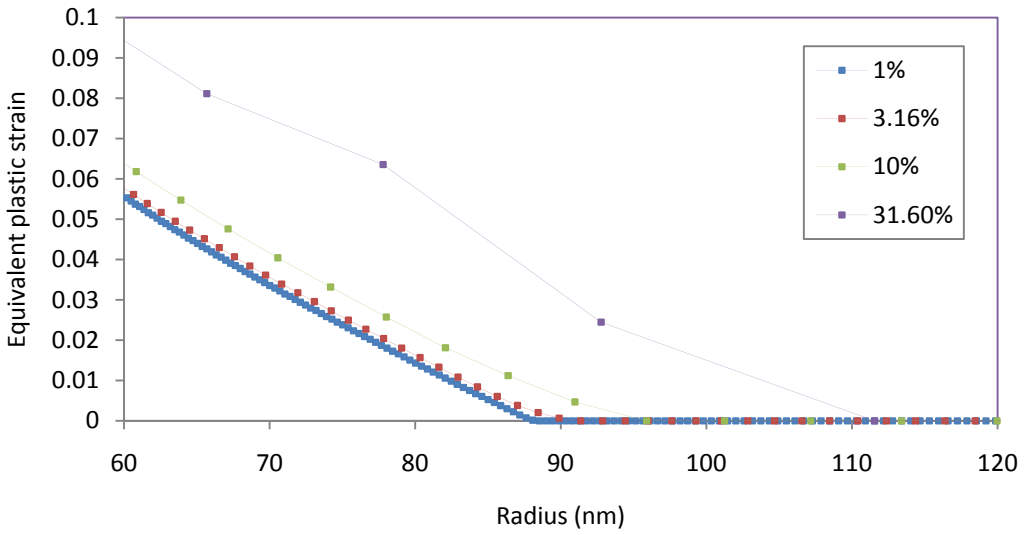

Figure 3.9. Equivalent plastic strain at the maximum penetration of 50nm for points on the surface of the specimen, around the last point in contact. Note that the amount of plastic strain is higher for coarser mesh which explains the increase of the hardness for coarser mesh.

3.6 Hardness

"The mean contact pressure, when determined under conditions of a fully developed plastic zone, is usually defined as the indentation hardness of the specimen material"(Fischer-Cripps, 2004). For self-similar indentation by sharp conical and pyramidal indenters, the mean contact pressure for any given material is expected to be constant, independent of the indentation depth. For each increment of load, the projected contact area increases by an equal amount. For determination of hardness, the load and the projected contact area that bears that load should be measured.

If the loading step size is controlled to be fine enough, it can be observed (see Figure 3.10) that the force versus displacement curve is smooth, but there is a stepwise increase in contact area whenever a new node comes into contact with the indenter. Therefore, the hardness value will have sudden drops as each new node comes into contact (see Figure 3.11). In the simulations reported in this work, the value of these maximums and minimums are expected to be a constant value, since the mesh is designed to have constant $\Delta A_c/A_c$. In order to determine these maximum and minimum values with a reasonable resolution and computational expense, the simulations were performed twice. First, they were simulated with maximum step size which recorded data at every 0.5nm. Then for a small time interval identified from the results, the simulations were rerun with higher time resolution around the two

last nodes coming into contact. At this second run, the maximum step size was set to record data every 0.005nm to identify the maximum and minimum hardness values more precisely.

In the case of experimental hardness measurement by static nanoindentation, the load is measured continuously during the loading segment, but the projected contact area is only determined at the maximum load, since the unloading curve is required to estimate the contact depth. Therefore only one value for hardness can be obtained from each indentation. However, in FEM simulations of static nanoindentation tests, the contact area can be continuously recorded. From the force and contact area obtained from nanoindentation simulation with the four designed meshes, continuous estimation of the hardness values are obtained, as shown in Figure 3.11 and Figure 3.12.

As seen before, a very fine mesh along the contact surface can reduce discretization errors and improve the resolution of contact area measurement. However, no matter how small the elements are, the error in determination of contact area has a finite value due to the discrete steps by which it increases. In ABAQUS, the area corresponding to one-half of the elements on both sides of the node is added to the contact area (CAREA) which results in a sudden drop in hardness. As can be seen in Figures 3.11 and 3.12, the hardness drops when the indenter comes into contact with a new node. The amount of decrease in hardness is a function of element size at the point of contact, contact radius and indenter's shape as shown in equation (3.8). Beyond this, the hardness increases as the indenter pushes into the material until the next node comes into contact. This occurs when the current contact area cannot support the applied load and additional area is required.

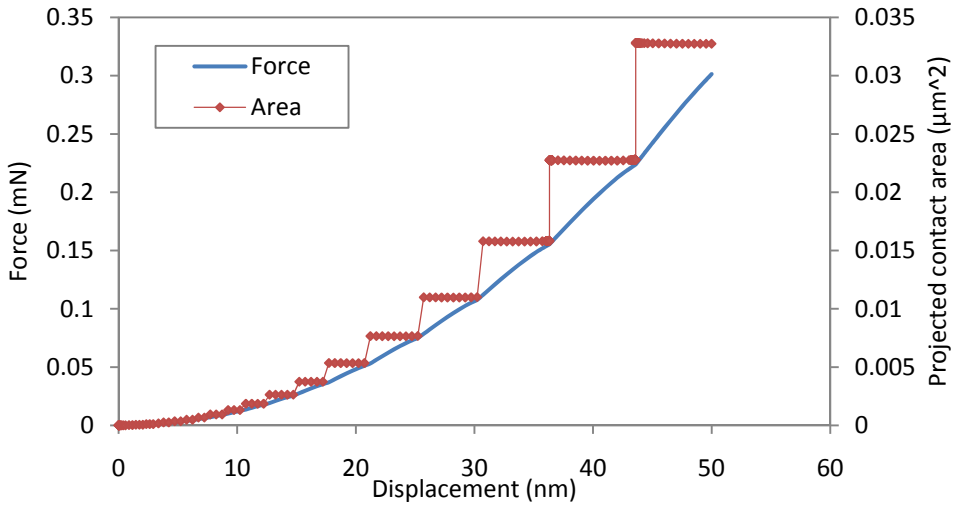

Figure 3.10. Force and projected contact area as a function of displacement. Note that the force curve is smooth, but there is a stepwise increase in contact area whenever a new node comes into contact with the indenter.

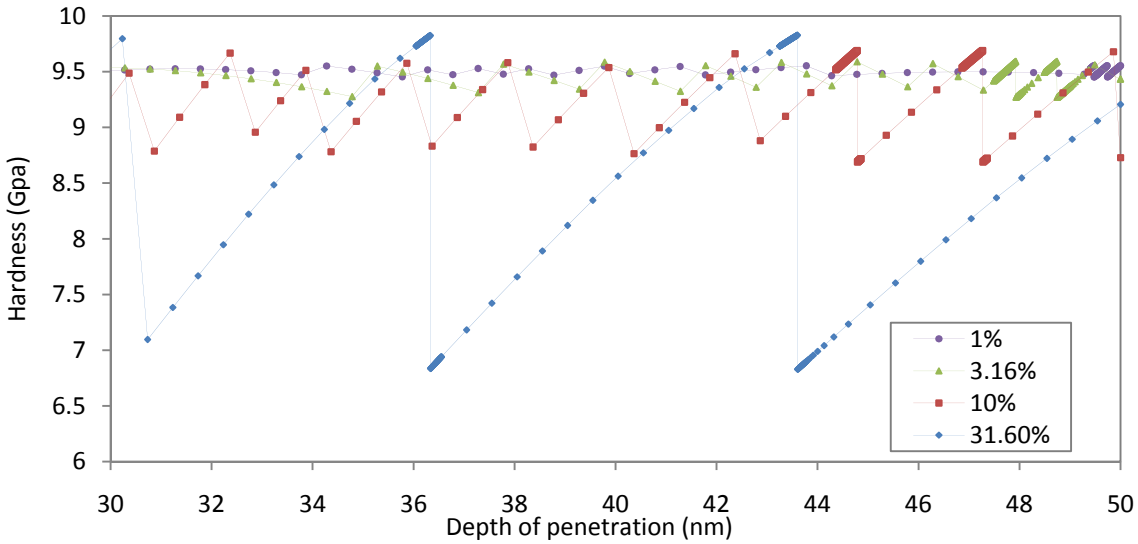

Figure 3.11. Hardness values for 31.6%, 10%, 3.16%, and 1% meshes.

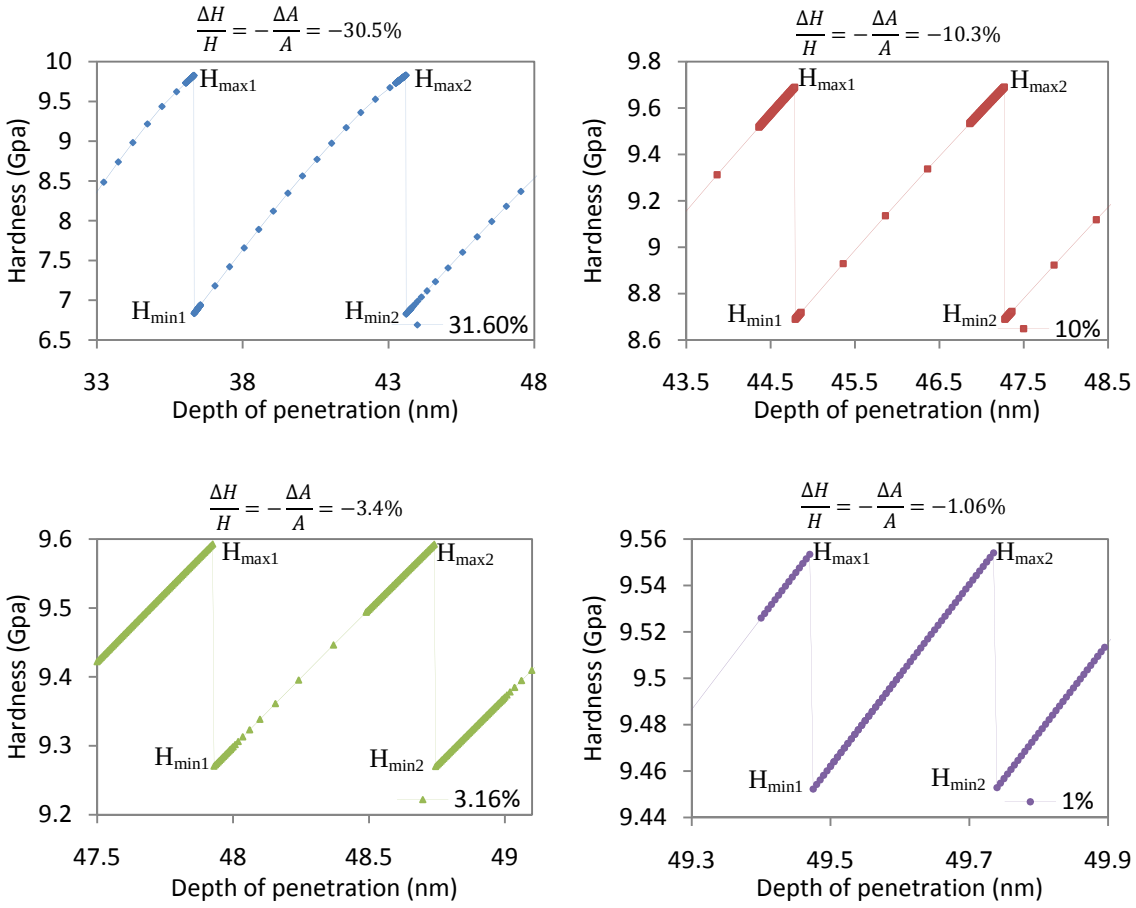

Figure 3.12. Separate graphs for Hardness values of 31.6%, 10%, 3.16%, and 1% meshes to show the similar behavior of all meshes.

The hardness vs. displacement curve is not differentiable at the point that a new node comes into contact. The left limit gives the maximum hardness and the right limit gives the minimum hardness for the mesh. The limits can be determined accurately by controlling the step size of the recorded increments in displacement to be very fine (0.005nm in this case). Since the mesh is designed to be self similar and have constant error over a wide range of penetration, successive maximums and minimums are the same, as shown in Figure 3.12, and calculating them only next to one node will be sufficient. The values of the maximum and minimum hardness obtained for the four meshes are listed in Table 3.2. Looking at results closely, reveals that the 0.005nm step sizes has resulted in consistent values of H_{max} to within 2.5MPa. Consistency of the results is a reflection of the self similarity of the mesh, since the hardness values are independent of the depth of penetration.

The actual maximum error in hardness due to the jumps in contact area can be calculated for each of the four meshes by considering the maximum hardness of that mesh as the reference $(H_{min}-H_{max})/H_{max}$. These maximum errors which are listed in Table 3.2 match very well with the expected error that the mesh was designed for. The slight differences arise from the fact that in typical approach the last node in contact is considered as the boundary of contact; however, the contact area increase due to a node coming into contact, given by the CAREA output variable in ABAQUS, includes half the area of elements on both sides of the node. There is also a slight difference between the desired constant gradient in mesh size required and the way that bias meshing works in ABAQUS/CAE.

As can be seen in Figure 3.13, the maximum hardness is not affected by the mesh as much as the minimum values are. The maximum hardness value is the best measure of hardness obtained from a given mesh since at that point, the contact area measurement error is minimum. This is a valid measure, since hardness is the maximum contact pressure that a given contact area can support.

TABLE 3.2

MAXIMUM AND MINIMUM HARDNESS VALUES (GPA) FOR 31.6%, 10%, 3.16%, AND 1% MESHES

Model	31.6% Mesh	10% Mesh	3.16% Mesh	1% Mesh
H_{max1}	9.8257	9.6897	9.5927	9.5534
H_{max2}	9.8282	9.6902	9.5924	9.5540
H_{min1}	6.8350	8.6896	9.2705	9.4522
H_{min2}	6.8280	8.6897	9.2701	9.4528
Max of maxes	9.8282	9.6902	9.5927	9.5540
Min of mins	6.8280	8.6896	9.2701	9.4522
(Min/Max)-1	-30.5%	-10.3%	-3.4%	-1.06%

Comparing H_{max} obtained with different meshes, it can be observed that H_{max} increases slightly as the mesh size increases. This is caused by the fact that a larger mesh size cannot track large gradients in stress, strain and shape of the surface that occur near the contact boundary. The actual hardness value of a material with given elastic and plastic properties would be obtained if one could mesh the specimen for 0% error, which will eliminate both contact area error and discretization error. As this is impossible, we introduce a new scheme for extrapolating the hardness values for different meshes (shown in Figure 3.9) to 0% error. It can be seen that second order equations fit the trends in maximum and minimum values well. It can also be seen that both second order fit predict the same value for the hardness for a 0% error mesh. Another approach, using two lines to fit to the maximum and minimum values from only the two finest meshes (Figure 3.14), also indicates the same value of hardness for zero error mesh. The lines intersect the zero percent error axis at almost same points: 9.5361 GPa and 9.5367 GPa. Therefore, it can be concluded that 9.536 GPa is the best estimate of true hardness value for this material after virtually removing contact area and discretization errors. This value is used to determine the actual amount of error obtained with H_{max} and H_{min} of each of the designed meshes which are listed in Table 3.3. Shim et al. (2005) reported a hardness value of 9.24 GPa from axisymmetric FEA simulations with the same material properties used here.

The constraint factor (C), which is the ratio of hardness to yield stress, can be precisely estimated to be 1.734 for this material since the true hardness value has been calculated very precisely. The estimate for this value based on the expanding cavity model proposed by Johnson (Johnson, 1985) and Sakai's Maxwellian model (Sakai, 2009) is 1.591.

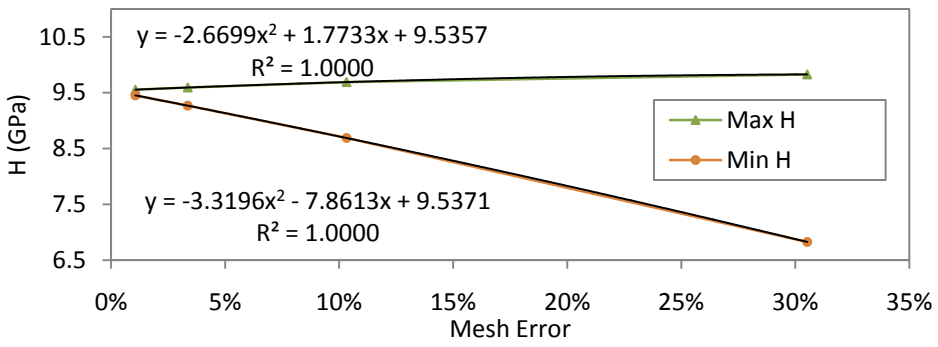

Figure 3.13. Minimum and maximum hardness values for 31.6%, 10%, 3.16%, and 1% meshes.

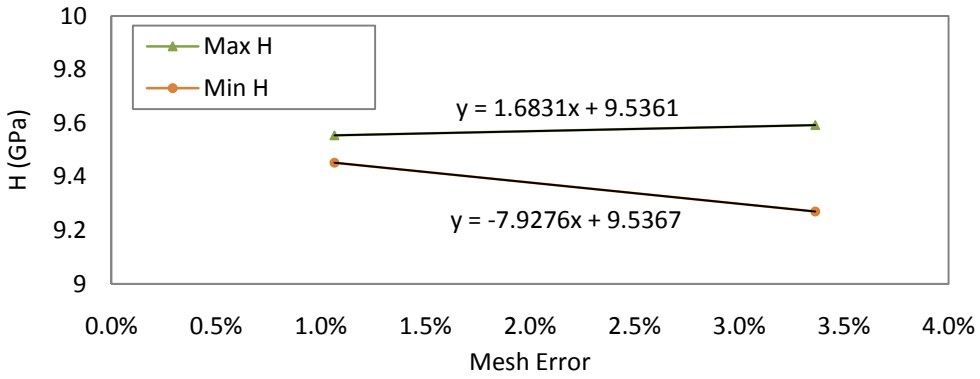

Figure 3.14. Minimum and maximum hardness values for 3.16% and 1% meshes. Linear extrapolation of both maximum values and minimum values intersects at the same point on zero error axis.

TABLE 3.3

The actual error of H_{max} and H_{min} of each of the designed meshes with respect to the hardness at virtually zero error (H_0=9.536GPa).

Error / Model	31.6% Mesh	10% Mesh	3.16% Mesh	1% Mesh
$\frac{H_{min}}{H_0} - 1$	3.1%	1.6%	0.6%	0.2%
$\frac{H_{max}}{H_0} - 1$	-28.4%	-8.9%	-2.8%	-0.9%

3.7 Elastic Modulus

While the actual elastic modulus used in the simulation is known, it is of interest to study the various sources of error in measurement of the elastic modulus from FEA results, using Sneddon's equation, which relates the modulus to the unloading stiffness and the projected contact area. The simulations showed that at the beginning of unloading and where a new node comes into contact, the calculated modulus does not result in stable value. It has been verified by some simulations that this noise can be reduced by tightening the convergence tolerances; however this is very expensive since the iterations required for convergence become very high. Without changing the default convergence tolerance, it is recommended to start unloading right before a new node comes into contact. As previously noted at this point the maximum force can be supported by the contact area is correctly reported and the slope of the force vs. the unloading displacement is also likely to be captured accurately. Additionally, this also permits the unloading slope to be determined for a reasonably long period before the perturbations due to the last node moving out of contact. Interestingly, it is noted that the contact area obtained from FEA increases during the

unloading process due to radial displacement of nodes before contact with the last node is lost. Even more interestingly, it is found that the unloading slope (the stiffness) increases slightly as unloading progresses (Figure 3.15), and the ratio of unloading stiffness to the square root of the contact area (the estimate for the elastic modulus) remains constant during unloading.

Getting the contact area directly from ABAQUS and assuming $\beta=1$, only the stiffness is required to calculate specimen's elastic modulus from equations (3.4) and (3.5). The stiffness is obtained from the local instantaneous slope of the load-displacement curve during elastic unloading. Specimen's elastic modulus calculated using instantaneous value of stiffness and contact area are shown in Figure 3.16 for 0.5nm of unloading with step size of 0.005nm. It can be seen that the elastic modulus calculated remains constant throughout, for each of the four designed meshes. This is correlated with the purely elastic deformation that takes place. Perturbations observed for the 1% mesh of about 0.4nm of unloading area is due to the step change in contact area when the node at the outer radius of contact moves out of contact. The average value over the initial plateau for each of the meshes is listed in Table 3.3 and graphed in Figure 3.17. A straight line is observed to fit the data very well and indicates that the elastic modulus calculated form a FEA model with zero mesh error would be equal to 77.742GPa with $\beta=1$. Shim et al. (2007) reported modulus value of 76.75 GPa from axisymmetric FEA simulation of the same elastic-perfectly-plastic model of fused silica with $\beta=1$.

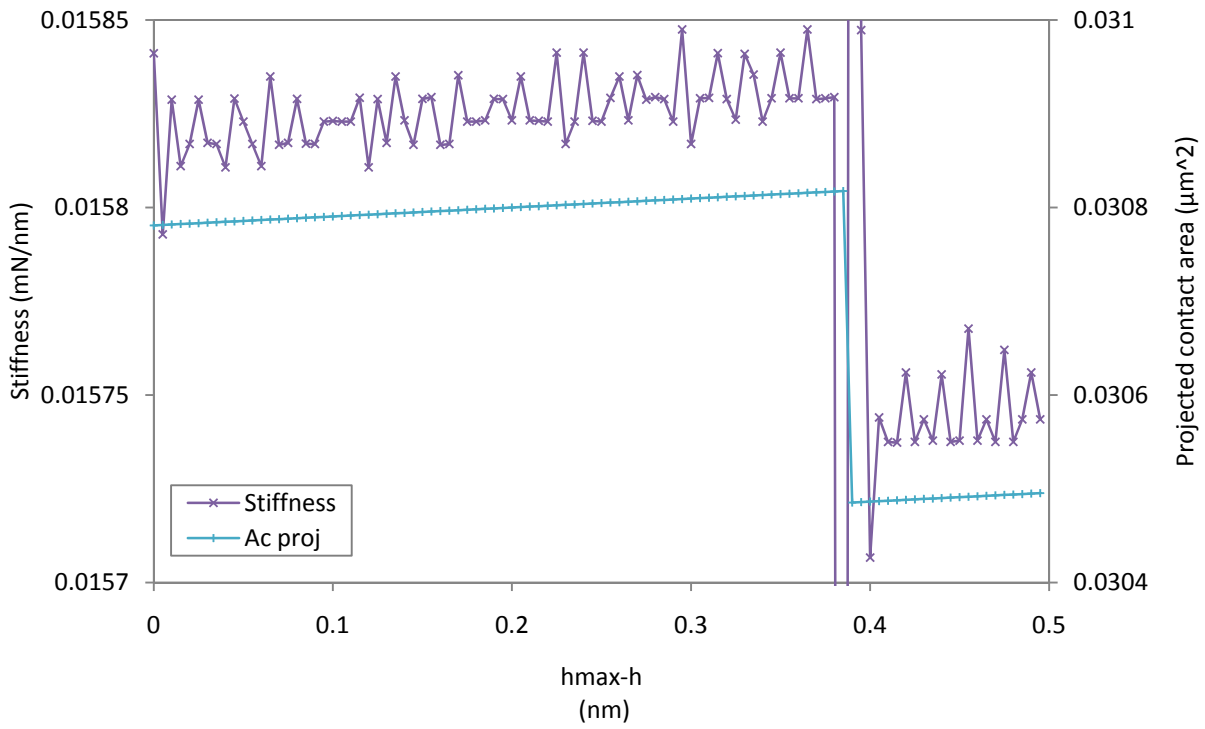

Figure 3.15. The instantaneous value of stiffness of unloading curve and projected contact area for the 1% mesh. Note that the contact area and also instantaneous stiffness of the unloading curve increases during the unloading process due to radial displacement of nodes before contact with the last node is lost.

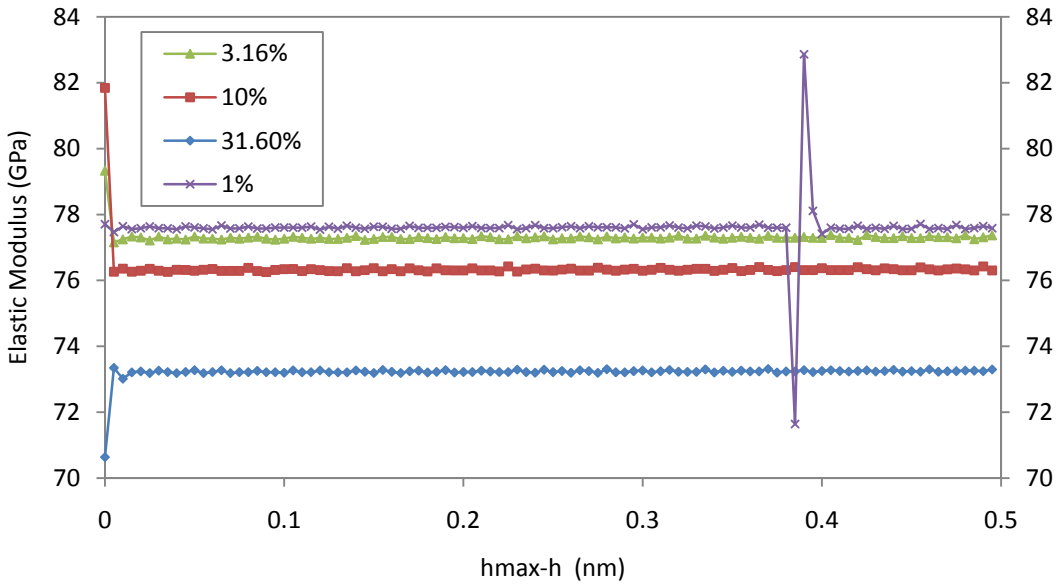

Figure 3.16. Elastic modulus values for 31.6%, 10%, 3.16%, and 1% meshes with β=1. The values are determined using instantaneous load and local slope of load-displacement curves.

TABLE 3.4

MODULUS OF ELASTICITY FOR 31.6%, 10%, 3.16%, AND 1% MESHES WITH β=1.

Model	31.6% Mesh	10% Mesh	3.16% Mesh	1% Mesh
Elastic Modulus (GPa)	73.231	76.315	77.285	77.605
Beta correction factor, β	1.0171	1.0599	1.0734	1.0778

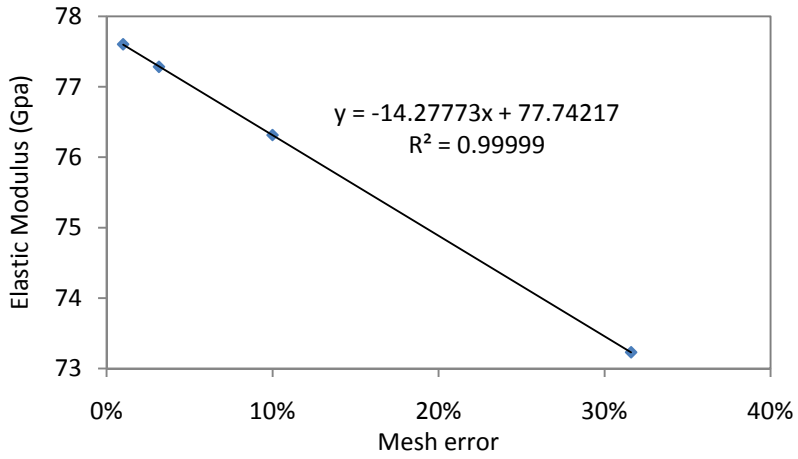

Figure 3.17. Elastic modulus values for 31.6%, 10%, 3.16%, and 1% meshes with β=1. Linear extrapolation is used to obtain the modulus at zero error as 77.742GPa.

Figure 3.16 and Figure 3.17 can be misleading since the coarser mesh seems to yield a calculated modulus value closer to the input modulus 72GPa. It should be noted that the β correction coefficient has not been applied to the data yet. The β correction factors for each mesh is determined based on the expected 72GPa value and are listed in Table 3.4. The extrapolated modulus value at virtually zero error (E=77.742 GPa) can be used to obtain the true β correction factor, β=1.0798. This value is in the range of recent analytical and experimental work as well. The analytical correction of Sneddon's solution, presented by Hay et al. (1999) results in β=1.095 for Poisson's ratio ν=0.17, and semi-cone angle θ=70.3º. Strader et al. (2006) suggested β=1.055 from experimental study of fused quartz using a Berkovich indenter. Shim et al. (2007) suggested β=1.059~1.068 from axisymmetric FEA simulation of elastic-perfectly-plastic fused silica. These values are expected from FEA with slightly coarse mesh as can be seen in Table 3.4. Note that, compared to the above work, the value of β has been estimated much more precisely in this study, since the value obtained here is for virtually zero size mesh.

3.8 Epsilon correction factor for O&P method

The same extrapolation approach can be used for obtaining an accurate value of the ε correction factor used to estimate the contact depth. The Oliver & Pharr equation for estimation of contact depth can be rearranged to equation (3.9). Using this equation, ε can be calculated from the modulus obtained with each of the meshes.

$$\varepsilon = \frac{S}{P_{max}}(h_{max} - h_c) \tag{3.9}$$

In this equation, h_c is the true contact depth in FEA simulation which can be simply calculated as

$$h_c = \sqrt{\frac{A_{proj}^{true}}{\pi \tan \theta^2}} \tag{3.10}$$

The data for obtaining the ε from each case are extracted and listed in Table 3.5. Figure 3.18 shows the plot of ε versus mesh error. The value of ε is obtained at virtually zero error mesh by fitting a line to the two finely meshed models which results in ε = 0.7690 as shown in Figure 3.18.

Shim et al. (2007) reported ε = 0.736~0.739 from axisymmetric FEA simulation of elastic-perfectly-plastic fused silica. Their reported range is closer to the theoretical value ε = 0.72, suggested by Sneddon for conical indentation (Hay et al., 1999).

TABLE 3.5

CORRECTION FACTOR, ε, FOR O&P ESTIMATION OF CONTACT AREA FOR 31.6%, 10%, 3.16%, AND 1% MESHES.

Model	31.6% Mesh	10% Mesh	3.16% Mesh	1% Mesh
True projected contact area (nm^2)	22780.1222	27404.9817	29445.1715	30780.9195
h_c(nm)	30.489	33.441	34.664	35.441
h_{max}(nm)	43.5250	47.2700	48.7400	49.7350
P_{max} (μN)	223.3982	265.5594	282.4490	294.0824
Stiffness (μN/nm)	12.8450	14.6758	15.4143	15.8169
ε	0.7495	0.7642	0.7682	0.7688

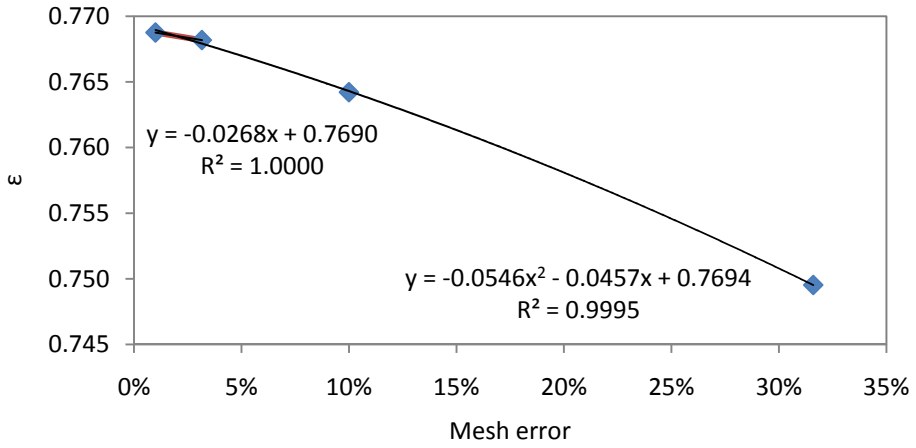

Figure 3.18. Correction factor ε for estimation of contact depth for O&P method for 31.6%, 10%, 3.16%, and 1% meshes. Linear extrapolation is used to obtain its value at zero error.

3.9 Discussion

There are many papers available in the literature, where FEA simulations are used to study various aspects of indentation. Most of these simulations are 2D axisymmetric simulations of conical indentation. As noted above, there will be discrete jumps in contact area and consequently in hardness. Since none of the other authors have explicitly mentioned this issue, or controlled the step size to detect H_{max}, it is conceivable that this is the main source of 'noise' that can be detected in FEA results represented in the literature (Shim et al., 2007; Chen and Vlassak, 2001).

Equations (3.8) can be used to estimate an approximate error bar, or range of results expected in the FEA simulations presented in the literature, in cases where the element sizes and the contact area have been given. The uncertainty in results for conical indentation simulations can be calculated from the element size at the point of contact, contact radius and the semi-cone angle. It should be remembered that this error bar is the minimum expected range of values, independent of other sources of error such as boundary conditions, contact type and so on.

For example Hay et al. (1999) have reported results of axisymmetric FEA of conical indentation by four different cones with half-included angles of 42.28º, 60º, 70.32º, and 80º. Noting that their mesh consisted of square elements 5nm on a side in the region of contact, the possible error in contact area results calculated from equation (3.8) for contact depths between 10nm and 100nm, is plotted in Figure 3.19.

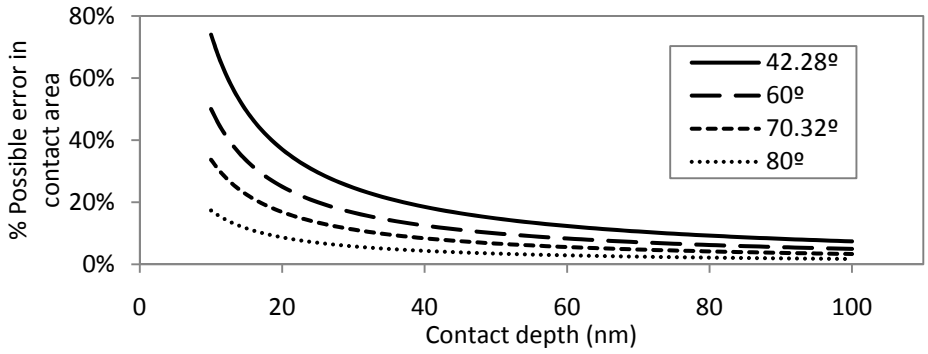

Figure 3.19. Possible error in contact area from error in measurement of true contact area for element size of 5nm for four different cones with half-included angles of 42.28º, 60º, 70.32º, and 80º.

This approach can be generalized to 3D FEA to estimate possible error from contact area measurement. Generally, the number of elements in contact, or more precisely, the number of elements on boundary of contact is the new parameter that comes to picture for determination of error bar of contact area measurement. This fact makes it almost impossible to design a mesh with a constant error bar in a specific range of penetration (specially for pyramidal indentation); however, one can easily calculate the ratio of projected contact area of one element to that of the entire indentation ($\Delta A/A$) and get a measure of the error from contact area measurement.

3.10 Conclusions

In this work the sources of error in FEA of nanoindentation are discussed and a method is developed to design the mesh at the contact surface to control the maximum possible error in contact area measurement. Self similar meshes with known amount of error were designed to determine the properties independent of the depth of penetration. The minimum and maximum hardness values from each of the four designed meshes were obtained precisely and the difference was found to agree with the expected error. It is also shown that the hardness can be measured very close to the true hardness even from very coarse meshes if the step size is controlled around the point where a new node comes into contact. It is also pointed out that the maximum of all hardness values for any mesh is the best measure of the hardness, not the average of them. It is shown that values of the constraint factor C, the modulus correction factor β, and the contact height correction factor ε, can be determined very precisely by extrapolating to virtually zero error mesh which accounts for both contact area measurement error and discretization error. This extrapolation approach is broadly applicable to problems where errors from mesh discretization can be quantified and controlled.

3.11 References

Bobji, M. S. & S. K. Biswas (1999) Deconvolution of hardness from data obtained from nanoindentation of rough surfaces. *Journal of Materials Research,* 14**,** 2259-2268.

Bolshakov, A. 1996. Finite element studies of mechanical property testing by nanoindentation methods. Rice University.

Bolshakov, A., W. C. Oliver & G. M. Pharr (1996) Influences of stress on the measurement of mechanical properties using nanoindentation .2. Finite element simulations. *Journal of Materials Research,* 11**,** 760-768.

Chen, X. & J. J. Vlassak (2001) Numerical study on the measurement of thin film mechanical properties by means of nanoindentation. *Journal of Materials Research,* 16**,** 2974-2982.

Fischer-Cripps, A. C. 2004. *Nanoindentation*. New York: Springer.

Hay, J. C., A. Bolshakov & G. M. Pharr (1999) A critical examination of the fundamental relations used in the analysis of nanoindentation data. *Journal of Materials Research,* 14**,** 2296-2305.

Johnson, K. L. 1985. *Contact mechanics*. Cambridge [Cambridgeshire] ; New York: Cambridge University Press.

Oliver, W. C. & G. M. Pharr (1992) AN IMPROVED TECHNIQUE FOR DETERMINING HARDNESS AND ELASTIC-MODULUS USING LOAD AND DISPLACEMENT SENSING INDENTATION EXPERIMENTS. *Journal of Materials Research,* 7**,** 1564-1583.

Prchlik, L. (2004) Input error sensitivity of hardness and elastic modulus evaluated from indentation load-displacement records by Oliver and Pharr method. *Journal of Materials Science,* 39**,** 1185-1193.

Sakai, M. (2009) Substrate-affected indentation contact parameters of elastoplastic coating/substrate composites. *Journal of Materials Research,* 24**,** 831-843.

Saket Kashani, M. & V. Madhavan. 2008. The effect of surface tilt on nanoindentation results. In *ASME International Mechanical Engineering Congress and Exposition, IMECE 2007*, 67-1071. Seattle, WA, United states: American Society of Mechanical Engineers, 3 Park Avenue, New York, NY 10016-5990, United States.

Shim, S., W. C. Oliver, and G. M. Pharr, (2007) A comparison of 3D finite element simulations for Berkovich and conical indentation of fused silica. *International Journal of Surface Science and Engineering,* 1**,** 259-273.

Strader, J. H., S. Shim, H. Bei, W. C. Oliver & G. M. Pharry (2006) An experimental evaluation of the constant ss relating the contact stiffness to the contact area in nanoindentation. *Philosophical Magazine,* 86**,** 5285-5298.

Warren, A. W. & Y. B. Guo (2006) Machined surface properties determined by nanoindentation: Experimental and FEA studies on the effects of surface integrity and tip geometry. *Surface & Coatings Technology,* 201**,** 423-433.

CHAPTER 4

THE VOLUME SAMPLED DURING NANOINDENTATION TEST FOR HARDNESS AND FOR MODULUS OF ELASTICITY

4.1 Abstract

In this paper, the size of the volume sampled by nanoindentation tests for hardness and modulus measurement is studied. This is done using finite element simulation of nanoindentation on a hemispherical particle embedded in a matrix with properties close to that of the particle. By monitoring the deviation of the measured hardness and modulus from those of the particle as the depth of penetration increases, the zones of influence for hardness results and modulus results are identified. In order to broaden the applicability of the study to a broad range of properties, the simulations are performed on two material systems, one that sinks in and another that piles up around the indenter and with two different cone angles of the indenter. It is found that for any elastic-perfectly plastic material, the intrinsic hardness of particle is measured until the contact radius reaches half the radius of particle, i.e. as long as the plastic region is still within the particle. For modulus, it is found that no specific volume is sampled beneath the indenter and the modulus measured by nanoindentation actually represents the elastic response of the specimen at the indentation point, which for all depths is a function of the properties of both the particle and the matrix. A relationship is developed to describe the observed behavior of the measured modulus as a function of the hemispherical particle-matrix configuration till the point when the contact radius reaches half the particle radius.

Keywords: FEA; Indentation; nanoindentation; dual phase; hardness; elastic modulus; stiffness

4.2 Introduction

The raw data from a quasi static nanoindentation test is nothing but continuous load versus displacement data for loading of an indenter with known geometry into a specimen followed by unloading. Oliver and Pharr (1992) applied Sneddon's solution for elastic indentation to analyze the initial unloading process and developed a method to relate the slope of the unloading curve to the area of contact. This approach enabled measurement of the hardness and the elastic modulus of the specimen.

When indenting into a homogenous bulk of material with a sharp indenter, it is expected that both the hardness and modulus would be independent of the depth of penetration; however, if the sample were not a semi-infinite homogenous bulk with uniform mechanical properties, the measured properties would be a function of depth of penetration, as observed in nanoindentation on thin film/substrate systems. There are numerous papers that address the mechanics of nanoindentation of thin films.

For measurement of properties of thin films, the conventional 10% of the thickness rule is most generally used, but the rule does not apply for measurement of modulus since there is always some elastic displacement of the substrate (Fischer-Cripps, 2004). Lichinchi et al. (1998) simulated 3D Berkovich nanoindentation of hard films on a soft substrate. They concluded for the TiN/HSS system, 15% of the thickness of the film is the critical depth at which the substrate begins to deform. Their simulations showed that soft substrate can begin to plastify at the interface region even before the plastic region in the film reaches the substrate. Bressan et al. (2005) presented some experimental and FEA work on the nanoindentation of bulk and thin film which still used the 10% of thin film as the rule of thumb.

Chen and Vlassak (2001) reported the results of their numerical study on the measurement of thin film mechanical properties by means of nanoindentation. They performed numerous simulations to study the effect of the substrate on the measured properties of the film for various combinations of indentation depth, strength and modulus. Figure 4.1 summarizes their results for the hardness as a function of indentation depth for different combinations of strength of materials.

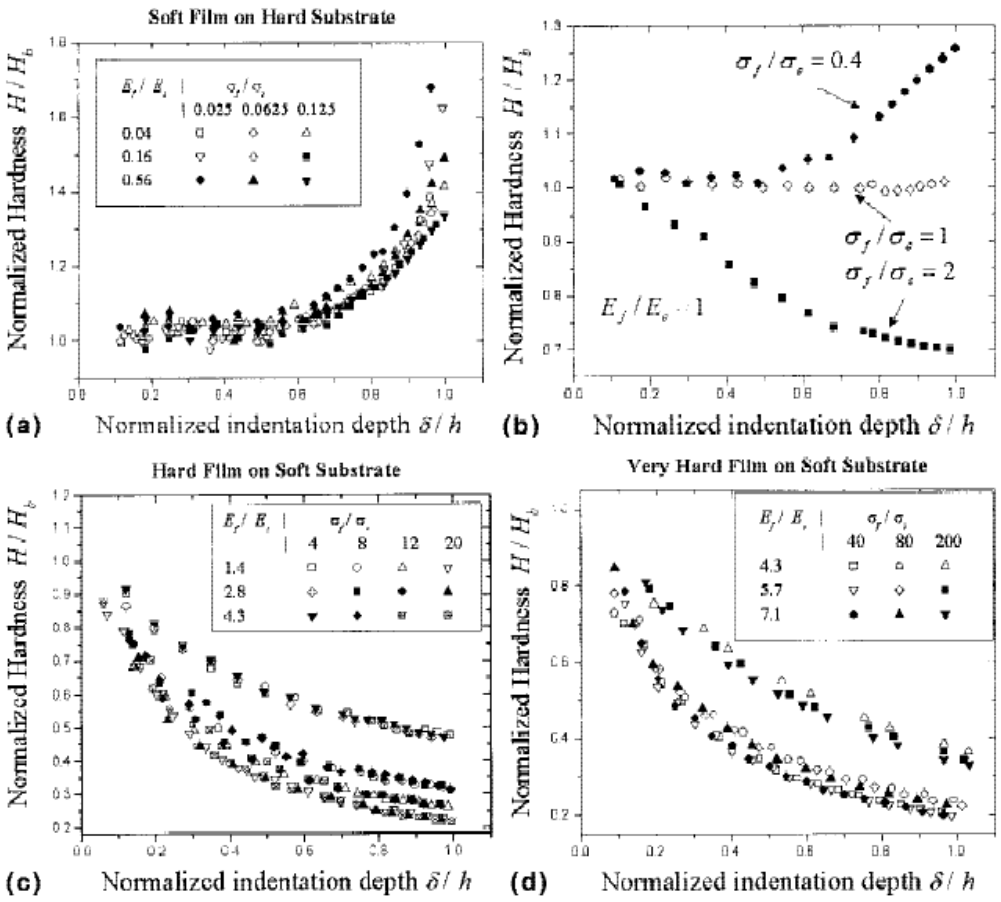

Figure 4.1. Variation of the normalized film hardness H/H_b with normalized indentation depth δ/h, as a function of σ_f/σ_s and E_f/E_s: (a) soft film on hard substrate; (b) the transition from $\sigma_f < \sigma_s$ to $\sigma_f > \sigma_s$; (c) hard film on soft substrate; and (d) very hard film on soft substrate (Chen and Vlassak, 2001).

From Figure 4.1(a) they concluded that the critical indentation depth is half of the thin film for the soft film on hard substrate system. We show in this paper that this has a small dependence on material properties and indenter geometry and is not a constant value.

From the data in Figures 4.1(b) and 4.1(c) they conclude that when the yield stress of the film is higher than that of the substrate, the normalized film hardness is no longer constant even for relatively small indentation depths. We show in this work that for two phase systems this can be improved, and that a critical depth of penetration for hard particle on soft matrix can be calculated, for slightly harder particles compared to the matrix. They have also shown in Figure 4.1(d) that for a very hard film on soft substrate ($\sigma_f/\sigma_s > 40$), the mechanism changes and the response to indentation is akin to that of a plate over an elastic foundation. They have also pointed out that the data in Figure 4.1 confirms that elastic mismatch plays a minor role in hardness measurement of thin film.

More recent FEA studies of thin film/substrate problem are presented by other researchers, with similar conclusions for various material types and simulation conditions (Chen and Bull, 2009; Pelegri and Huang, 2008; Wang et al., 2007).

Saha and Nix (2002) experimentally studied the effect of the substrate on the determination of thin film mechanical properties by nanoindentation on the same thin film, deposited on four different substrates. Their experimental results support the findings of Chen and Vlassak (2001) qualitatively. They also presented an extension to King's solution (King, 1987) to account for the influence of substrate compliance by including a term due to the substrate effect in the reduced modulus equation for conical indentation

$$\frac{1}{E_r}=\frac{1-\nu_i^2}{E_i}+\frac{1-\nu_f^2}{E_f}\left(1-e^{-\frac{\alpha(t-h)}{a}}\right)+\frac{1-\nu_s^2}{E_s}\left(e^{-\frac{\alpha(t-h)}{a}}\right) \tag{4.1}$$

where α is a numerically determined scaling parameter, h is the indenter displacement, a is the indentation contact radius, and t is the film thickness. They (Saha and Nix, 2002) showed that equation (4.1) predicts the expected film modulus reasonably well for indentation depths less than 50% of the film thickness.

Han et al. (2005) used the reduced modulus given by equation (4.1) to estimate the resultant hardness as a function of depth. They used the relationship presented by Josling and Oliver (1990) in equation (4.2) to estimate hardness as long as the modulus estimation is valid.

$$\frac{H}{{E_r}^2}=\beta^2\frac{4}{\pi}\frac{P}{S^2} \tag{4.2}$$

Yu et al. (1990) presented an elastic solution of the axisymmetric Boussinesq problem for indentation on a film/substrate system. "The results are obtained by solving a Fredholm integral equation of the second kind with a continuous symmetrical kernel which depends on the bonding conditions". Numerical results are given for several combinations of film and substrate elastic moduli and film thickness. Later Chen and Vlassak (2001) showed that Yu's elastic solution agrees well with finite element simulations and can be used for estimation of elastic modulus of the composite where the elastic properties of film and substrate are known. Han, Saha, and Nix (2006) used Yu's elastic solution to calculate a relationship between the reduced contact stiffness and contact radius. Thus, they used this analysis to determine contact areas during indentation and to calculate the hardness as a function of indentation depth. Their experimental results show applicability of this method for several elastic mismatch ratios up to indentation depths of more than 80% of the film thickness. They showed that since the method is based on the

contact radius, the pile-up error would be taken care of and the method would be applicable to elastic-plastic indentation as well as elastic indention.

Sakai (2009) also used Yu's elastic solution along with FE simulations to define a spatially graded modulus and spatially graded yield stress and showed these two parameters perfectly lie on his Maxwelian relation for compliance factor (H/Y) as a function of plastic index ($E_r \tan\beta/Y$). He showed that the analytical model perfectly matches with FEA results. He also presented some relations that can be used to simplify the application of Yu's solution.

Li and Vlassak (2009) used Yu's method and other works to simplify the use of this elastic solution for thin film/substrate systems instead of Sneddon's equation that is developed for indentation into homogenous materials. Their proposed procedure which is similar to the widely accepted procedure of Oliver and Pharr (1992), is applicable over a much larger range of indentation depths.

Durst et al (2004) included the thin film configuration as one among three different configurations characteristic of dual phase systems. Their categories are based on the ratio of height to thickness of the second phase: thin film, columnar second phase, and particle (Figure 4.2). They showed how the load curve for the dual phase system change from that of the phase being indented to load curve of the second phase as conical indenter goes deeper into the phase being indented.

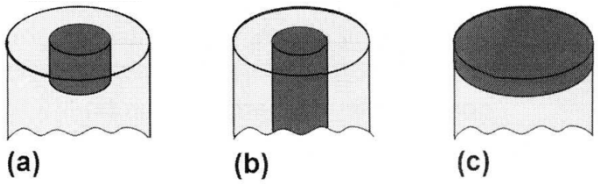

Figure 4.2. Model systems for sectioned particle-matrix compounds: (a) thin film, (b) columnar, (c) particle.(Durst et al., 2004)

It was decided that the transition from the properties of the phase being indented to those of substrate occur due to progressive increase in the volume where properties are sampled by the indenter. Study of this transition can lead to understanding of the volume that is sampled for determining each of the measured mechanical properties. Knowing this, educated guesses can be made about the size of the indents that would be best for any specific study, providing maximum information about the phase of interest with minimal noise. In addition, for the case of indenting on a second phase grain (Sun et al., 2008) or for capturing the gradient of variation of properties over a

small region (Saket Kashani and Madhavan, 2007), tracking the changes with depth of penetration will help to understand the influence of the material around the region of indentation on determined results.

In this paper, we present some dual phase studies using FEA to understand the extent of the sampled material beneath the indenter for measurement of hardness and modulus. For the first time, a hemispherical particle is assumed with slightly different properties compared to those of the matrix. This allows understanding the volume sampled in a bulk material since the behavior of the two materials are not significantly different. The shape of the particle in the matrix is shown in Figure 4.3 schematically as compared to the ones in Figure 4.2.

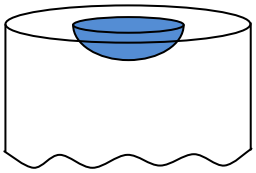

Figure 4.3. Schematic demonstration of hemispherical particle in matrix.

4.3 Finite element model

The nanoindentation test is simulated using an axisymmetric finite element model with linear full integration elements. The specimen is modeled as a hemisphere of radius 200 μm and meshed with a gradient in the contact region to keep the error in area measurement below 1% (explained in chapter 3). The geometry of the specimen and detail of the mesh are shown in Figure 4.4. This self-similar, constant-error mesh is applied to the range up to the radius of 500nm. More details about the mesh design and error control are reported in an earlier work (chapter 3) on the accuracy of FEA of nanoindentation. The indenter is modeled as an analytical rigid cone with semi-cone angle of 70.3º, with area function equivalent to that of a Berkovich indenter and 42.28º semi-cone angle for cone equivalent to a cube corner. Frictionless contact is used between the indenter and the surface of the specimen and fixed boundary conditions are applied to the outer radius of the specimen.

Poon et al. (2008) have shown that if the height of the specimen is more than 100 times larger than the maximum depth of penetration, the elastic results would not be affected by the boundary conditions. In this work the maximum depth of penetration is only 100nm while the radius of the hemispheric model is 200μm. Even though the 2000 times larger specimen is very conservative for avoiding the boundary effects, it is shown later in this paper that there is still a slight effect of the boundary on the modulus calculated.

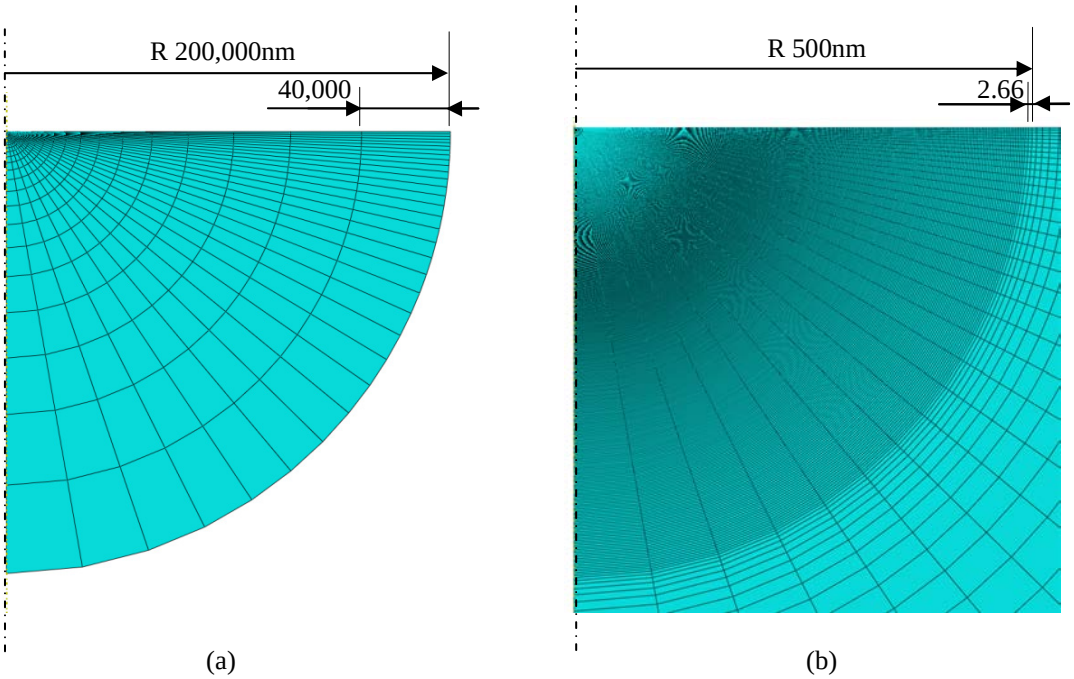

Figure 4.4. Mesh designed for 1% error (units in nm). (a) Axisymmetric model of hemispherical model, (b) close up at the contact region with 1% error, gradient mesh.

Two material systems are considered as representatives of the materials that sink-in and pile-up around the indenter. These materials are designed around the properties of glass (Y= 2662MPa, ν= 0.25, E= 70Gpa) and aluminium (Y= 228.5MPa, ν = 0.25, E= 70Gpa) which have E/Y of 26 and 306 respectively, both assumed to be elastic-perfectly plastic (Bolshakov, 1996). It is expected that glass would exhibit sink-in while pile-up will be expected for aluminium for the equivalent cone of Berkovich indenter (Bolshakov and Pharr, 1998). It should be noted that glass exhibits pile-up for the equivalent cone of cube corner indenter.

The equivalent plastic strain distributions and von Mises stress distributions beneath the indenter are shown for these two materials in Figures 4.5 and 4.6. It is clear that the shape and size of the plastic zone is different in these two materials. The von Mises plots (Figure 4.6) also depict clear difference in the distribution of stress in these two representative materials. It can be concluded that the volume sampled for hardness and modulus measurements could be dependent on material properties and needs to be studied for a range of materials.

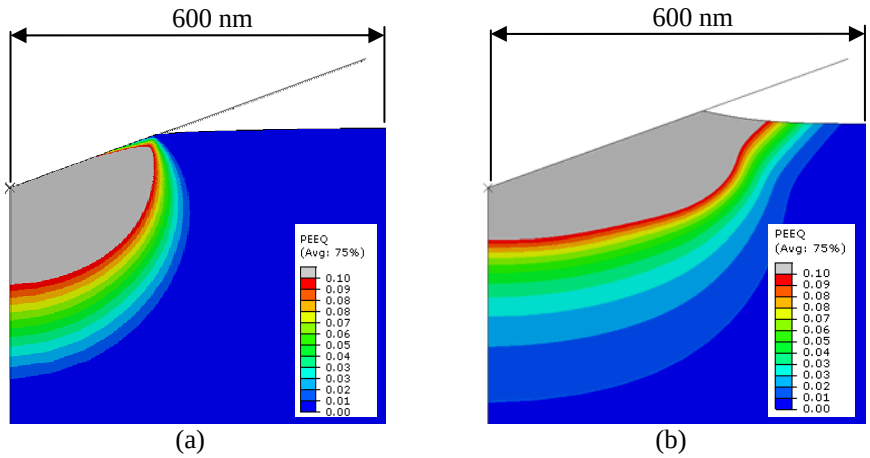

Figure 4.5. Equivalent plastic strain distribution at maximum depth of penetration, 100nm (a) for glass (b) for aluminum.

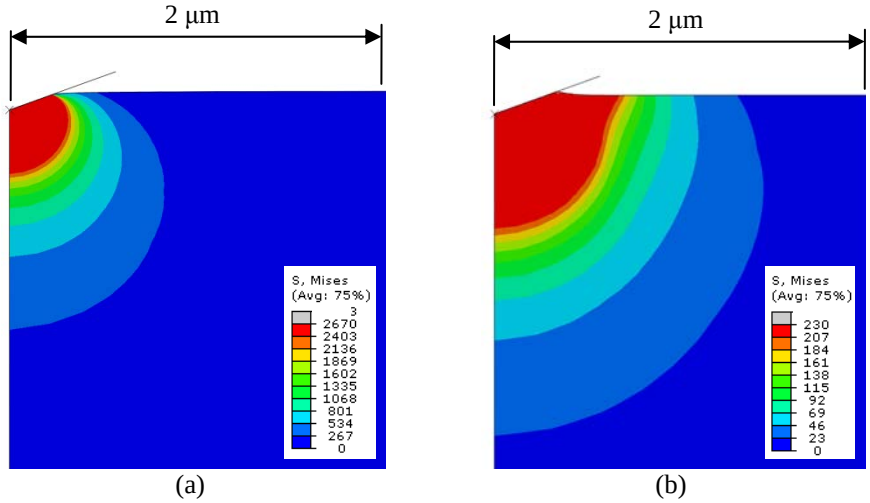

Figure 4.6. Von Mises stress distribution at maximum depth of penetration, 100nm, in MPa (a) for glass (b) for aluminum.

4.4 Volume sampled for hardness

In order to determine the volume sampled for measurement of hardness by nanoindentation, the hemispherical particle is modelled as a material with either 10% larger or 10% smaller yield stress with respect to that of the bulk phase. All other properties of the particle and the bulk are equal.

Nanoindentation simulations were performed on only the bulk material (without the particle) to obtain the baseline value of hardness. Using the instantaneous load and the projected contact area directly obtained from FEA, the hardness can be determined from equation (4.3) where P is the load and $A_{c\ proj}$ is the instantaneous projected contact area that carries the load. In Figure 4.7 and 4.8 it can be seen that the hardness value stabilizes after sufficient number of elements is used for discretizing the contact area and plastic zone. It was shown in our previous

work (chapter 3) that the noise in hardness in the stabilized region comes from area measurement noise and the best estimate of hardness is the maximum value in that region. Therefore unique values are extracted from hardness curves corresponding to each material which are listed in Table 4.1.

$$H = \frac{P}{A_{c\ proj}} = \frac{P}{A_c \sin\theta} \tag{4.3}$$

TABLE 4.1

HARDNESS VALUES FROM INDENTING ON BULK MATERIALS WITH DIFFERENT YIELD STRESS

Material	Yield stress (Mpa)	Hardness (GPa)
Al0.9Y	205.7	0.530
Aluminum	228.5	0.593
Al1.1	251.4	0.653
Gl0.9Y	2396	5.439
Glass	2662	5.902
Gl1.1Y	2928	6.350

Two dual phase simulations were performed for each material system by assuming hemispherical particles embedded in the matrix. In all simulations, the matrix had the properties of original materials (glass or aluminum), but the yield stress of the particle was altered to be either 10% lower or 10% higher than that of the matrix. The four dual phase simulations were Gl0.9Y-on-Gl, Gl1.1Y-on-Gl, Al0.9Y-on-Al, and Al1.1Y-on-Al. The second phase was modeled by simply assigning new material properties to the elements inside the particle, which has a radius of 279nm in these simulations. The particle and matrix are perfectly connected by shared nodes and no sliding is allowed between them, modeling consistent deformation of the two phases. Indentation was simulated by linear displacement of the indenter to a maximum penetration of 100nm into the particle. Figure 4.7 and 4.8 also show continuous plots of the hardness vs. normalized depth of penetration for the dual phase simulations, in addition to results of indentation into single phase glass and aluminum.

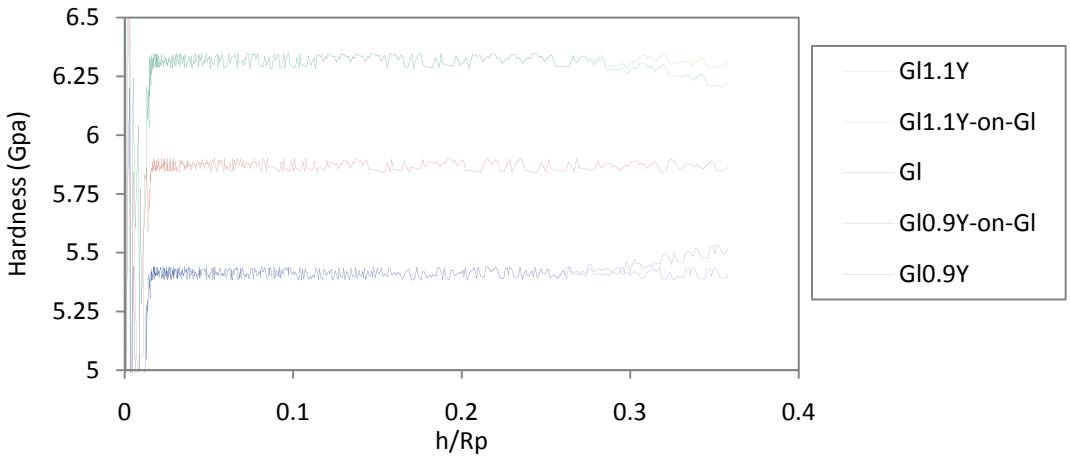

Figure 4.7. Hardness vs. normalized depth of penetration for glass material system.

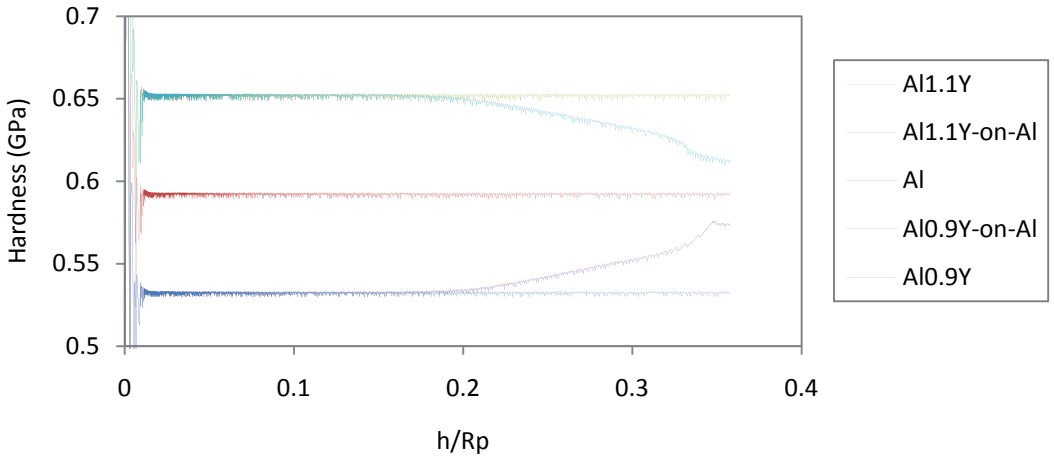

Figure 4.8. Hardness vs. normalized depth of penetration for aluminum material system.

In order to study the deviation of hardness measured, from that of the particle, the hardness measurement error relative to the expected value for the particle is plotted as a function of normalized depth of penetration (Figure 4.9). It can be noted that the deviations for 10% higher and lower hardness are symmetric about the x-axis. The measured hardness begins to deviate from the hardness of the particle for penetrations greater than 25% of particle radius for the case of glass and for penetrations greater than 15% of particle radius for aluminum. This shows that recommendation of a constant percentage penetration for all materials is not valid.

In order to study other parameters that may affect the critical depth of penetration, one more case was modeled within the glass material system, where in the particle has yield stress of 80% of that of glass. Additionally, cube corner indentation into a particle having yield stress equal to 90% of glass was simulated, to study the effect of cone angle. The results of these two new cases are also shown in Figure 4.9. It can be seen that the hardness of a

Gl0.8 particle on glass begins to be affected by the substrate at the same depth of penetration as observed in the other glass simulations, which is 25% of the particle size. However, the cube corner simulation shows negligible error in hardness measurement until the depth of penetration reaches 58% of the particle radius. This means that cube corner indenter samples a smaller volume compared to the Berkovich indenter, for the same depth of penetration.

It is well known in the literature that the amount of sink-in and pile-up changes as a function of $E_r tan\beta/Y$ (Bolshakov and Pharr, 1998; Cheng and Cheng, 2000). Chen and Vlassak (2001) showed that pile-up of a thin film on a substrate may be different from that of the same material in bulk form. Therefore, the amount of pile-up would be a function of E_r/Y, indenter geometry, thin film configuration and normalized depth of penetration. Since it is noted in Figures 4.5 and 4.6 that the pile-up when indenting into aluminum causes the contact radius to be higher for the same depth of penetration, and since Figure 4.9 show that the true deviations in hardness of the particle begin at a smaller penetration, it is of intent to study the deviation as a function of the contact radius.

Figure 4.10 shows the hardness error as a function of versus the normalized contact radius. It can be seen that all curves begin to get affected by matrix properties when the contact radius exceeds 50% of the radius of particle. This is a good rule of thumb that can be considered to be broadly applicable, for different materials and indenter sharpnesses, for all elastic-perfectly materials. To help understand the reason for this, Figure 4.11 shows the error vs. normalized radius of the plastic zone, which shows that the hardness measured starts to deviate from that of the particle's hardness when the plastic zone spreads into the matrix.

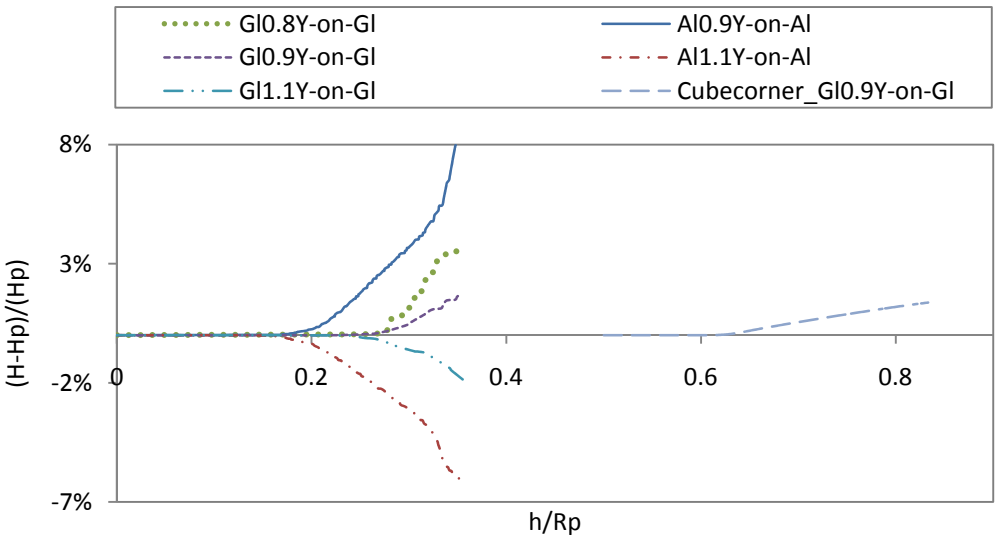

Figure 4.9. Hardness error versus normalized depth of penetration.

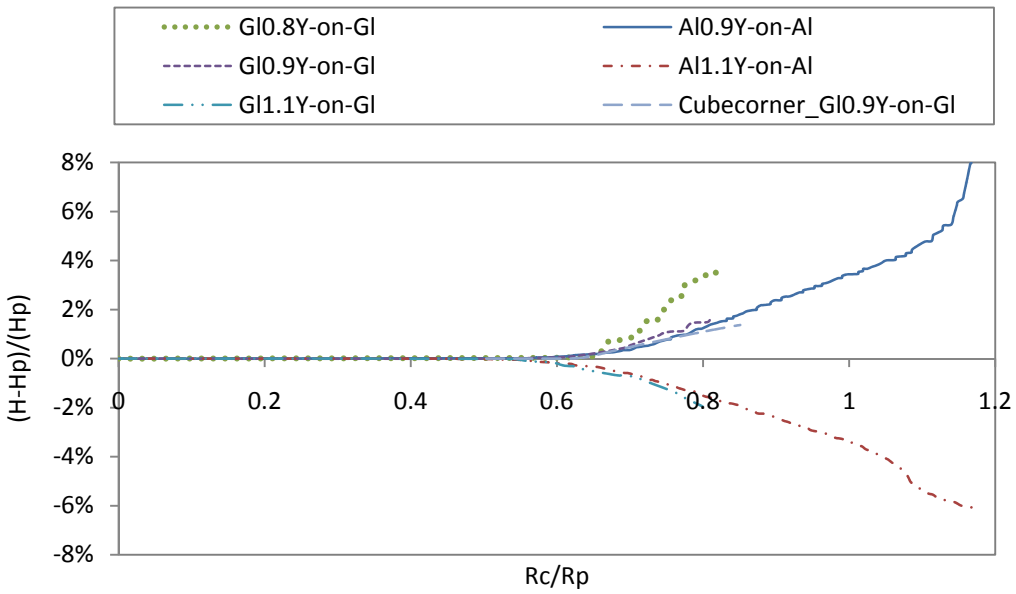

Figure 4.10. Hardness error versus normalized contact radius.

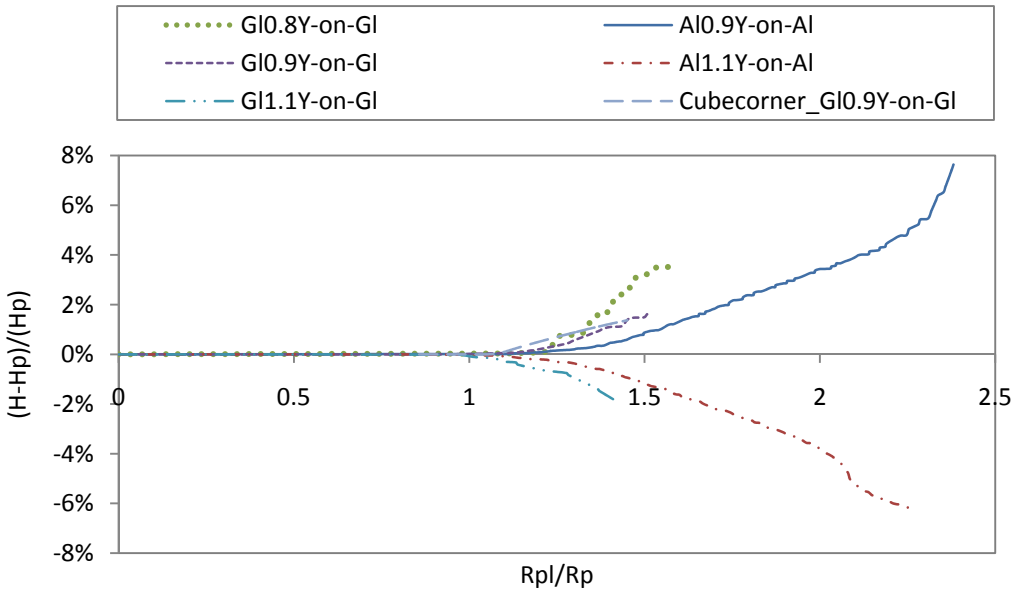

Figure 4.11. Hardness error versus normalized radius of plastic zone.

The radius of the plastic zone was calculated using the relationship developed by Harvey et al. (1993) for estimation of size of the plastic zone for elastic-perfectly plastic materials based on Johnson's expanding cavity model (1985).

$$R_{pl} = \sqrt{3\ P/2\pi Y} \tag{4.4}$$

Since the hardness can be written as:

$$H = \frac{P}{A_c} = \frac{P}{\pi {R_c}^2} \tag{4.5}$$

A relation for R_c/R_{pl} can be obtained by eliminating force from equations (4.4) and (4.5) by use of the definition of the constraint factor (C=H/Y). The resultant relation can be written as

$$\frac{R_c}{R_{pl}} = \sqrt{\frac{2}{3C}} \tag{4.6}$$

From the results given in Table 4.1, it should be noted that the constraint factor of the materials used in this paper range from 2.2 to 2.6. Further simulations show that 2.6 is the maximum value of C attainable for frictionless simulations, which results in a minimum possible value of 0.51 for R_c/R_{pl}. Therefore one can conclude that for any elastic-perfectly plastic material, the intrinsic hardness of particle is measured until the contact radius reaches half of the radius of particle since the plastic region would be still within the particle. This is valid as long as the cavity expansion model can be used for modeling of the indentation of the composite system. For the cases of large mismatch between elastic modulus of the two materials or the yield stress values, the validity of this conclusion remains to be verified. This conclusion is definitely not valid for very hard particles in soft matrices for reasons noted in several thin film studies available in the literature (Chen and Vlassak, 2001; Sakai, 2009).

4.5 Volume sampled for measurement of elastic modulus

A similar approach using hemispherical particles, but with different modulii, is used to study the volume sampled for measurement of elastic modulus. A new set of materials are designed around the properties of glass and aluminum. The yield stress and Poisson's ratio of the particle are kept the same as those of the present materials, and the elastic modulus of the particle is changed to be 10% higher or 10% lower. The material properties used in the simulations are listed in Table 4.2.

TABLE 4.2

LIST OF MATERIALS FOR MODULUS STUDIES WITH ALTERED MODULUS OF ELASTICITY.

Material	Yield stress (Mpa)	Elastic modulus (Gpa)
Al0.9E	228.5	63
Aluminum	228.5	70
Al1.1E	228.5	77
Gl0.9E	2662	63
Glass	2662	70
Gl1.1E	2662	77

To study the variation of measured modulus as a function of depth of penetration, the indentation simulations are performed in displacement mode and stopped every 10nm for a 0.1nm unloading step. The slope of the unloading curve is used to calculate the modulus of elasticity at each unloading step. This results in 10 data points for each simulation since the maximum depth of penetration is 100nm. Performing a simulation with only one unloading step at 100nm confirmed that the small unloading steps do not affect the measurements in subsequent steps.

The specimen's modulus of elasticity E_s can be obtained from equation (4.7) for the case of indentation with a rigid indenter where S is the stiffness of unloading curve, ν_s is the Poisson's ratio of specimen, and β is a constant that depends primarily on the geometry of the indenter (Oliver and Pharr, 1992).

$$E_s = \frac{\sqrt{\pi}}{2\beta}\frac{S}{\sqrt{A_{c\,proj}}}(1-\nu_s^2) \tag{4.7}$$

First, the simulations were done for the bulk aluminum and glass and other materials listed in Table 4.2 to determine the reference values. As can be seen in Figure 4.12, the obtained value for glass and aluminum is not exactly the same even though they have the same input elastic modulus. This means that the β correction factor is slightly different for these two materials. It is also interesting to note that even though a constant modulus value is expected for bulk material simulations, there is a slight linear increase in measured modulus as the depth of penetration increases. This may be attributed either to the fixed boundary condition at the outer radius of the specimen or to the increasing distortion of the elements at the center.

In order to understand the dependency of the modulus increase to model size, three other simulations are performed on glass with model sizes of 20μm, 400μm, and infinity. Note that all previous simulations used a model

with outer radius of 200μm. Figure 4.13 depicts that the elastic modulus increases linearly as a function of contact radius with a specific dependency on model size. Notice that all the lines intersect with the vertical axis at the same value which is the elastic modulus independent from depth of penetration, E_0. It can be also seen that even for infinite model size, which is simulated using axisymmetric fully integrated continuum infinite elements (CINAX4) at the outer radius of the model, the modulus increases slightly. This clarifies that the stiffness increase is not only because of the fixed boundary conditions in far field, but also because of the lack of self similarity or the increase of the amount of distortion of elements at the center of the model. Identification of the true sources of this effect remains to be verified.

As noted during the hardness study, if the changes in modulus are normalized with respect to their values at zero penetration (which is the intercept of the lines with vertical axis), and the horizontal axis is considered as the contact radius, all data points collapse into one line as shown in Figure 4.14, which shows the modulus increase is the same for all simulations performed on same model size. The straight line equations given within Figure 4.14 can be rearranged so that the modulus can be written as

$$E = E_0(1 + bR_c) \tag{4.8}$$

where E_0 is the modulus at zero depth of penetration, which is determined by extrapolation, and b is equal to the slope of each line in Figure 4.14.

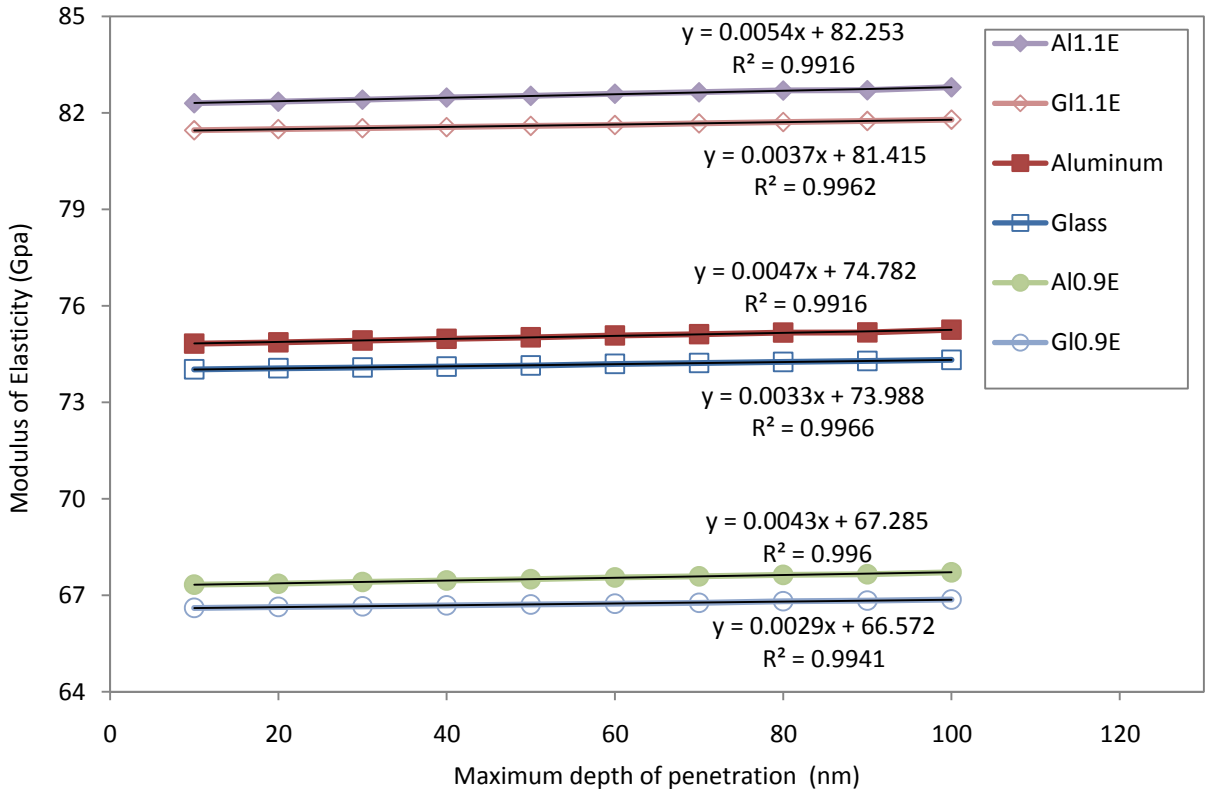

Figure 4.12. The elastic modulus obtained from indentation on bulk of each homogenous material increases slightly as depth of penetration increases. (β=1 is assumed)

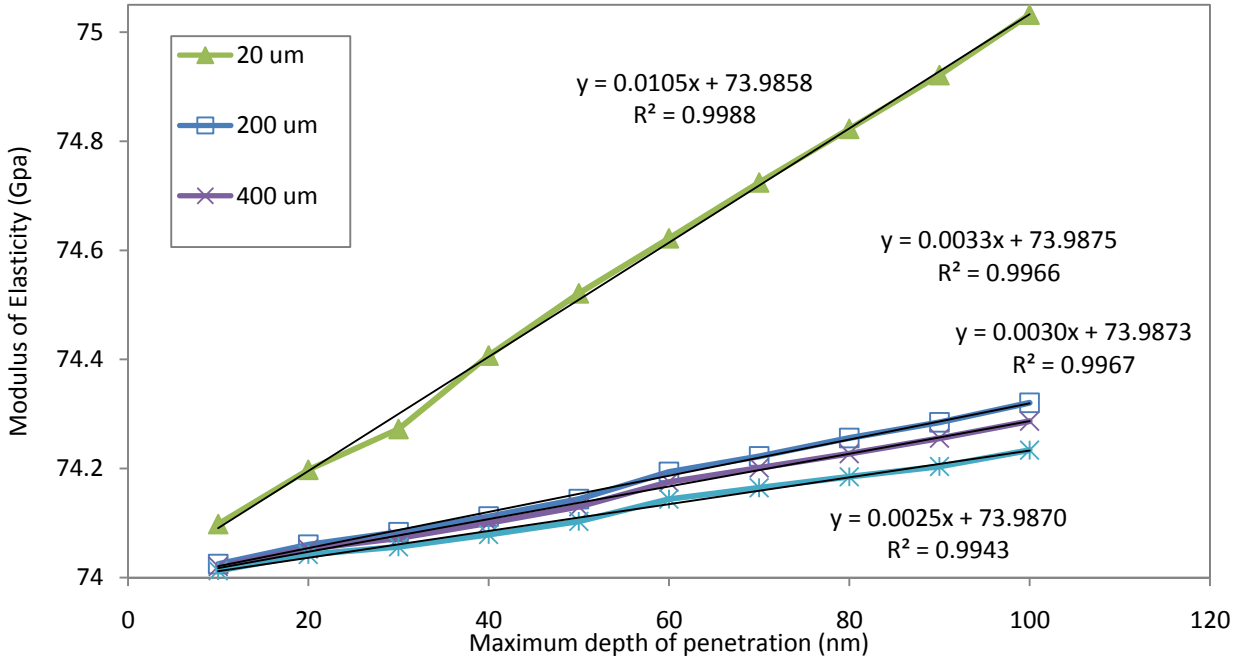

Figure 4.13. The elastic modulus obtained from indentation on bulk of glass increases linearly as depth of penetration increases with a dependence on model sizes. (β=1 is assumed)

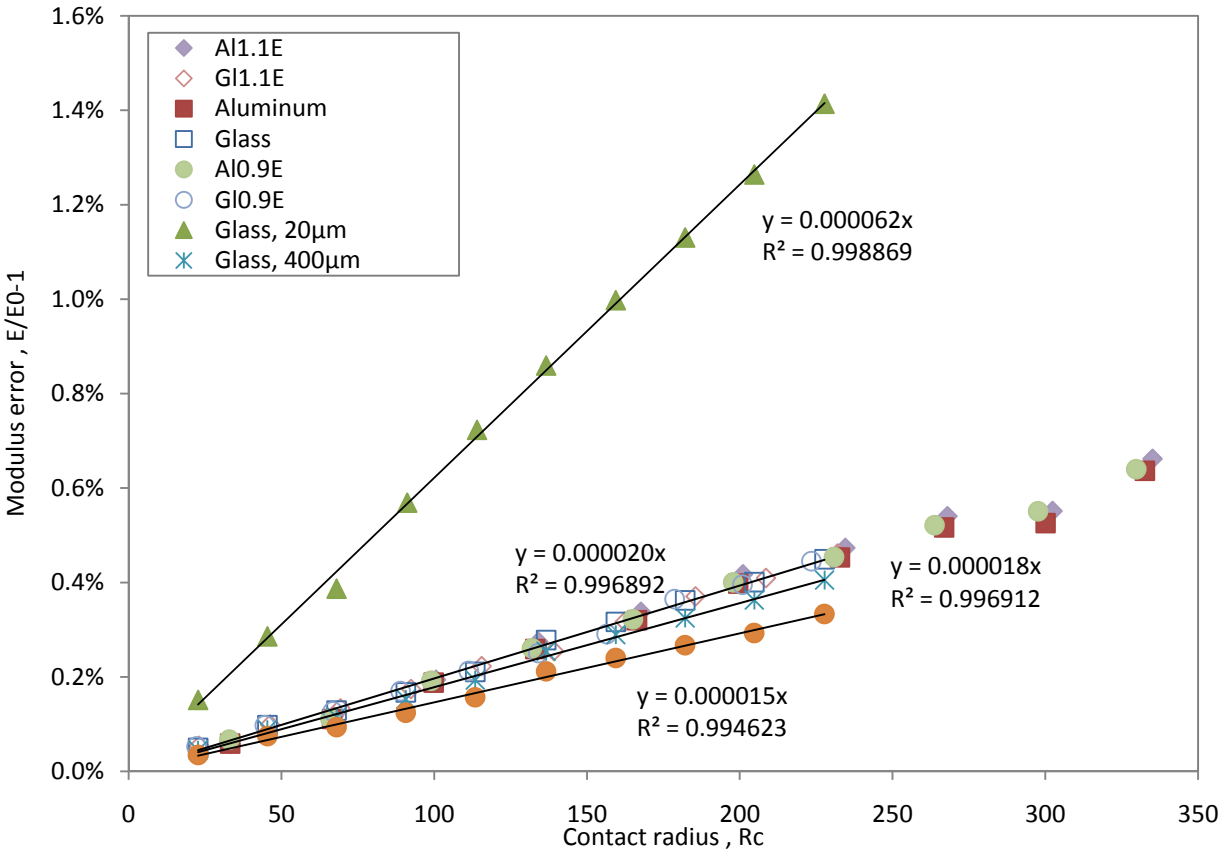

Figure 4.14. The error in elastic modulus with respect to its value at zero penetration versus normalized contact radius for the studied materials with the 200µm model and also for glass with various model sizes. Note that the error in modulus measurement increases faster for smaller model sizes.

Dual phase simulations are performed with a particle of size 1083nm, with modulus either 10% lower or 10% higher than that of the matrix in which it is embedded. The deviation of the measured modulus from that of the particle is determined at the discrete depths of penetration. The reason for assuming a larger particle radius in modulus study compared to what used in hardness study is the fact that, for the same particle size, measured modulus sees the effect of matrix properties at much shallower depths of penetration compared to hardness. Larger particle size is used to be able to simulate the test within the same range of 100nm and 0.1nm unloading step at every 10nm. Figure 4.15 shows the plot of modulus error versus the normalized depth of penetration. It can be seen that for all cases the measured modulus is influenced by the matrix properties even at the very first data point where the penetration depth is less than 1% of the particle radius. This clearly shows that it is not possible to identify a finite volume that is sampled beneath the indenter and the modulus measured by nanoindentation actually represents the elastic response of the entire specimen at the indentation point, which is a function of the elastic modulus of the entire volume with a dependence on the distance from the indentation point.

Figure 4.16 show that if the errors are plotted versus normalized contact radius, the curves for glass and aluminum (Gl0.9E on glass, Al0.9E on aluminum) as well as the curves for different cone angles (cubecorner-Gl0.9E on glass) merge together. This implies that all systems with particle modulus 10% less than that of matrix, behave the same, even independent of cone angle.

The slopes of these lines in Figure 6.16 are related to the ratio of modulus of the particle to that of matrix (Slope $\propto (1 - E_p/E_m)$). Therefore, if the error is normalized with respect to the difference between the particle and matrix properties, a single relationship that relates the deviations of the measured modulus of the particle to R_c/R_p and E_p/E_m is obtained, as shown in Figure 4.17.

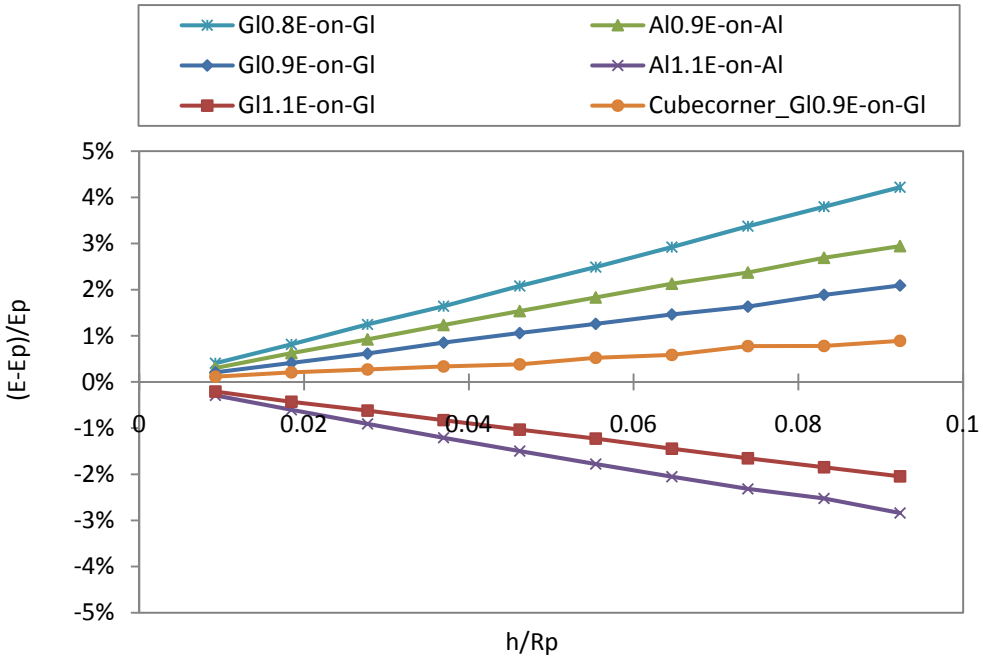

Figure 4.15. Modulus error vs. normalized depth of penetration.

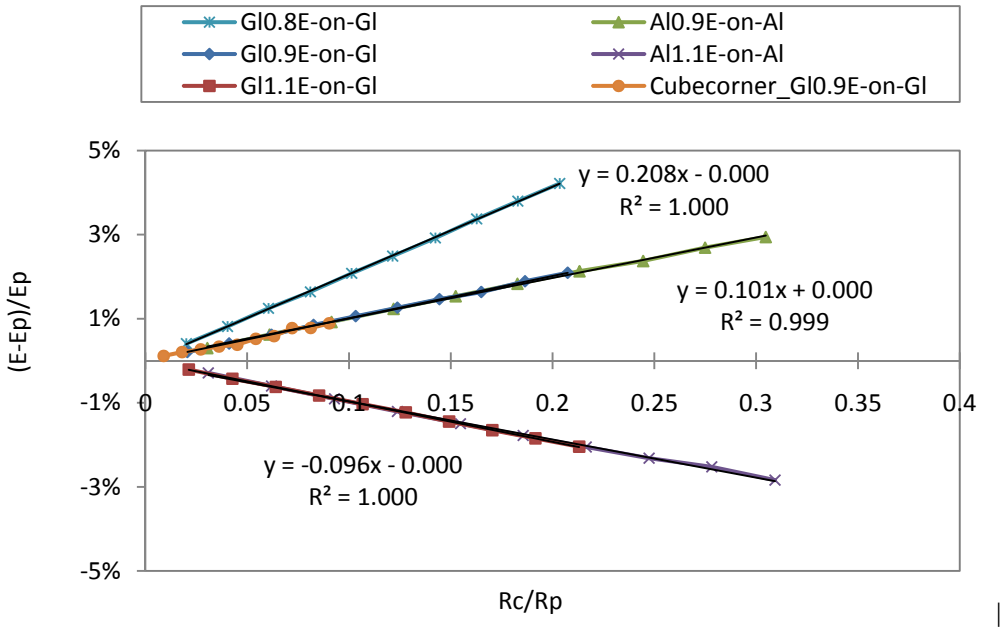

Figure 4.16. Modulus error vs. normalized depth of penetration.

In Figure 4.17 the vertical axis is the ratio of the deviation to $(1 - E_p/E_m)$, which is found to make the slopes of all curves equal to unity. The relationship can be written as:

$$\left(\frac{E}{E_p} - 1\right) \cong \frac{R_c}{R_p}\left(1 - \frac{E_p}{E_m}\right) \tag{4.9}$$

Notice that the data are shown only up to contact radius of about 30% of the particle radius. Considering that much deeper indents ($R_c \gg R_p$) should result in measurement of the modulus of matrix without much effect of the particle, the linear behavior shown in Figure 4.17 can be inferred to be valid only for small R_c/R_p ratios. To study the transition between these two se regimes, indentation into a particle of Gl0.9E on glass has been simulated to higher R_c/R_p ratios. Figure 4.18 show that the modulus measured shows linear behaviour until the contact radius reaches one-half of the particle radius. This means that equation (4.9) can be suggested as a model for the measured modulus only within this range, and can be rewritten as shown below to make the dependence of the measured modulus on contact radius explicit.

$$E \cong E_p\left[1 + \left(\frac{E_m - E_p}{E_m}\right)\frac{R_c}{R_p}\right] \tag{4.10}$$

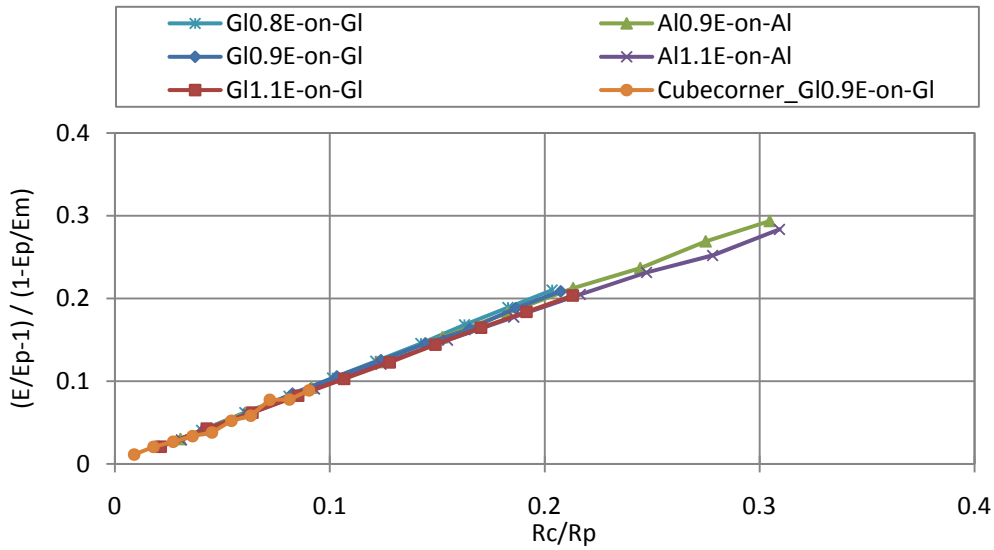

Figure 4.17- Normalized modulus deviation relative to the maximum possible deviation, weighted by the ratio of modulus of particle to that of matrix vs. normalized contact radius for all studied cases

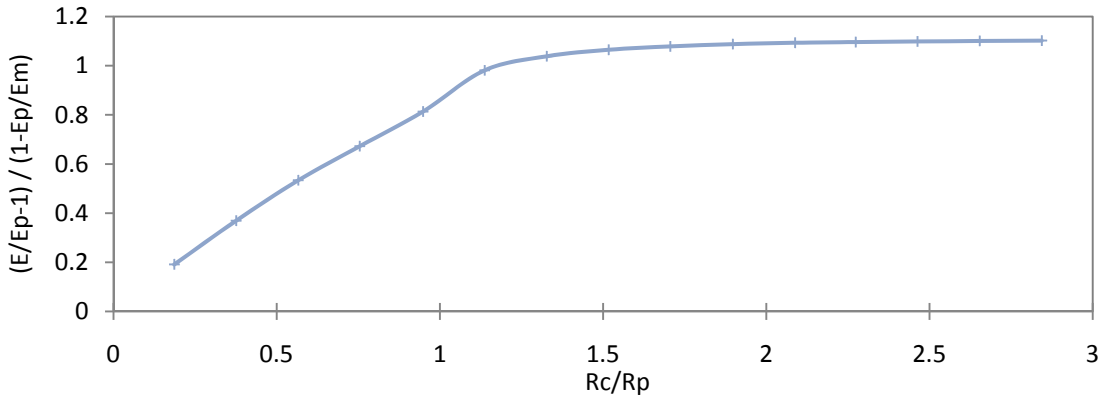

Figure 4.18. Normalized modulus deviation relative to the maximum possible deviation, weighted by the ratio of modulus of particle to that of matrix vs. normalized contact radius for the case of Gl0.9E-on-Glass

Equation (4.10) is similar to the form of the relation developed by Nagao et al. (2009) for determination of Young's modulus for pyramidal indentation into thin film/substrate system. They used a one dimensional linear analysis which models the system as a set of linear springs. There are other works in the literature that also show the spring model to result in good agreement with experiments (Bec et al., 2006).

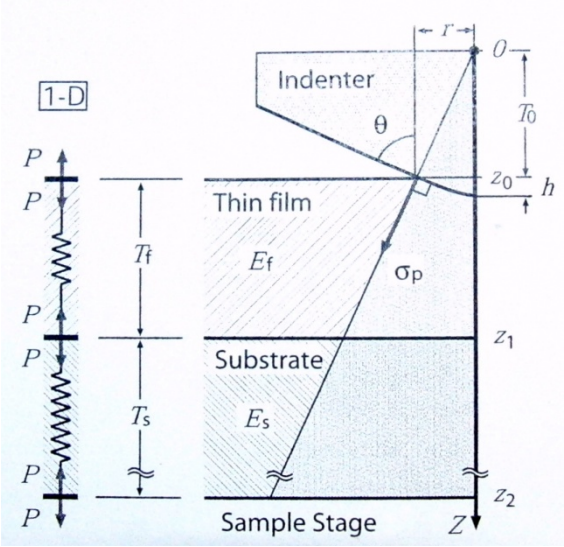

Figure 4.19. Geometry of the axisymmetric model of pyramidal indentation into thin film/substrate system and analogous 1D representation of a linear set of springs (Nagao et al., 2009).

Figure 4.19 shows the geometry of the axisymmetric model proposed by Nagao et al. (2009). They defined the parameter τ as the parameter describing substrate effect where displacement of indenter can be expressed as summation of displacement in film and substrate.

$$\delta h = \delta h_f + \delta h_s = \delta h_f(1+\tau) \tag{4.11}$$

which can be used for $\tau \ll 1$ to obtain a relation between the measured modulus and the modulii of the film and substrate.

$$E_r \cong (1-\tau)E_f + \tau E_s. \tag{4.12}$$

They showed that for a practical system in which the film thickness is very small compared to that of the substrate, $T_s \gg T_f + T_0$, (T_0 defined in Figure 4.19) the parameter τ would be

$$\tau_{film/substrate} = \frac{E_f}{E_s}\frac{T_0}{T_f} = \frac{E_f}{E_s}\frac{h}{T_f}tan^2\,\theta \tag{4.13}$$

which results in

$$E_r \cong E_f\left[1+\left(\frac{E_s-E_f}{E_s}\right)\frac{h}{T_f}tan^2\,\theta\right] \tag{4.14}$$

Equation (4.14) relates the measured modulus of the thin film system to the modulus of the film and matrix and also the penetration ratio. Comparing this to equation (4.10), τ, the parameter describing matrix effect for a hemispherical particle within a matrix is:

$$\tau_{particle/matrix} = \frac{E_p}{E_m}\frac{R_c}{R_p} \tag{4.15}$$

Note that equation (4.15) is developed for small values of matrix effect, $\tau \ll 1$. Therefore the proposed relation is valid for relatively shallow indents compared to the particle radius and also it works better for compliant particle in stiff matrix since it has smaller matrix effect compared to a stiff particle embedded in compliant matrix.

4.6 Discussion

Based on the understanding gained, that the hardness measured is identical to that of the particle so long as the plastic zone is confined within the particle, displacement and load limits can be formulated for maximum penetration before the matrix influences the hardness measurement for any elastic-perfectly plastic material. Equation (4.6) can be used to obtain the displacement limit

$$\mathrm{h_c} < \frac{R_p}{\tan\theta}\sqrt{\frac{2}{3\mathrm{C_p}}} \tag{4.16}$$

As can be seen the maximum contact depth is a function of particle radius R_p, semi-cone angle θ and the normalized hardness of the particle material $\mathrm{C_p} = \mathrm{H_p}/\mathrm{Y_p}$. This supports the common knowledge that believes sharper indents can go deeper on a film/substrate system. Equation (4.4) also can be used to come up with a maximum limit on the load if the hardness of particle is desired to be measured without any influence from the matrix:

$$\mathrm{P} < \frac{2\pi}{3} Y_p {R_p}^2 \tag{4.17}$$

The force limit as can be seen in equation (4.17) is a function of yield stress of particle Y_p and its radius R_p. These conclusions are valid only so long as the plastic region is confined to the particle. For the cases that the particle is harder than the matrix, another condition should also be satisfied, which avoids indentation of the particle into matrix. This condition can be simply expressed as:

$$\mathrm{P} < \pi H_m {R_p}^2 \tag{4.18}$$

or simply

$$Y_p < \frac{3}{2} H_m \tag{4.19}$$

Therefore, if the yield stress of the particle is more than 1.5 times of hardness of the matrix, the maximum permissible contact radius would be smaller, due to indentation of the matrix by the particle.

Using the maximum possible constraint factor in equation (4.16), a conservative rule of thumb can be obtained which says the intrinsic hardness of particle is measured by nanoindentation until the contact radius reaches half of particle radius as long as condition given in equation (4.18) holds true.

For the case of modulus measurement, it was shown that fixed boundary conditions in far field affect the measured modulus even for very shallow indents. The effect of the fixed boundary on measured modulus of bulk materials is formulated by equation (4.8). The behavior of the effect of matrix properties on measured modulus of a particle/matrix is also modeled using equation (4.10). It should be noted that the data that were used to develop equation (4.10) are the modulus of matrix and particle at specific contact radius and not a constant value of modulus. These two equations can be used to develop equation (4.20) for a particle/matrix configuration that includes the effect of boundary into account as well. In this equation, E_{p_0} and E_{m_0} are the intrinsic modulus of the particle and matrix respectively. Equation (4.20) yields into equation (4.8) for indentation on bulk material since the second term would be equal to one.

$$E \cong E_{p_0}(1 + bR_c)\left[1 + \left(1 - \frac{E_{p_0}}{E_{m_0}}\right)\frac{\mathrm{R_c}}{R_p}\right] \tag{4.20}$$

4.7 Conclusions

In this paper, the size of the volume sampled for hardness and modulus measurement during nanoindentation test is studied. FEA simulations of nanoindentation test on a hemispherical particle embedded in a matrix are performed and the hardness and modulus are measured as a function of penetration depth. The deviation of hardness and modulus from those of particle are monitored which reveal the size of the zones that influence hardness and modulus results. It is found that for any elastic-perfectly plastic material, the intrinsic hardness of particle is measured until the contact radius reaches half of the radius of particle and until the plastic region is still within the particle. For modulus, it is shown that no specific volume is sampled beneath the indenter and the modulus measured by nanoindentation actually represents the elastic response of the entire specimen. It is shown that even for indentation on homogenous bulk material, the effect of the fixed boundary conditions in far field can be seen on indentation modulus, and the magnitude of the effect is a function of the contact radius and the model radius. A relationship is developed that shows the effect of matrix on resultant indentation modulus at low depths of

penetration for hemispherical particle/matrix system. The relation shows the specific dependency of the modulus on ratio of R_c/R_p and E_p/E_m.

4.8 References

Bec, S., A. Tonck & J. L. Loubet (2006) A simple guide to determine elastic properties of films on substrate from nanoindentation experiments. Philosophical Magazine, 86, 5347-5358.

BOLSHAKOV, A., 1996, FINITE ELEMENT STUDIES OF MECHANICAL PROPERTY TESTING BY NANOINDENTATION METHODS: PHD DISSERTATION THESIS, RICE UNIVERSITY.

Bolshakov, A. & G. M. Pharr (1998) Influences of pileup on the measurement of mechanical properties by load and depth sensing indentation techniques. Journal of Materials Research, 13, 1049-1058.

Bressan, J. D., A. Tramontin & C. Rosa (2005) Modeling of nanoindentation of bulk and thin film by finite element method. Wear, 258, 115-122.

Chen, J. & S. J. Bull (2009) On the factors affecting the critical indenter penetration for measurement of coating hardness. Vacuum, 83, 911-920.

Chen, X. & J. J. Vlassak (2001) Numerical study on the measurement of thin film mechanical properties by means of nanoindentation. Journal of Materials Research, 16, 2974-2982.

Cheng, Y. T. & C. M. Cheng (2000) What is indentation hardness? Surface & Coatings Technology, 133, 417-424.

Durst, K., M. Goken & H. Vehoff (2004) Finite element study for nanoindentation measurements on twO&Phase materials. Journal of Materials Research, 19, 85-93.

Fischer-Cripps, A. C. 2004. Nanoindentation. New York: Springer.

Han, S. M., R. Saha & W. D. Nix (2006) Determining hardness of thin films in elastically mismatched film-on-substrate systems using nanoindentation. Acta Materialia, 54, 1571-1581.

Han, S. M., R. Shah, R. Banerjee, G. B. Viswanathan, B. M. Clemens & W. D. Nix (2005) Combinatorial studies of mechanical properties of Ti-Al thin films using nanoindentation. Acta Materialia, 53, 2059-2067.

Harvey, S., H. Huang, S. Venkataraman & W. W. Gerberich (1993) MICROSCOPY AND MICROINDENTATION MECHANICS OF SINGLE-CRYSTAL FE-3 WT-PERCENT-SI .1. ATOMIC-FORCE MICROSCOPY OF A SMALL INDENTATION. Journal of Materials Research, 8, 1291-1299.

Johnson, K. L. 1985. Contact mechanics. Cambridge [Cambridgeshire] ; New York: Cambridge University Press.

Joslin, D. L. & W. C. Oliver (1990) A NEW METHOD FOR ANALYZING DATA FROM CONTINUOUS DEPTH-SENSING MICROINDENTATION TESTS. Journal of Materials Research, 5, 123-126.

KING, R. B., 1987, ELASTIC ANALYSIS OF SOME PUNCH PROBLEMS FOR A LAYERED MEDIUM: INTERNATIONAL JOURNAL OF SOLIDS AND STRUCTURES, V. 23, P. 1657-1664.

Li, H. & J. J. Vlassak (2009) Determining the elastic modulus and hardness of an ultra-thin film on a substrate using nanoindentation. Journal of Materials Research, 24, 1114-1126.

Lichinchi, M., C. Lenardi, J. Haupt & R. Vitali (1998) Simulation of Berkovich nanoindentation experiments on thin films using finite element method. Thin Solid Films, 312, 240-248.

Nagao, S., M. Fujikane, N. Tymiak & R. Nowak (2009) Achieving consistency of Young's modulus determination from nanoscale deformation of low-k films. Journal of Applied Physics, 105.

Oliver, W. C. & G. M. Pharr (1992) AN IMPROVED TECHNIQUE FOR DETERMINING HARDNESS AND ELASTIC-MODULUS USING LOAD AND DISPLACEMENT SENSING INDENTATION EXPERIMENTS. Journal of Materials Research, 7, 1564-1583.

Pelegri, A. A. & X. Huang (2008) Nanoindentation on soft film/hard substrate and hard film/soft substrate material systems with finite element analysis. Composites Science and Technology, 68, 147-155.

Poon, B., D. Rittel & G. Ravichandran (2008) An analysis of nanoindentation in linearly elastic solids. International Journal of Solids and Structures, 45, 6018-6033.

Saha, R. & W. D. Nix (2002) Effects of the substrate on the determination of thin film mechanical properties by nanoindentation. Acta Materialia, 50, 23-38.

Sakai, M. (2009) Substrate-affected indentation contact parameters of elastoplastic coating/substrate composites. Journal of Materials Research, 24, 831-843.

Sun, Y., J. Liang, Z. H. Xu, G. F. Wang & X. D. Li (2008) Nanoindentation for measuring individual phase mechanical properties of lead free solder alloy. Journal of Materials Science-Materials in Electronics, 19, 514-521.

Wang, T. H., T. H. Fang & Y. C. Lin (2007) Analysis of the substrate effects of strain-hardening thin films on silicon under nanoindentation. Applied Physics a-Materials Science & Processing, 86, 335-341.

Yu, H. Y., S. C. Sanday & B. B. Rath (1990) THE EFFECT OF SUBSTRATE ON THE ELASTIC PROPERTIES OF FILMS DETERMINED BY THE INDENTATION TEST - AXISYMMETRICAL BOUSSINESQ PROBLEM. Journal of the Mechanics and Physics of Solids, 38, 745-764.

CHAPTER 5

A NEW ITERATIVE PROCEDURE FOR ESTIMATION OF MECHANICAL PROPERTIES OF ELASTIC-PERFECTLY PLASTIC MATERIALS BY NANOINDENTATION: A PILE-UP CORRECTION METHOD

5.1 Abstract

A new iterative procedure is proposed to estimate hardness, elastic modulus, and also yield stress of a elastic-perfectly plastic material from nanoindentation load curve data. This procedure converges to accurate values independent of amount of pile-up or sink-in, which is an advantage over the classic Oliver and Pharr method. Finite element simulations have been carried out for a range of materials to study the effect of plastic index ($E_r \tan\beta\ /Y$) on the constraint factor, ratio of contact depth to the depth of penetration and the beta correction factor. It is shown that the beta correction factor remains constant for the range of material properties studied. Relations are developed to describe the contact depth ratio and the constraint factor as functions of the plastic index, $E_r \tan\beta\ /Y$. Starting with an initial value for the plastic index, the constraint factor and contact depth ratio are calculated and consequently an improved estimate of plastic index is obtained. This is used to improve the estimate of the contact depth and the constraint factor and the iteration continue until convergence is achieved. It is shown that the iterative method improves the accuracy of the estimated mechanical properties independent of the amount of pile-up.

Keywords: Nanoindentation; Finite element analysis; Hardness; Elastic behavior; Pile-up

5.2. Introduction

The main challenge in determining hardness and modulus from nanoindentation load curve data is accurate estimation of the contact area. Oliver and Pharr (1992) proposed a method for estimation of the contact depth, and by extension the contact area, that enabled hardness and modulus measurements from depth sensing indentation. However, it was shown by numerous researchers that the O&P method results in large errors in estimation of contact area for materials that exhibit pile-up around the indenter. Casals and Alcala (2005) blamed the duality in mechancial property extractions from nanoindention on the lack of a good measurement method for the amount of pile-up through further analysis of the load curve.

The paper by Cheng and Cheng (1998) was one of the first works that showed that the Oliver and Pharr (O&P) method (Oliver and Pharr, 1992) cannot be used with confidence for materials that show pile-up around the

indenter. They refined their results in a more recent work (Cheng and Cheng, 2000) and concluded that O&P is valid for highly elastic materials, $Y/E > 0.05$. For a Berkovich indenter, this can be stated in term of the plastic index as $PI < 7.16$. They also showed that as the ratio of Y/E decreases, the error of O&P method increases, and that the error is smaller for materials that work harden.

Bolshakov presented a comprehensive study correlating the amount of pile-up to the ratio of residual depth of indentation after unloading, h_f to the maximum penetration depth, h_{max} (Bolshakov, 1996; Bolshakov and Pharr, 1998). The correlation between pile-up and sink-in and the ratio of h_f/h_{max} can be seen in Figures 5.1 and 5.2. Their FEA simulations also showed that elastic perfectly plastic materials begin to show pileup for $h_f/h_{max} > 0.85$ corresponding to $Y/E < 0.012$, or $PI > 29.8$, and that significant deviation from O&P results for $h_f/h_{max} > 0.73$ corresponding to $Y/E < 0.029$, or $PI > 12.5$ (Figure 5.2). From Figure 5.2, it is also be noted that there is no pile-up for strongly work hardening materials, even at PI up to 220, and O&P method is able to track the actual contact area quite well.

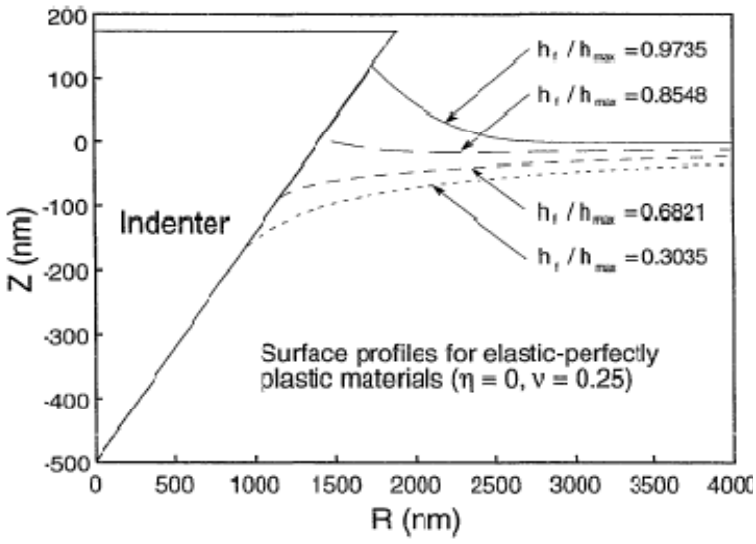

Figure 5.1. Surface profiles for various ratio of h_f/h_{max} for elastic-perfectly plastic materials. (Bolshakov, 1996)

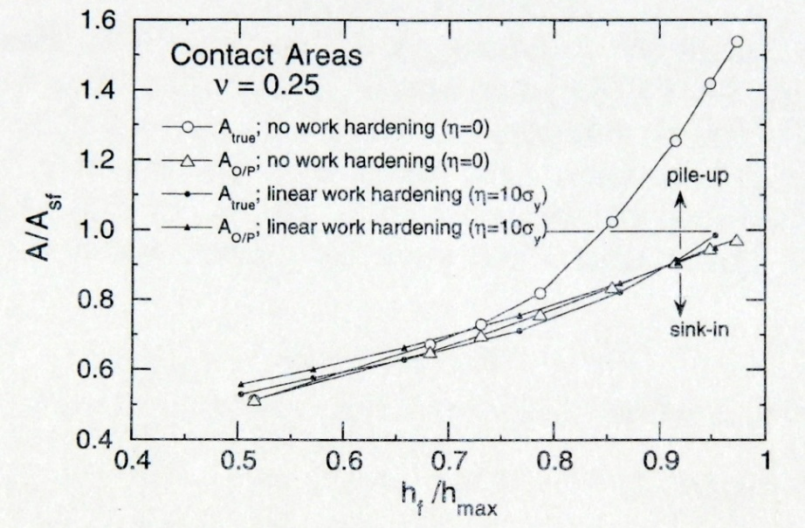

Figure 5.2. Normalized contact area for various ratio of h_f/h_{max}. The contact areas are normalized with respect to area from indenter shape function evaluated at the maximum depth of penetration.(Bolshakov and Pharr, 1998)

Shu et al. (2007) proposed a different approach for accounting for error caused by pile-up, taking both the ratio of E/Y of the material and the work hardening exponent into consideration. They carried out a large number of FEA studies for different ratios of E/Y, as well as different work hardening exponents for two different cone angles. They used the loading curvature and the work done by the indenters to obtain E/Y and n from indentation load curves. Then they used E/Y and n ratios to look up the amount of error of O&P method for estimation of hardness and modulus. The relative errors of the hardness and modulus of O&P method with respect to outcome of their FEA results are shown in Figure 5.3 and 5.4 respectively.

Kese and Li (2006) proposed a method for accounting for the pile-up by considering the added pile-up contact area as semi-ellipses around Berkovich triangular impression. This was done by post AFM scanning of the indented surface and measurement of the pile-up contact width for each of the three possible pile-up lobes. Lee et al. (2007) proposed a different approach by measuring the modulus of the material from early Hertzian loading analysis and using it to predict the pile-up. Some recent works in this field have reported study of pile-up around spherical indenters (Taljat and Pharr, 2004), spherical-conical indenters (Maneiro and Rodriguez, 2005), and also the effect of pile-up on thin film system measurements (Zhou et al., 2008).

In this article, a new iterative method is proposed that uses the observed dependence of the constraint factor and the contact height ratio (h_c/h_{max}) on the plastic index, to obtain the hardness, modulus and also yield stress independent from O&P method.

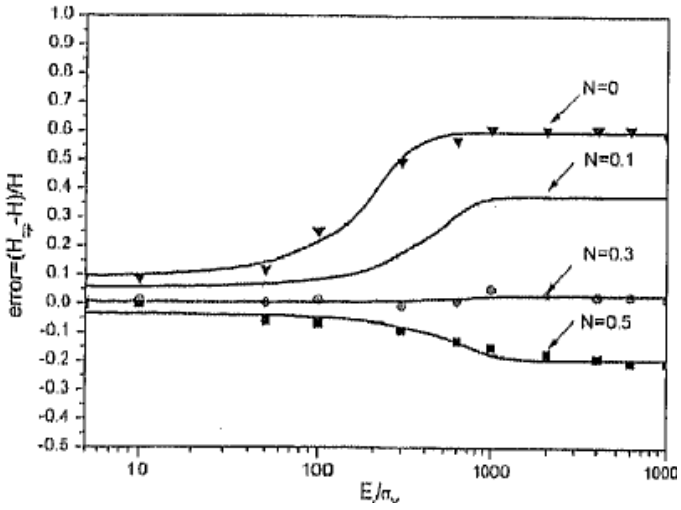

Figure 5.3. The error in the hardness obtained from O&P method. (Shu et al., 2007)

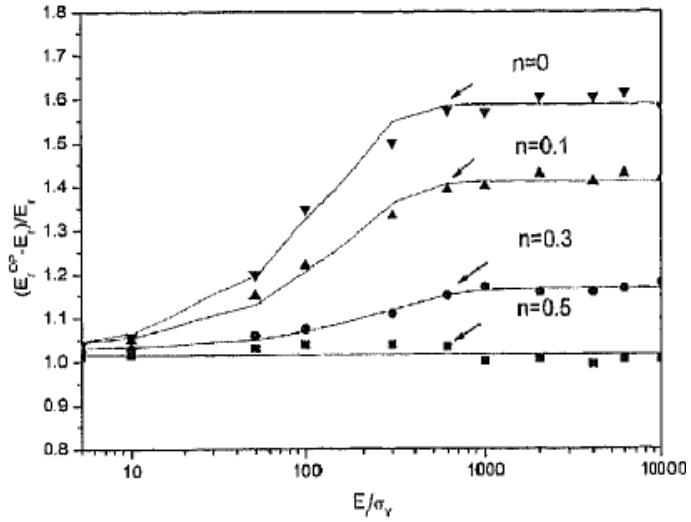

Figure 5.4. The error in the modulus obtained from O&P method. (Shu et al., 2007)

5.3. Finite element simulations

2D axisymmetric finite element simulations of conical indentation are carried out in ABAQUS/Standard. The specimen is modeled as a hemisphere, discretized using linear fully integrated elements (CAX4) and meshed with a constant gradient of element size such that the size of the elements increases linearly with radius ($L_e = R_c/188$), so that the error in contact area is below 1% for all indentation depths of interest. The indenter is modeled as an analytical rigid surface with semi-cone angle of 70.3º, which has an area function equivalent to that of the

Berkovich indenter. Frictionless contact is used between the indenter and the surface of the specimen and fixed boundary conditions are applied at the outer radius of the specimen.

The material is assumed to be elastic-perfectly plastic, and several simulations are performed for different E/Y ratios. Elastic modulus is kept constant at 70GPa and the Poisson's ratio is taken to be 0.25. The yield stress of the materials are varied between 114.25MPa to 26620MPa, using the same values as used by Bolshakov (1996), to cover a broad range of plastic indices ($PI = E_r \tan\beta\ /Y = 1..234$, where E_r is the reduced elastic modulus, β is the angle between the cone surface and specimen i.e. 90-θ, where θ is the semi-cone angle; β=19.7° for equivalent cone of Berkovich and Y is the yield stress). Simulations were performed to an indentation depth, h_{max}, of 20nm and then unloading the indenter by 0.1nm. The load curves for these simulations are shown in Figure 5.5. As noted earlier (chapter 3), though the unloading depth is very small, it is sufficient to obtain the stiffness accurately. To obtain true hardness for each material, maximum load and true projected contact area at maximum load are used from FEA results. Inputs and outputs of the simulations are listed in Table 5.1.

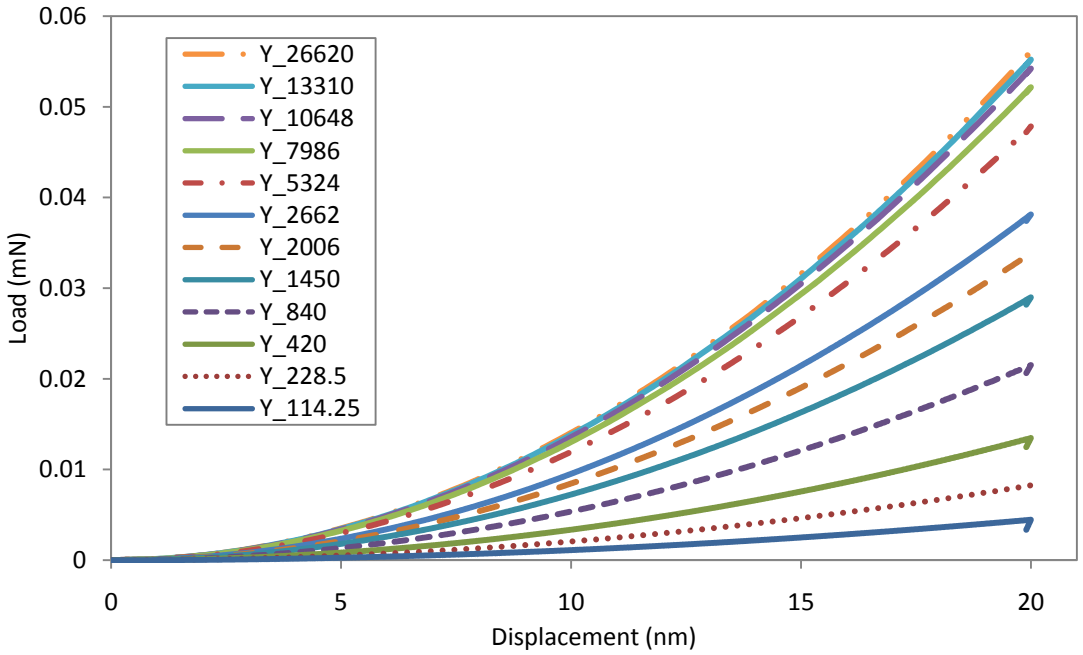

Figure 5.5. Load curves from the FEA simulations of nanoindentation for the range of the materials for loading up to 20nm penetration and 0.1nm unloading for determination of stiffness at maximum load.

Figure 5.6 shows the dependence of constraint factor (normalized hardness, H/Y) on the plastic index ($E_r \tan\beta\ /Y$) as obtained from our FEA results. This is very close to the results of Bolshakov (1996). Sakai (2009) also obtained similar results and developed an elastoplastic Maxwellian model that describes the normalized

hardness as a function of the plastic index over the entire range from purely elastic deformation to fully ductile. Their equation is given as:

$$\frac{H}{Y} = \frac{C}{\left[1 + \left(\frac{2C}{E_r \tan\beta / Y}\right)^{1/n}\right]^n} \tag{5.1}$$

where they suggested $C = 2.65$ and $n = 2/3$ to best match their FEA results.

As can be seen in Figure 5.6, the equation (5.1) suggested by Sakai does not fit well to the FEA results from this work. Therefore equation (5.1) is modified to a more general form of

$$\frac{H}{Y} = \frac{C_1}{\left[1 + \left(\frac{C_2}{E_r \tan\beta / Y}\right)^{1/n}\right]^n} \tag{5.2}$$

where constants were determined by numerically fitting equation (5.2) to the FEA data; $n = 2/3$, C_1=2.62 and C_2=4.1 resulted in least mean square error.

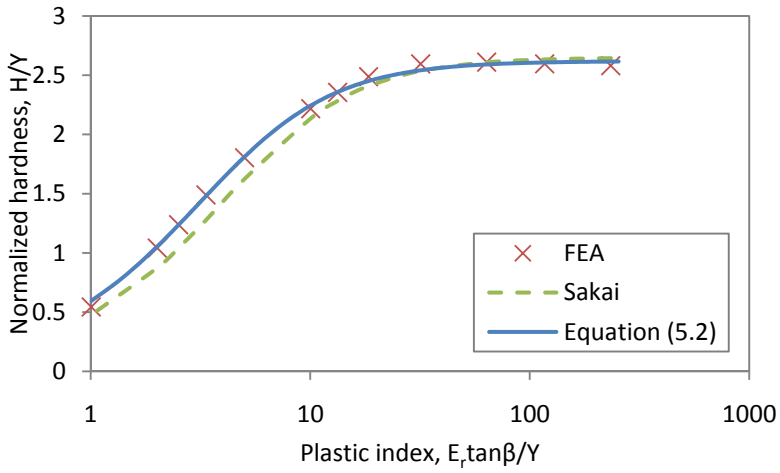

Figure 5.6. Normalized hardness vs. plastic index for FEA results, Sakai Maxwellian model and from equation (5.2)

TABLE 5.1

PROPERTIES OF THE MATERIALS MODIFIED AND THE RESULTS OBTAINED FROM FEA

Inputs					Results			
Material	Y (Mpa)	E (Gpa)	E_r (Gpa)	$E_r tan\beta/Y$	A_c_FEA (μm²)	P_{max} (mN)	Hardness (Gpa)	Stiffness (mN/nm)
Y_114.25	114.25	70	74.67	234.000	0.015	0.004	0.295	0.0110
Y_228.5	228.5			117.000	0.014	0.008	0.593	0.0106
Y_420	420			63.654	0.012	0.013	1.096	0.0100
Y_840	840			31.827	0.010	0.022	2.180	0.0089
Y_1450	1450			18.438	0.008	0.029	3.606	0.0080
Y_2006	2006			13.327	0.007	0.034	4.723	0.0076
Y_2662	2662			10.043	0.006	0.038	5.902	0.0072
Y_5324	5324			5.022	0.005	0.048	9.602	0.0063
Y_7986	7986			3.348	0.004	0.052	11.892	0.0059
Y_10648	10648			2.511	0.004	0.054	13.189	0.0057
Y_13310	13310			2.009	0.004	0.055	13.860	0.0057
Y_26620	26620			1.004	0.004	0.056	14.478	0.0056

The O&P method (Oliver and Pharr, 1992) is used for processing the data to determine the hardness and modulus so that these values can be compared to the true values obtained from FEA. Equation (5.3) is the basis of O&P method that estimates the contact depth h_c as a function of maximum depth of penetration h_{max}, maximum load P_{max}, and stiffness at the maximum load S. The constant ε is a geometrical constant suggested to be equal to 0.75 for conical indentation based on the experimental work. Knowing the contact depth, the projected contact area $A_{c\,proj}$ can be determined from the geometry of the indenter (θ being the semi-cone angle) as:

$$h_c = h_{max} - \varepsilon \frac{P_{max}}{S} \tag{5.3}$$

$$A_{c\,proj} = \pi h_c^2 \tan^2\theta \tag{5.4}$$

The hardness can be calculated from equation (5.5), and reduced elastic modulus E_r from Sneddon's equation (5.6) where β is a constant that depends primarily on the geometry of the indenter which is assumed equal to 1 for the sake of comparison (Oliver and Pharr, 1992). Having the reduced elastic modulus, one can determine the modulus of the specimen using equation (5.7), where the indenter's modulus E_i, its Poisson's ratio ν_i, and the specimen's Poisson's ratio ν_s are known. In the case of rigid indenter, the second term simply is zero.

$$H = \frac{P_{max}}{A_{c\,proj}} \tag{5.5}$$

$$E_r = \frac{1}{2\beta}\frac{\sqrt{\pi}}{\sqrt{A_{c\,proj}}}S \tag{5.6}$$

$$\frac{1}{E_r} = \frac{1\text{-}\nu_s^2}{E_s} + \frac{1\text{-}\nu_i^2}{E_i} \tag{5.7}$$

Since the accuracy of hardness and modulus estimated by O&P method depends on the accuracy of determination of the contact area, which in turn directly depends on the accuracy of determination of contact height h_c, the true contact area FEA and used to determine the true contact depth using equation (5.4). Figure 5.7 compares the ratio of contact depth to the maximum depth of penetration obtained from FEA with that from the O&P method (equation 5.3) for different values of the plastic index. It can be seen that, O&P does not predict the contact area at large values of the plastic index (PI>10) where there is pile-up around the indenter. These results match the findings of Bolshakov (1996) and Chen and Vlassak (2001). Figure 5.7 also show that equation (5.7), which is similar to equation (5.3) but has different constants, reproduces the FEA observations faithfully.

$$\frac{h_c}{h_{max}} = C_1 + \frac{C_2}{\left[1 + \left(\frac{C_3}{E_r \tan\beta\,/Y}\right)^{1/n}\right]^n} \tag{5.8}$$

The purely elastic solution of conical indentation on an elastic material presented by Sneddon leads to h_c/h_{max} =2/π=0.637 (Hay et al., 1999). Chen and Vlassak (2001) showed through FEA simulations that h_c/h_{max} varies between 0.64 and 1.26. Assuming the same numbers for fitting the data, the constants C_1=0.64 for $Y = \infty$ (purely elastic) and C_2=0.62 for $Y = 0$ (Perfectly plastic) would be known. The numerical solution results in C_3=36 and $n = 2/3$ as the best fit to FEA data as shown in Figure 5.7. The main reason for lack of good agreement between equation (5.8) and FEA results our forcing the fit so that the elastic solution is not violated.

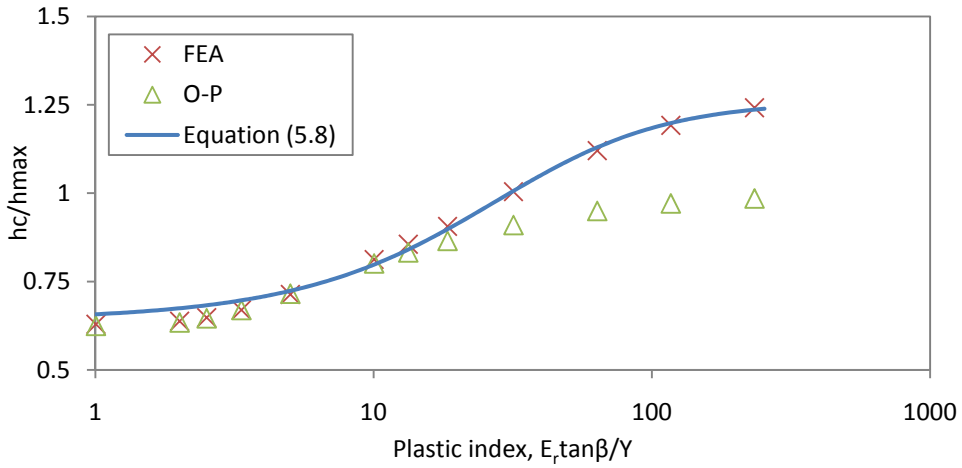

Figure 5.7. The ratio of contact depth to the maximum depth of penetration from FEA , O&P and equation (5.8)

Figure 5.8 shows the true value of β that gives the exact input value for modulus as a function of plastic index. It can be seen that changes in β are negligible for the range of properties studied. Therefore the constant value of 1.065 is used for the iterative procedure. This number is close to the values reported in the literature (Hay et al., 1999; Shim et al., 2007; Strader et al., 2006).

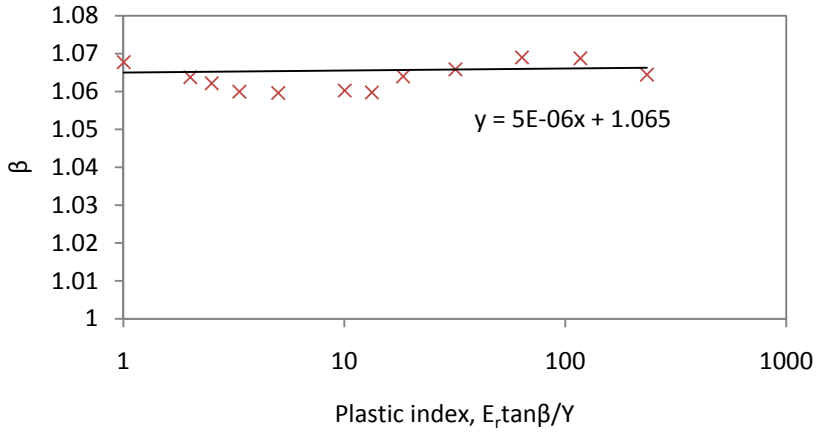

Figure 5.8. The true β value obtained from FEA results.

5.4 A new iterative procedure to obtain H, E and Y

A new iterative procedure is developed, utilizing the effect of the plastic index on the constraint factor and the contact height ratio (equations 5.2 and 5.8) to estimate hardness, modulus and yield stress of an elastic-perfectly plastic material. The objective of the iteration is to find a combination of H, E_r and Y that satisfies equations (5.2) and (5.8). As can be seen in the flowchart of the procedure in Figure 5.9, the only input for the calculations are the maximum load, maximum depth of penetration, and the stiffness of the unloading curve at maximum load. To begin

the iterative loop, an initial value should be assumed for E_r/Y, e.g. $E_r/Y = 1$ and the plastic index (PI) should be calculated. As shown later, the convergence of the solution is independent of this initial value, but the closer the initial value is to the actual ratio, the faster the procedure would converge. For this plastic index, constraint factor H/Y and contact height ratio h_c/h_{max} can be calculated from equations (5.2) and (5.8) respectively. Then calculated h_c/h_{max} can be used to estimate the projected contact area since the cone angle and maximum depth of penetration are known. Based on the estimated projected contact area, the hardness (H) and reduced modulus (E_r) are calculated from equations (5.5) and (5.6). The new hardness and the current estimate of the constraint factor H/Y are used to calculate the estimated yield stress (Y) using the estimated value of Y and E_r, a new value of the ratio of E_r/Y is estimated and compared with the old ratio to check for convergence of the iterations. If the ratio has not converged to a constant value, a new iteration is performed beginning with the new ratio of E_r/Y as shown in the flowchart in Figure 5.9. The values of H, E_r and Y when convergence is achieved are the final estimates determined by this procedure.

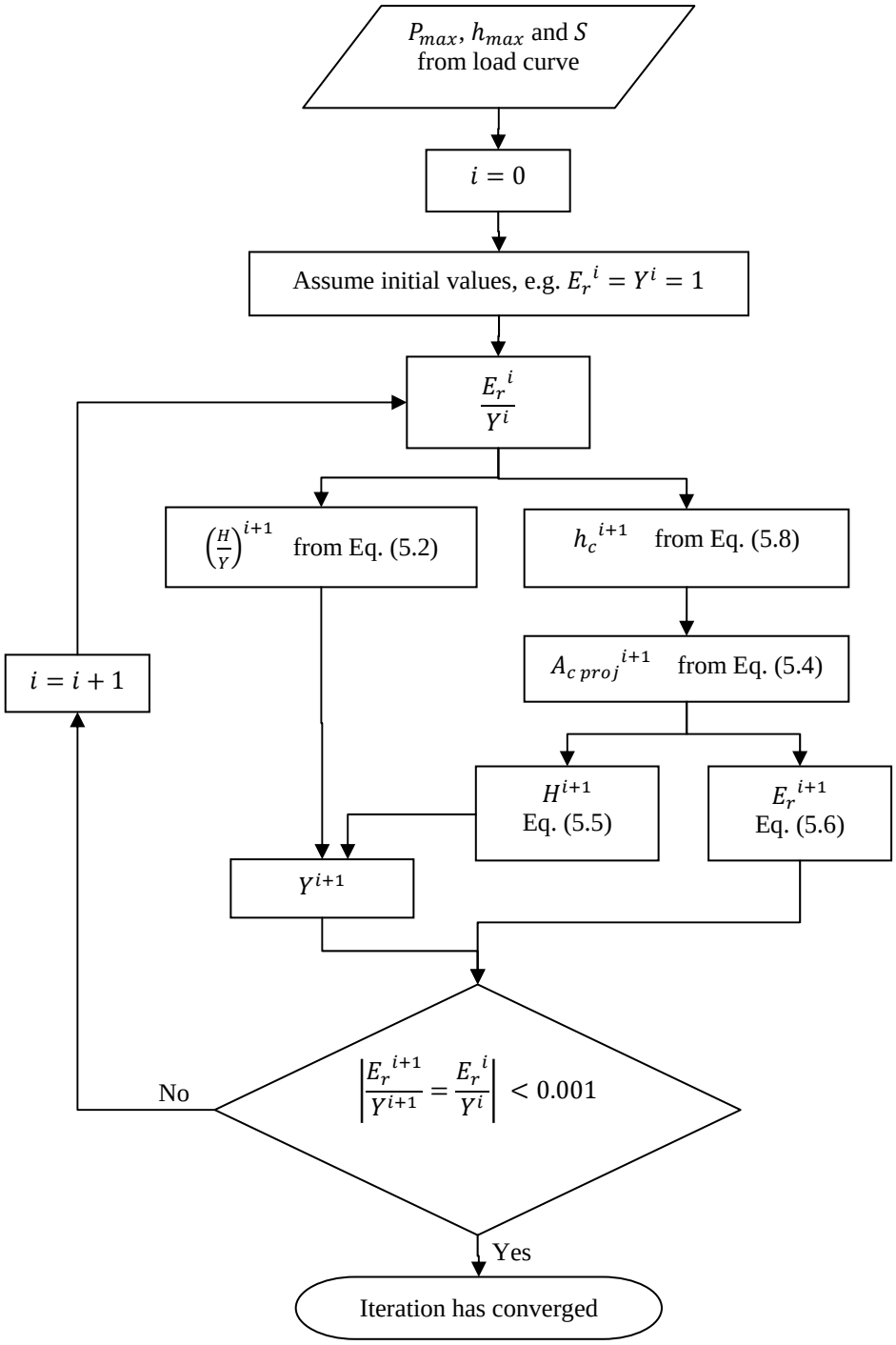

Figure 5.9. Flowchart of the iterative procedure for determining the hardness, modulus, and the yield stress

5.5. Results

The effectiveness of the proposed method is demonstrated in Figures 5.10, 5.11 and 5.12 for the error in hardness, modulus, and yield stress of which the first two can be compared with the results of O&P method. It can be seen that the proposed iterative method improves the estimation of hardness and modulus compared to the Oliver

and Pharr method and also gives a good estimation of the yield stress for all values of plastic index greater than 10. For instance, for the worst case (Y=114.25MPa), while the O&P method results in 58.9% hardness error and 26.0% modulus error, the iterative method results in 0.5% and 0.2% error in hardness and modulus, respectively. For plastic indices smaller than 10, O&P method yields in good agreement with expected values, which makes the use of the iterative method unnecessary.

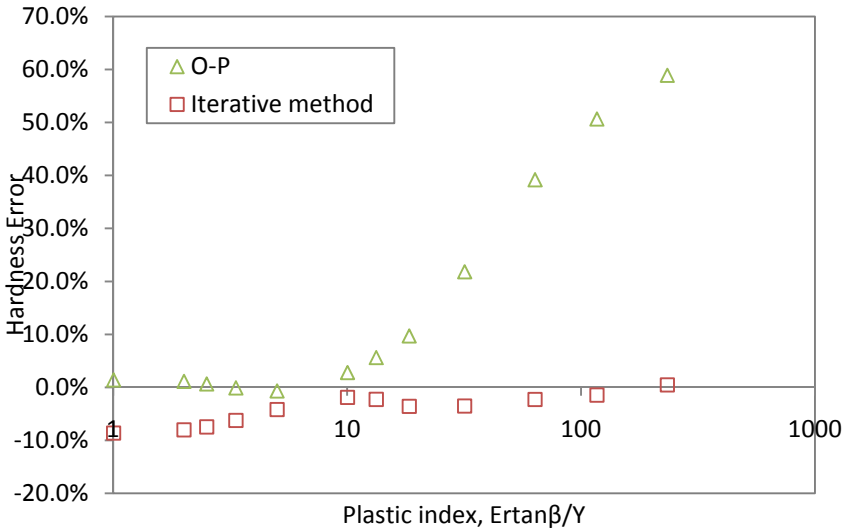

Figure 5.10. Hardness error with respect to the expected value vs. plastic index for the developed iterative method and the O&P method

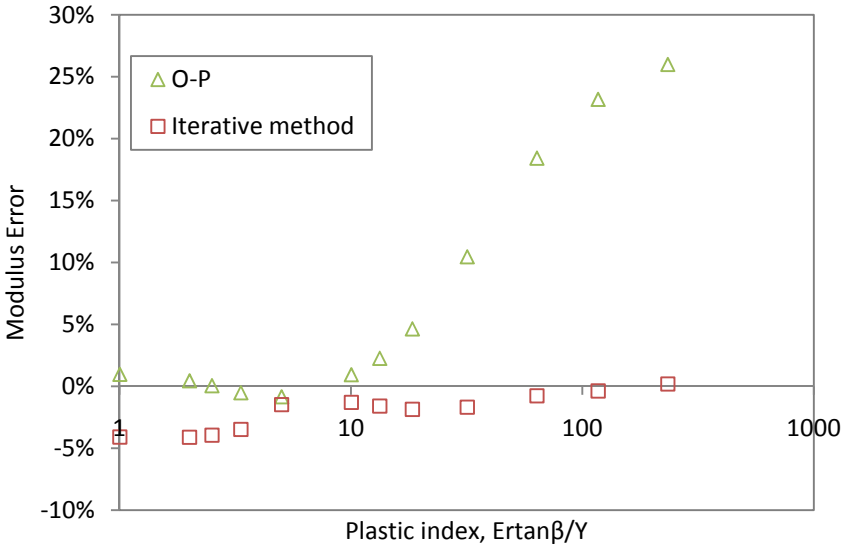

Figure 5.11. Modulus error with respect to the expected value vs. plastic index for the developed iterative method and the O&P method

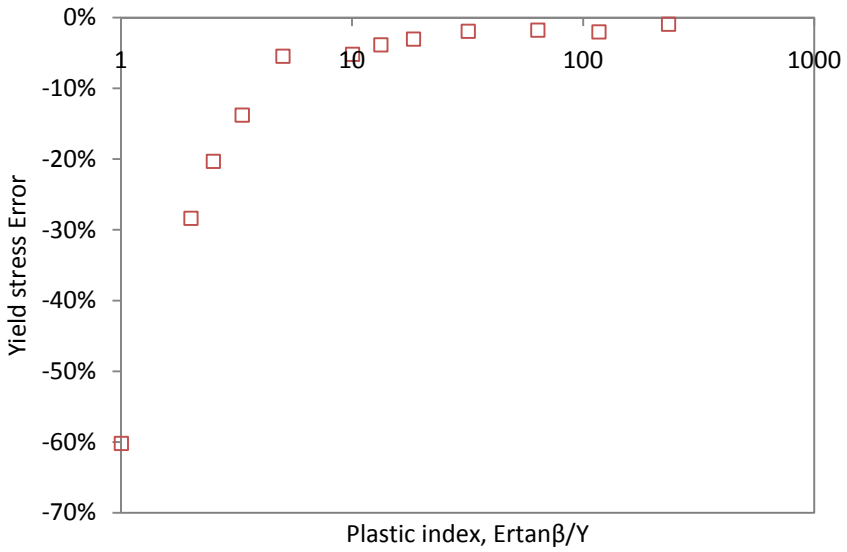

Figure 5.12. Yield stress error vs. plastic index for the developed iterative method

5.6. Discussion

This iterative approach converged for all cases, but the number of iterations, with the initial value of $E_r/Y = 1$ is plotted against the plastic index in Figure 5.13. It can be seen that the number of iterations increases as the plastic index decreases. The convergence path on normalized hardness graph and h_c/h_{max} graph for three cases are shown in Figure 5.14 and 5.15. Additionally, it is noted that the actual value of the plastic index is slightly different from the value to which the iteration converges.

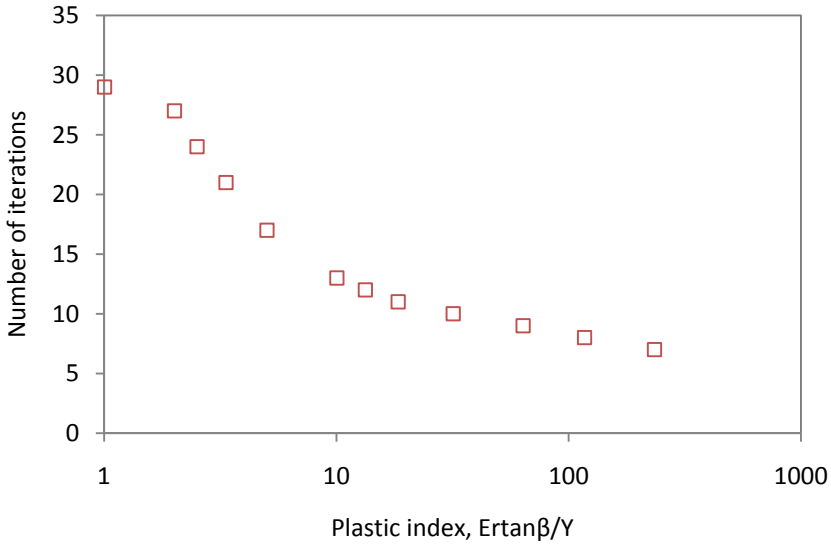

Figure 5.13. The number of iterations to converge to definite values vs. plastic index

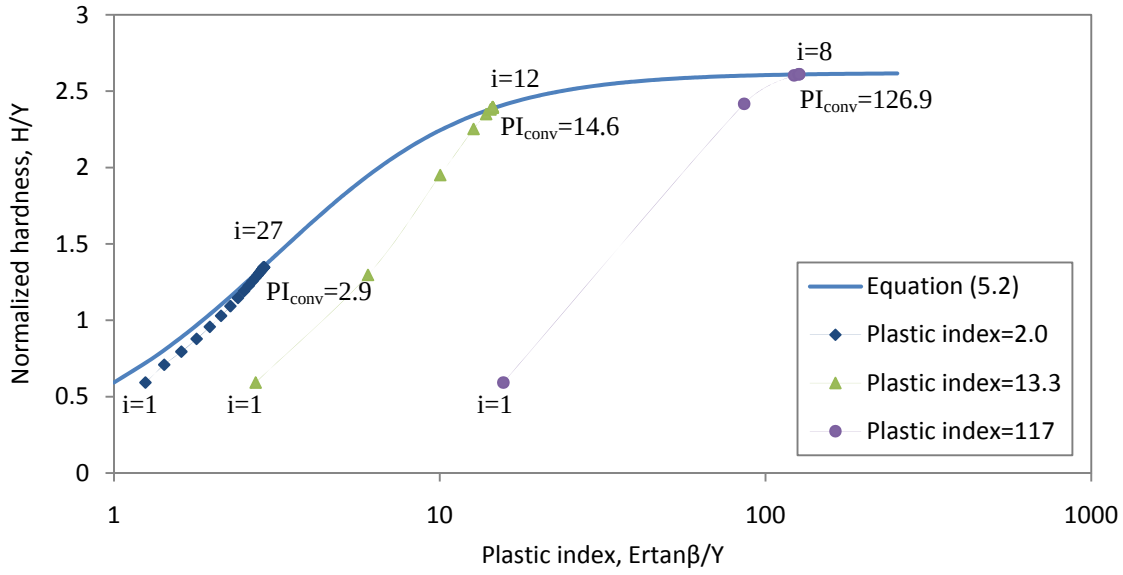

Figure 5.14. The convergence path on H/Y curve vs. plastic index for three cases. The first iteration and last iteration is shown for each path.

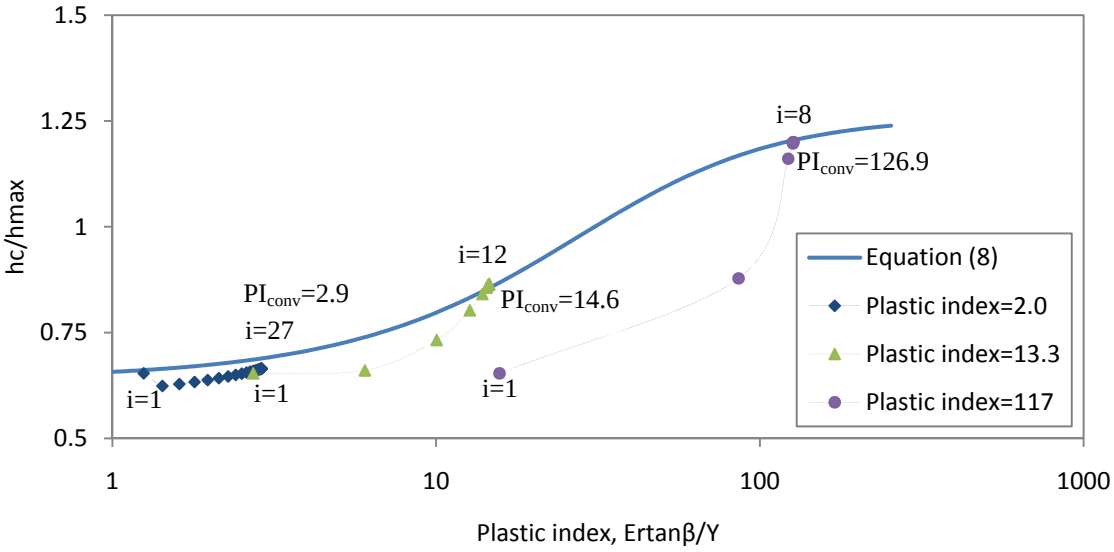

Figure 5.15. The convergence path on h_c/h_{max} curve vs. plastic index for three cases. The first iteration and last iteration is shown for each path.

5.7. Conclusions

A new iterative procedure is developed to estimate hardness, elastic modulus, and also yield stress from a single nanoindentation load curve data. This procedure is insensitive to pile-up and can be used for the cases the Oliver and Pharr method does not estimate the contact area due to pile-up. This method is developed for elastic-perfectly plastic material and is expandable to other materials types. This procedure converges to accurate values of

hardness, elastic modulus, and yield stress independent of the amount of pile-up or sink-in. It is shown from FEA that the beta correction factor to the Sneddon's equation remains constant for the studied range of materials; however, the contact depth ratio and the constraint factor vary for different plastic indices, $E_r \tan\beta\,/Y$. It is found that the proposed iterative method improves the estimation of hardness and modulus compared to the Oliver and Pharr method and also gives a good estimation of the yield stress for materials with plastic index greater than 10. For the case with maximum pile-up, the iterative method results in less than 1% error while O&P results in 59% hardness error and 26% modulus error.

5.8. References

Bolshakov, A. 1996. Finite element studies of mechanical property testing by nanoindentation methods. Rice University.

Bolshakov, A. & G. M. Pharr (1998) Influences of pileup on the measurement of mechanical properties by load and depth sensing indentation techniques. Journal of Materials Research, 13, 1049-1058.

Casals, O. & J. Alcala (2005) The duality in mechanical property extractions from Vickers and Berkovich instrumented indentation experiments. Acta Materialia, 53, 3545-3561.

Chen, X. & J. J. Vlassak (2001) Numerical study on the measurement of thin film mechanical properties by means of nanoindentation. Journal of Materials Research, 16, 2974-2982.

Cheng, Y. T. & C. M. Cheng (1998) Effects of 'sinking in' and 'piling up' on estimating the contact area under load in indentation. Philosophical Magazine Letters, 78, 115-120.

Cheng, Y. T. & C. M. Cheng (2000) What is indentation hardness? Surface & Coatings Technology, 133, 417-424.

Hay, J. C., A. Bolshakov & G. M. Pharr (1999) A critical examination of the fundamental relations used in the analysis of nanoindentation data. Journal of Materials Research, 14, 2296-2305.

Kese, K. & Z. C. Li (2006) Semi-ellipse method for accounting for the pile-up contact area during nanoindentation with the Berkovich indenter. Scripta Materialia, 55, 699-702.

Lee, Y. H., U. Baek, Y. I. Kim & S. H. Nahm (2007) On the measurement of pile-up corrected hardness based on the early Hertzian loading analysis. Materials Letters, 61, 4039-4042.

Maneiro, M. A. G. & J. Rodriguez (2005) Pile-up effect on nanoindentation tests with spherical-conical tips. Scripta Materialia, 52, 593-598.

Oliver, W. C. & G. M. Pharr (1992) AN IMPROVED TECHNIQUE FOR DETERMINING HARDNESS AND ELASTIC-MODULUS USING LOAD AND DISPLACEMENT SENSING INDENTATION EXPERIMENTS. Journal of Materials Research, 7, 1564-1583.

Sakai, M. (2009) Substrate-affected indentation contact parameters of elastoplastic coating/substrate composites. Journal of Materials Research, 24, 831-843.

Shu, S. Q., J. Lu & D. F. Li (2007) A systematic study of the validation of Oliver and Pharr's method. Journal of Materials Research, 22, 3385-3396.

Strader, J. H., S. Shim, H. Bei, W. C. Oliver & G. M. Pharry (2006) An experimental evaluation of the constant ss relating the contact stiffness to the contact area in nanoindentation. Philosophical Magazine, 86, 5285-5298.

Taljat, B. & G. M. Pharr (2004) Development of pile-up during spherical indentation of elastic-plastic solids. International Journal of Solids and Structures, 41, 3891-3904.

Zhou, X. Y., Z. D. Jiang, H. R. Wang & R. X. Yu (2008) Investigation on methods for dealing with pile-up errors in evaluating the mechanical properties of thin metal films at sub-micron scale on hard substrates by nanoindentation technique. Materials Science and Engineering a-Structural Materials Properties Microstructure and Processing, 488, 318-332.

CHAPTER 6

CONCLUSIONS AND FUTURE WORK

6.1 Conclusions

In the following, we summarize the important results detailed in this dissertation and show how, taken together, they help improve experimental and FEA nanoindentation studies.

As described in chapter 2, one of the parameters that can introduce error in the mechanical properties determined by nanoindentation is presence of sample tilt. 3D FEA of conical indentation on tilted samples of materials which show pile-up or sink-in around the indenter reveals that:

- the boundary of contact lies along a plane,
- this plane is nearly parallel to the surface of the tilted specimen,
- the contact depth, measured as the distance between the indenter tip and the intersection of the axis of the indenter with the plane containing the boundary of contact, is independent of tilt angle.

The above observations justify the use of a geometrical correction for compensating for the effect of sample tilt. The analytical area function equation is obtained for conical and pyramidal indentation into tilted sample and it is shown that the contact area increases faster with contact depth than that on non-tilted surfaces. The geometric correction can be applied by simply multiplying the usual area function of ideal indentation by a correction factor given in equation (6.1) and (6.2), for conical and pyramidal indentation.

$$\frac{A_{tilted}}{A_{ideal}} = (1 - \tan\theta^2 \tan\eta^2)^{-1.5} \tag{6.11}$$

$$\frac{A_{tilted}}{A_{ideal}} = (1 - 3\tan^2\varphi \tan^2\eta - 2\tan^3\varphi \tan^3\eta \cos 3\zeta)^{-1} \tag{6.2}$$

where θ is semi-cone angle, φ is the pyramid face angle, η is the sample tilt angle, and ζ is the rotation angle of the pyramidal indenter with respect to tilt direction. The first two are known from geometry of the indenter and the two later can be obtained from surface scans of the indentation impression.

The accuracy of the area function for tilted indentation is verified by the results of 3D FEA of nanoindentation of tilted samples. If the sample tilt is not taken into account and the standard area function is used, the contact area would actually be underestimated, leading to overestimation of the hardness and modulus. For indentation with a cone of semi-cone angle 70.3º, with area function equivalent to the Berkovich indenter, on a

specimen tilted five degrees, the contact area is underestimated by 8%, leading to 8% overestimation in hardness and 4% overestimation in modulus which would be perfectly corrected for if the proposed correction factor is applied. The presented results improves the understanding about the effect of sample tilt since a previous study reported approximately 100% underestimation of contact area, 130% overestimation of hardness, and 50% overestimation of elastic modulus (Xu and Li, 2007).

The results are experimentally validated by performing Berkovich nanoindentations on ideally mounted fused silica and on tilted one. It was shown that the proposed correction method reduces the induced error if the indenter is infinitely stiff in horizontal direction. It was shown experimentally that lack of infinite stiffness in horizontal direction causes side creep during indentation which leads to even less sensitivity of results to tilt angle.

The findings of chapter 3 facilitate the design of a mesh that results in a known amount of error in the pre-designed range of depths of penetration. This would enable FEA study of a parameter that affects the mechanical properties as the depth of indentation varies. The study also improves the understanding of various sources of error in finite element analysis of nanoindentation test in order to obtain the true mechanical properties of a material with given plastic and elastic properties.

In comparison with small errors arising from the convergence tolerance of the iterative solution process, errors due to discretization are found to be significant. Errors due to discretization arise from discrete jumps in contact area as each additional surface element comes into contact, and from higher indentation forces required for plastic deformation of larger element near the boundary of contact. It is shown that a graded mesh, that permits self-similar growth of the displacement strain field with increase in indentation depth, can be used to keep the percentage error in hardness due to discretization constant at pre-set values. It is shown that sudden jumps in projected contact area because of a new node coming into contact can be obtained as a function of element size L_e at contact radius R_c for a cone with semi-cone angle of θ. This inverse translation of this error to hardness error is verified in this work.

$$\frac{\Delta A}{A} = 2\frac{L_e \sin\theta}{R_c} \tag{6.3}$$

It is also found that the hardness can be measured very close to the true hardness even from a coarse mesh if the step size is controlled around the point where a new node comes into contact as long as the mesh is capable of conforming to deformation geometry. It is also found that the maximum of all hardness values obtained from any mesh is the best measure of the hardness, and not the average of them only and only if the plastic region is completely formed.

It is also shown that results obtained from different meshes with different pre-set error percentages can be extrapolated to determine the exact value of hardness that will be obtained with infinitesimally small elements. Using this approach, true hardness for a given set of elastoplatic properties commonly used for fused silica is determined to within 0.01%, 100 times more accurately than in earlier work. This extrapolation approach is also applied for calculation of precise values of the ε correction factor used in the O&P method for estimation of contact depth and of the β correction factor in Sneddon's equation. This extrapolation approach is broadly applicable to problems where errors from mesh discretization can be quantified and controlled.

The interesting study of the volume sampled underneath nanoindenter for hardness and modulus measurements given in chapter 4 was made possible by using the results of chapter 3. The comprehensive study improves the understanding of measurement of mechanical properties in a dual phase system with slight variation of properties between particle and matrix. A locally damaged region in a bulk material is a good example of such systems.

This study is done by simulating nanoindentation test on a hemispherical particle embedded in a matrix with properties close to that of particle. By monitoring the deviation of hardness and modulus from those of particle as the depth of penetration increases, the zone of influence on hardness results and modulus results are identified. In order to generalize the conclusions of the study over a range of properties, the simulations are performed on two material systems, one of which sinks in and the other piles up around the indenter.

It is found that the intrinsic hardness of particle is measured by nanoindentation as long as the plastically deformed region is within the particle, which is satisfied so long as equation (6.4) holds true. This condition is simplified to a conservative rule of thumb using the maximum constraint factor value, which says the intrinsic hardness of particle is measured so long as the radius of contact is less than one half the radius of the particle. However, it is shown that, if the yield stress of the particle is more than 1.5 times of hardness of the matrix (equation 6.6), the maximum permissible contact radius would be smaller, due to indentation of the matrix by the particle (equation 6.5).

$$\mathrm{h_c} < \frac{R_p}{\tan\theta}\sqrt{\frac{2}{3\mathrm{C}}} \tag{6.4}$$

$$\mathrm{P} < \frac{2\pi}{3} Y_p {R_p}^2 \tag{6.5}$$

$$Y_p < \frac{3}{2} H_m \tag{6.6}$$

For measurement of modulus of elasticity it is shown that no specific volume is sampled beneath the indenter and the measured modulus by nanoindentation method actually represents the elastic response of the entire specimen at the indentation point.

It is shown that even for indentation on homogenous bulk material; the effect of fixed boundary condition in far field can be seen on indentation modulus. A relationship is developed that shows the effect of boundary conditions and matrix on resultant indentation modulus at low depths of penetration for hemispherical particle/matrix system in equation (6.7). The relation shows the specific dependency of the modulus on boundary effects and the dependency on ratio of R_c/R_p and E_p/E_m for matrix effects. The equation is valid for small values of $(R_c/R_p)(E_p/E_m)$.

$$E \cong E_{p_0}(1 + bR_c)\left[1 + \left(1 - \frac{E_{p_0}}{E_{m_0}}\right)\frac{\mathrm{R_c}}{R_p}\right] \tag{6.7}$$

The fifth chapter of the dissertation explains development of a new iterative method that estimates the hardness, modulus and yield stress of the material from load curve of a single indent. This is a very useful method since it works very well for the range of materials that show pile-up around the indenter.

Finite element simulations have been carried out for a range of materials to study the variations of constraint factor, ratio of contact depth to the depth of penetration and the beta correction factor in Sneddon's equation. It is shown that the beta correction factor remains constant for the studied range of materials; however, the contact depth ratio and the constraint factor vary for different plastic indices, $E_r \tan\beta\ /Y$.

It is found that the proposed iterative method improves the estimation of hardness and modulus compared to the Oliver and Pharr method and also gives a good estimation of the yield stress for materials with plastic index greater than 10. For the case with maximum pile-up, the iterative method results in less than 1% error while O&P results in 59% hardness error and 26% modulus error.

6.2 Future work

Nanoindentation test method is relatively a young and active research field in mechanics. There are numerous issues that need to be addressed in great detail to improve the applicability of this method to different cases. In this section, some future work is suggested to extend the findings in this dissertation.

In regard with sample tilt studies, a calibration method for measurement of side stiffness of the indenter's stem and the transducer that results in complicated creep behavior of the material is needed. Further studies can result in generation of knowledge about side creep effects on final results. This can be used to introduce nanoindentation as a method to measure mechanical properties on a significantly tilted sample. Further FEA and experimental studies on the effect of side stiffness of the indenter's stem and the transducer are required for such applications. The first step in this study would be the use of two-dimensional transducers that makes the measurement of side force possible. Two-dimensional transducers are commercially available and are mostly used for scratch tests. Having the load curved in both directions during indentation on a tilted sample, would give much more information about the amount of creep and its effects on measured properties. This can lead to development of stiffness correction relations to improve the accuracy of nanoindentation test.

To study the accuracy of results of FEA of nanoindentation further, one can use infinite boundary conditions to compare the effect of boundaries on measured modulus. The other interesting study that can be carried out by designing new FEA simulations is the study of the effect of mesh distortion. This can be done by remeshing and rezoning to new meshes which will help to understand this effect on the extracted parameters. It is also of value to address the issues of simulation of indentation of indenters with small cone angles since very large distortion was observed in the mesh, especially for the case of frictionless contact.

It would be of value to validate the results of dual phase studies experimentally. The expansion of relations for various material combinations would be also of great value for the use of nanoindentation test in an actual dual phase specimen. A ferrite/pearlite system would be a good candidate to develop the method for and study the applicability of the findings.

Further study on the proposed iterative procedure can be of great value in the field of nanoindentation. The expansion of the method to work hardening materials should be pretty straight forward. Validating the method experimentally would improve the chances of the method to get widely recognized. The systematic error in convergence, especially for yield stress can be elevated by further study of the method.

BIBLIOGRAPHY

BIBLIOGRAPHY

Antunes, J. M., L. F. Menezes, and J. V. Fernandes, 2007, Influence of Vickers tip imperfection on depth sensing indentation tests: International Journal of Solids and Structures, v. 44, p. 2732-2747.

Basaran, C., H. Tang, and S. Nie, 2004, Experimental damage mechanics of microelectronic solder joints under fatigue loading: Mechanics of Materials, v. 36, p. 1111-1121.

ISO14577-2, 2002, International Standard Organization.

Antunes, J. M., L. F. Menezes, and J. V. Fernandes, 2007, Influence of Vickers tip imperfection on depth sensing indentation tests: International Journal of Solids and Structures, v. 44, p. 2732-2747.

Basaran, C., H. Tang, and S. Nie, 2004, Experimental damage mechanics of microelectronic solder joints under fatigue loading: Mechanics of Materials, v. 36, p. 1111-1121.

Bec, S., A. Tonck, and J. L. Loubet, 2006, A simple guide to determine elastic properties of films on substrate from nanoindentation experiments: Philosophical Magazine, v. 86, p. 5347-5358.

Bobji, M. S., and S. K. Biswas, 1999, Deconvolution of hardness from data obtained from nanoindentation of rough surfaces: Journal of Materials Research, v. 14, p. 2259-2268.

Bolshakov, A., 1996, Finite element studies of mechanical property testing by nanoindentation methods: PhD Dissertation thesis, Rice University.

Bolshakov, A., W. C. Oliver, and G. M. Pharr, 1996, Influences of stress on the measurement of mechanical properties using nanoindentation .2. Finite element simulations: Journal of Materials Research, v. 11, p. 760-768.

Bolshakov, A., and G. M. Pharr, 1998, Influences of pileup on the measurement of mechanical properties by load and depth sensing indentation techniques: Journal of Materials Research, v. 13, p. 1049-1058.

Bressan, J. D., A. Tramontin, and C. Rosa, 2005, Modeling of nanoindentation of bulk and thin film by finite element method: Wear, v. 258, p. 115-122.

Casals, O., and J. Alcala, 2005, The duality in mechanical property extractions from Vickers and Berkovich instrumented indentation experiments: Acta Materialia, v. 53, p. 3545-3561.

Chen, J., and S. J. Bull, 2009, On the factors affecting the critical indenter penetration for measurement of coating hardness: Vacuum, v. 83, p. 911-920.

Chen, X., and J. J. Vlassak, 2001, Numerical study on the measurement of thin film mechanical properties by means of nanoindentation: Journal of Materials Research, v. 16, p. 2974-2982.

Chen, X., Y. Xiang, and J. J. Vlassak, 2006, Novel technique for measuring the mechanical properties of porous materials by nanoindentation: Journal of Materials Research, v. 21, p. 715-724.

Cheng, C. M., and Y. T. Cheng, 1997, On the initial unloading slope in indentation of elastic-plastic solids by an indenter with an axisymmetric smooth profile: Applied Physics Letters, v. 71, p. 2623-2625.

Cheng, Y. T., and C. M. Cheng, 1998, Effects of 'sinking in' and 'piling up' on estimating the contact area under load in indentation: Philosophical Magazine Letters, v. 78, p. 115-120.

Cheng, Y. T., and C. M. Cheng, 2000, What is indentation hardness?: Surface & Coatings Technology, v. 133, p. 417-424.

Durst, K., M. Goken, and H. Vehoff, 2004, Finite element study for nanoindentation measurements on twO&Phase materials: Journal of Materials Research, v. 19, p. 85-93.

Ellis, J. D., S. T. Smith, and R. J. Hocken, 2008, Alignment uncertainties in ideal indentation styli: Precision Engineering-Journal of the International Societies for Precision Engineering and Nanotechnology, v. 32, p. 207-214.

Fischer-Cripps, A. C., 2004, Nanoindentation: Mechanical engineering series: New York, Springer, xxii, 263 p. p.

Fleck, N. A., H. Otoyo, and A. Needleman, 1992, INDENTATION OF POROUS SOLIDS: International Journal of Solids and Structures, v. 29, p. 1613-1636.

Han, S. M., R. Saha, and W. D. Nix, 2006, Determining hardness of thin films in elastically mismatched film-on-substrate systems using nanoindentation: Acta Materialia, v. 54, p. 1571-1581.

Han, S. M., R. Shah, R. Banerjee, G. B. Viswanathan, B. M. Clemens, and W. D. Nix, 2005, Combinatorial studies of mechanical properties of Ti-Al thin films using nanoindentation: Acta Materialia, v. 53, p. 2059-2067.

Harvey, S., H. Huang, S. Venkataraman, and W. W. Gerberich, 1993, MICROSCOPY AND MICROINDENTATION MECHANICS OF SINGLE-CRYSTAL FE-3 WT-PERCENT-SI .1. ATOMIC-FORCE MICROSCOPY OF A SMALL INDENTATION: Journal of Materials Research, v. 8, p. 1291-1299.

Hay, J. C., A. Bolshakov, and G. M. Pharr, 1999, A critical examination of the fundamental relations used in the analysis of nanoindentation data: Journal of Materials Research, v. 14, p. 2296-2305.

Johnson, K. L., 1985, Contact mechanics: Cambridge [Cambridgeshire] ; New York, Cambridge University Press, xi, 452 p. p.

Joslin, D. L., and W. C. Oliver, 1990, A NEW METHOD FOR ANALYZING DATA FROM CONTINUOUS DEPTH-SENSING MICROINDENTATION TESTS: Journal of Materials Research, v. 5, p. 123-126.

Kese, K., and Z. C. Li, 2006, Semi-ellipse method for accounting for the pile-up contact area during nanoindentation with the Berkovich indenter: Scripta Materialia, v. 55, p. 699-702.

King, R. B., 1987, ELASTIC ANALYSIS OF SOME PUNCH PROBLEMS FOR A LAYERED MEDIUM: International Journal of Solids and Structures, v. 23, p. 1657-1664.

Kumar, D. R., R. K. Kumar, and P. K. Philip, 2001, Numerical investigations of pyramid indentation on powder compacts: Scripta Materialia, v. 44, p. 2713-2719.

Larsson, P. L., A. E. Giannakopoulos, E. Soderlund, D. J. Rowcliffe, and R. Vestergaard, 1996, Analysis of Berkovich indentation: International Journal of Solids and Structures, v. 33, p. 221-&.

Lee, Y. H., U. Baek, Y. I. Kim, and S. H. Nahm, 2007, On the measurement of pile-up corrected hardness based on the early Hertzian loading analysis: Materials Letters, v. 61, p. 4039-4042.

Li, H., and J. J. Vlassak, 2009, Determining the elastic modulus and hardness of an ultra-thin film on a substrate using nanoindentation: Journal of Materials Research, v. 24, p. 1114-1126.

Lichinchi, M., C. Lenardi, J. Haupt, and R. Vitali, 1998, Simulation of Berkovich nanoindentation experiments on thin films using finite element method: Thin Solid Films, v. 312, p. 240-248.

Madhavan, V., and A. H. Adibi-Sedeh, 2005, Understanding of finite element analysis results under the framework of Oxley's machining model: Machining Science and Technology, v. 9, p. 345-368.

Maneiro, M. A. G., and J. Rodriguez, 2005, Pile-up effect on nanoindentation tests with spherical-conical tips: Scripta Materialia, v. 52, p. 593-598.

Nagao, S., M. Fujikane, N. Tymiak, and R. Nowak, 2009, Achieving consistency of Young's modulus determination from nanoscale deformation of low-k films: Journal of Applied Physics, v. 105.

Oliver, W. C., and G. M. Pharr, 1992, AN IMPROVED TECHNIQUE FOR DETERMINING HARDNESS AND ELASTIC-MODULUS USING LOAD AND DISPLACEMENT SENSING INDENTATION EXPERIMENTS: Journal of Materials Research, v. 7, p. 1564-1583.

Pelegri, A. A., and X. Huang, 2008, Nanoindentation on soft film/hard substrate and hard film/soft substrate material systems with finite element analysis: Composites Science and Technology, v. 68, p. 147-155.

Poon, B., D. Rittel, and G. Ravichandran, 2008, An analysis of nanoindentation in linearly elastic solids: International Journal of Solids and Structures, v. 45, p. 6018-6033.

Prchlik, L., 2004, Input error sensitivity of hardness and elastic modulus evaluated from indentation load-displacement records by Oliver and Pharr method: Journal of Materials Science, v. 39, p. 1185-1193.

Saha, R., and W. D. Nix, 2002, Effects of the substrate on the determination of thin film mechanical properties by nanoindentation: Acta Materialia, v. 50, p. 23-38.

Sakai, M., 2009, Substrate-affected indentation contact parameters of elastoplastic coating/substrate composites: Journal of Materials Research, v. 24, p. 831-843.

Saket Kashani, M., and V. Madhavan, 2007, Study of damage distribution over primary shear zone in metal cutting process by nanoindentation: Materials Science and Technology Conference and Exhibition, MS and T'07 - "Exploring Structure, Processing, and Applications Across Multiple Materials Systems", p. 2609-2617.

Saket Kashani, M., and V. Madhavan, 2008, The effect of surface tilt on nanoindentation results: ASME International Mechanical Engineering Congress and Exposition, IMECE 2007, p. 67-1071.

Shim, S., 2007, A comparison of 3D finite element simulations for Berkovich and conical indentation of fused silica: International Journal of Surface Science and Engineering, v. 1, p. 259-273.

Shu, S. Q., J. Lu, and D. F. Li, 2007, A systematic study of the validation of Oliver and Pharr's method: Journal of Materials Research, v. 22, p. 3385-3396.

Strader, J. H., S. Shim, H. Bei, W. C. Oliver, and G. M. Pharry, 2006, An experimental evaluation of the constant ss relating the contact stiffness to the contact area in nanoindentation: Philosophical Magazine, v. 86, p. 5285-5298.

Sun, Y., J. Liang, Z. H. Xu, G. F. Wang, and X. D. Li, 2008, Nanoindentation for measuring individual phase mechanical properties of lead free solder alloy: Journal of Materials Science-Materials in Electronics, v. 19, p. 514-521.

Taljat, B., and G. M. Pharr, 2004, Development of pile-up during spherical indentation of elastic-plastic solids: International Journal of Solids and Structures, v. 41, p. 3891-3904.

Tasan, C. C., J. P. M. Hoefnagels, and M. G. D. Geers, 2009, A critical assessment of indentation-based ductile damage quantification: Acta Materialia, v. 57, p. 4957-4966.

Wang, T. H., T. H. Fang, and Y. C. Lin, 2007, Analysis of the substrate effects of strain-hardening thin films on silicon under nanoindentation: Applied Physics a-Materials Science & Processing, v. 86, p. 335-341.

Warren, A. W., and Y. B. Guo, 2006, Machined surface properties determined by nanoindentation: Experimental and FEA studies on the effects of surface integrity and tip geometry: Surface & Coatings Technology, v. 201, p. 423-433.

Xiang, Y., X. Chen, T. Y. Tsui, J. I. Jang, and J. J. Vlassak, 2006, Mechanical properties of porous and fully dense low-kappa dielectric thin films measured by means of nanoindentation and the plane-strain bulge test technique: Journal of Materials Research, v. 21, p. 386-395.

Xu, Z. H., and X. Li, 2007, Effect of sample tilt on nanoindentation behaviour of materials: Philosophical Magazine, v. 87, p. 2299-2312.

Yu, H. Y., S. C. Sanday, and B. B. Rath, 1990, THE EFFECT OF SUBSTRATE ON THE ELASTIC PROPERTIES OF FILMS DETERMINED BY THE INDENTATION TEST - AXISYMMETRICAL BOUSSINESQ PROBLEM: Journal of the Mechanics and Physics of Solids, v. 38, p. 745-764.

Zhou, X. Y., Z. D. Jiang, H. R. Wang, and R. X. Yu, 2008, Investigation on methods for dealing with pile-up errors in evaluating the mechanical properties of thin metal films at sub-micron scale on hard substrates by nanoindentation technique: Materials Science and Engineering a-Structural Materials Properties Microstructure and Processing, v. 488, p. 318-332.